

# **Microscopy**

# Microscope

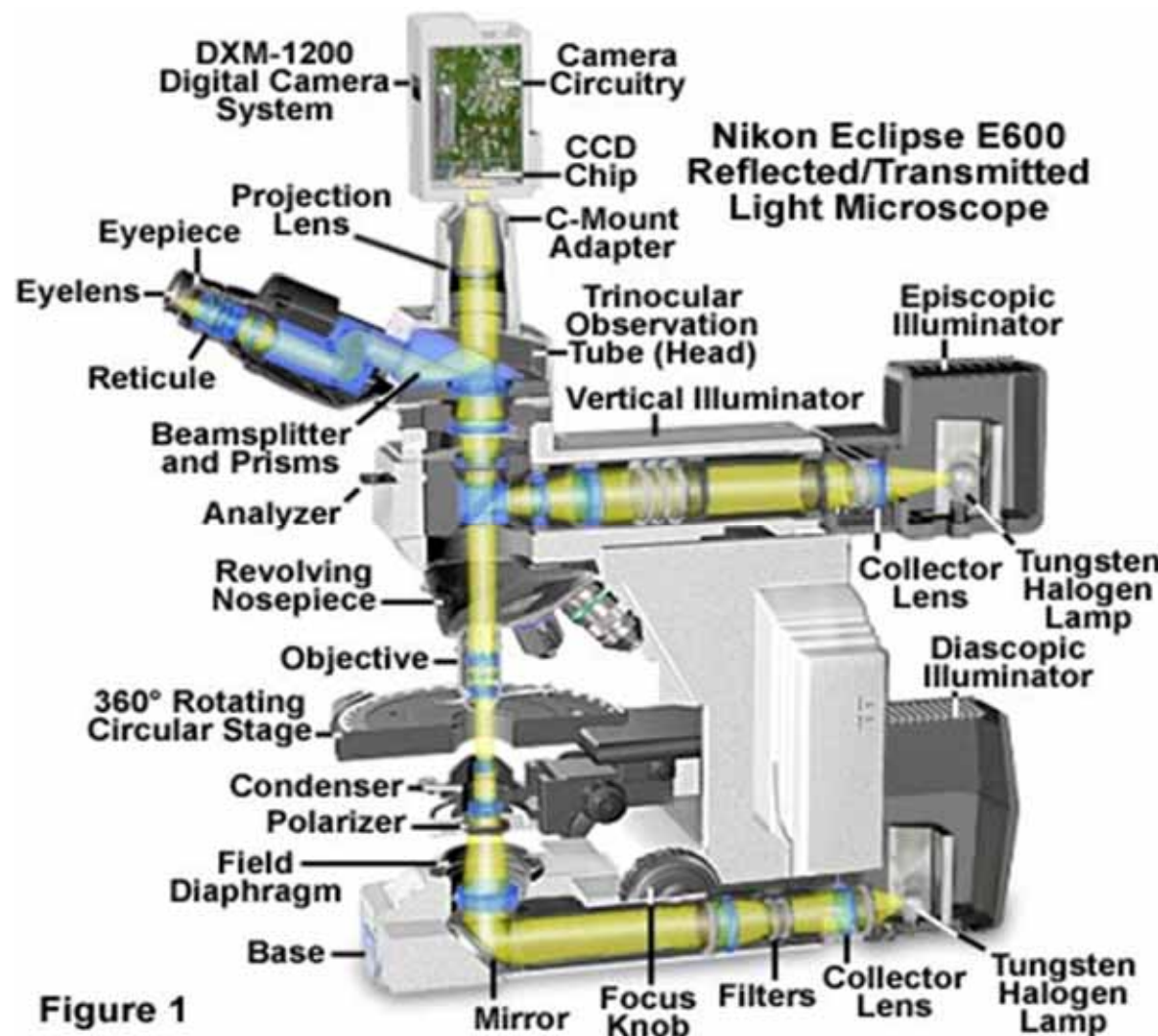


Figure 1

# Conjugate Plan

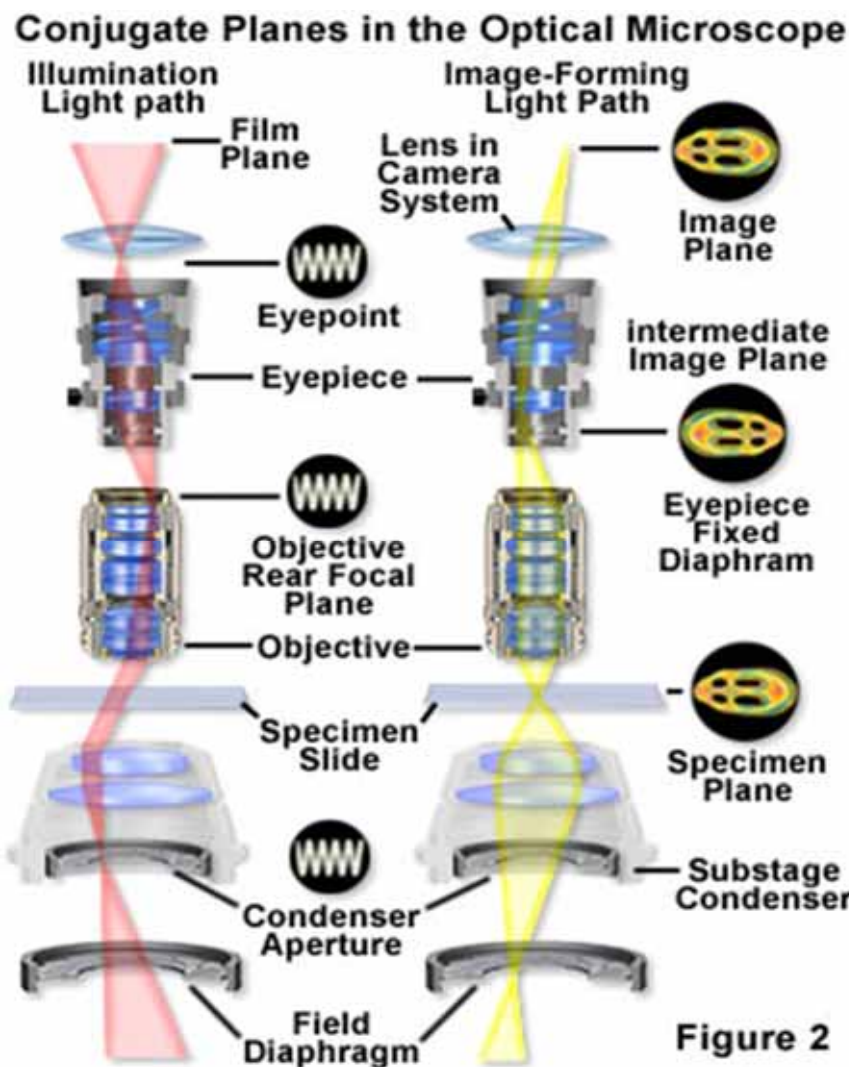
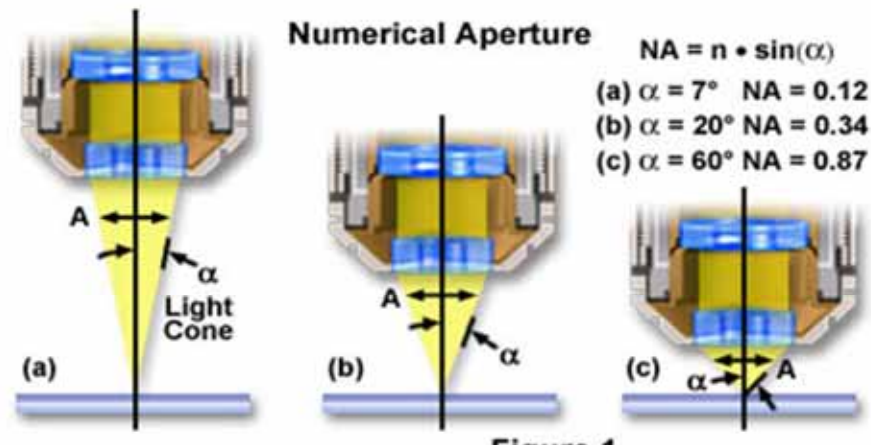


Figure 2

# Numerical Aperture

Numerical Aperture (NA) =  $n \cdot \sin(\mu)$  or  $n \cdot \sin(\alpha)$



## Numerical Aperture versus Objective Magnification

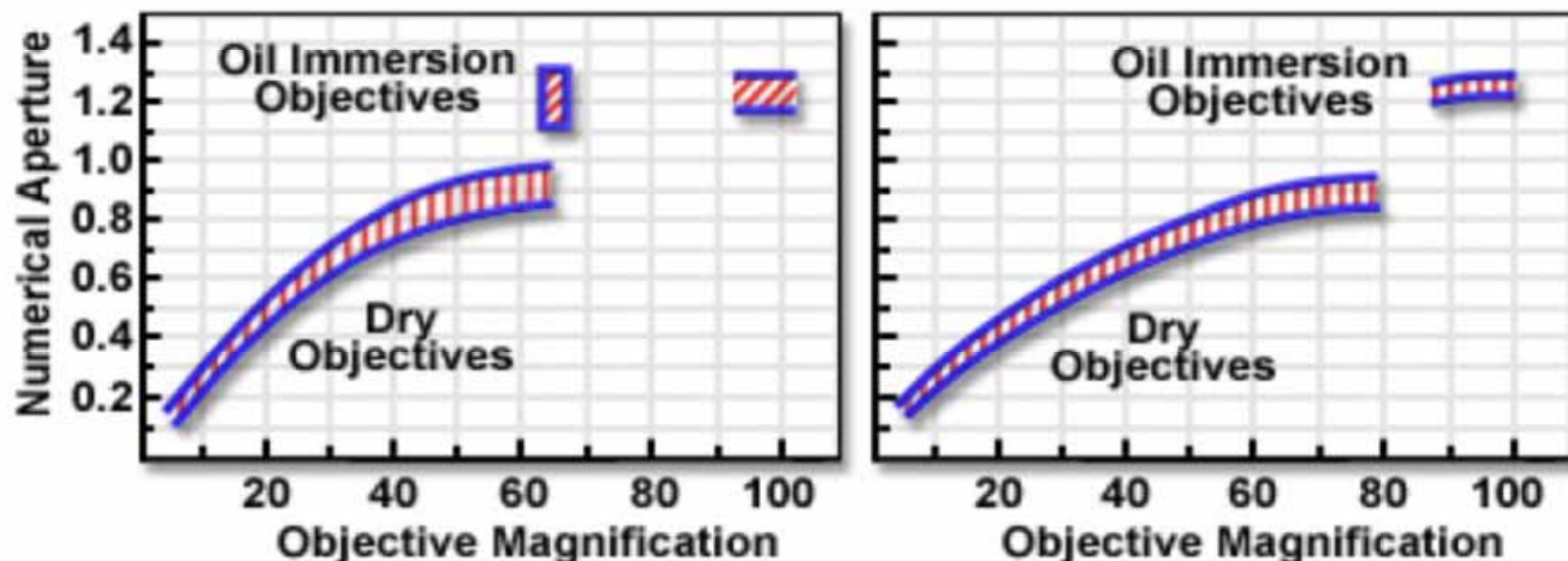
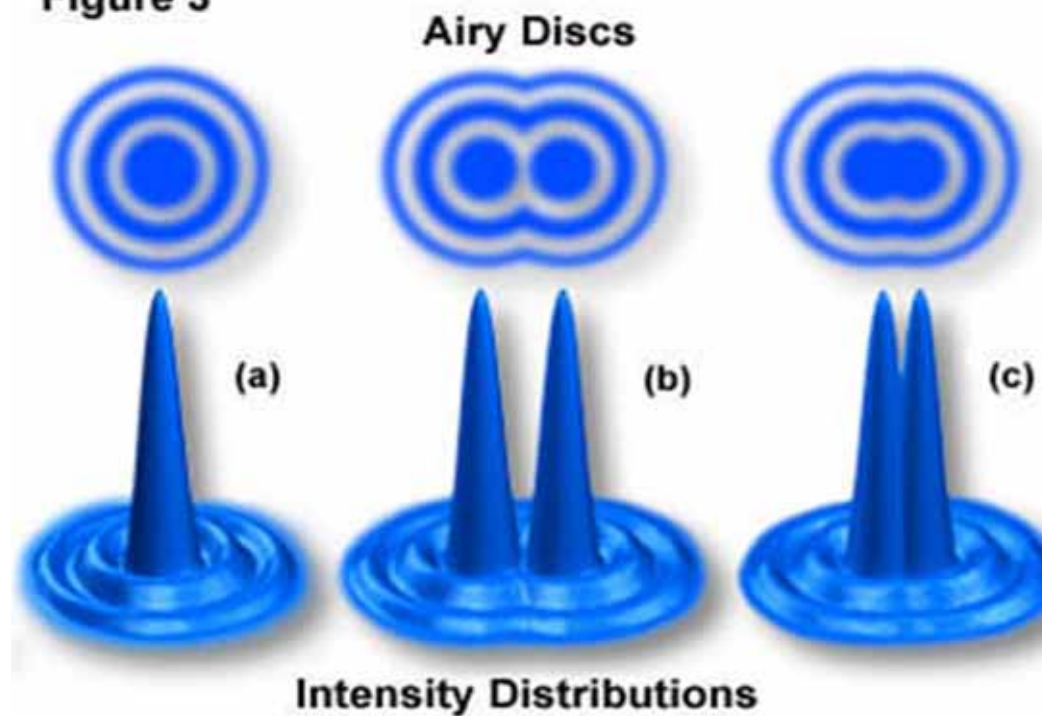


Figure 2

# Resolution

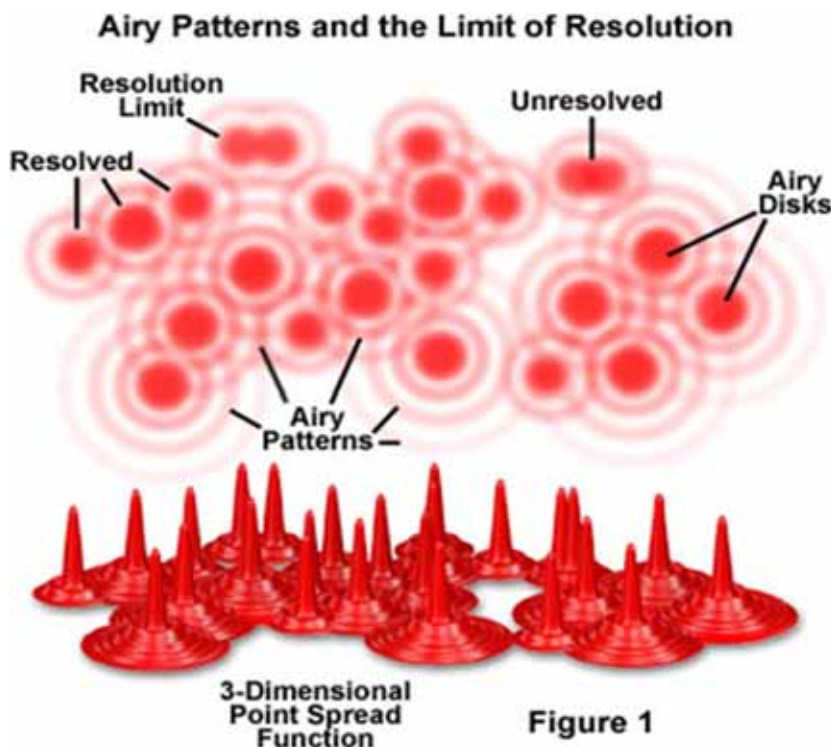
Figure 3



$$\text{Resolution (r)} = \lambda / (2\text{NA}) \quad (1)$$

$$\text{Resolution (r)} = 0.61 \lambda / \text{NA} \quad (2)$$

$$\text{Resolution (r)} = 1.22 \lambda / (\text{NA(obj)} + \text{NA(cond)}) \quad (3)$$



Objective Type						
Magnification	N.A.	Plan Achromat		Plan Fluorite		Plan Apochromat
		Resolution (μm)	N.A.	Resolution (μm)	N.A.	Resolution (μm)
4x	0.10	2.75	0.13	2.12	0.20	1.375
10x	0.25	1.10	0.30	0.92	0.45	0.61
20x	0.40	0.69	0.50	0.55	0.75	0.37
40x	0.65	0.42	0.75	0.37	0.95	0.29
60x	0.75	0.37	0.85	0.32	0.95	0.29
100x	1.25	0.22	1.30	0.21	1.40	0.20

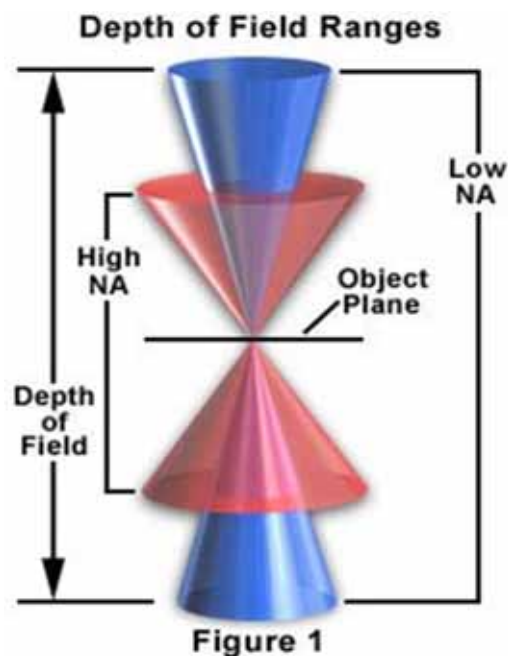
N.A. = Numerical Aperture

### Resolution versus Wavelength

Wavelength (Nanometers)	Resolution (Micrometers)
360	.19
400	.21
450	.24
500	.26
550	.29
600	.32
650	.34
700	.37

$$\text{N.A.} = 0.95$$

# Depth of Focus



Magnification	Numerical Aperture	Depth of Field (μm)	Image Depth (mm)
4x	0.10	55.5	0.13
10x	0.25	8.5	0.80
20x	0.40	5.8	3.8
40x	0.65	1.0	12.8
60x	0.85	0.40	29.8
100x	0.95	0.19	80.0

# Magnification

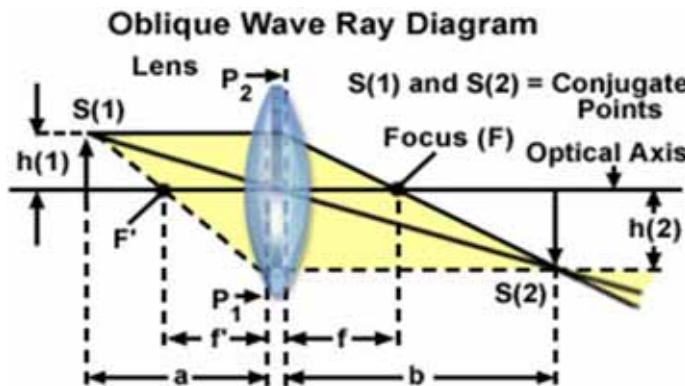
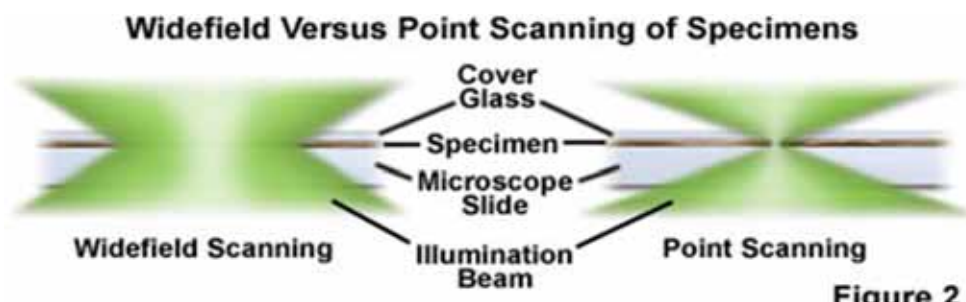
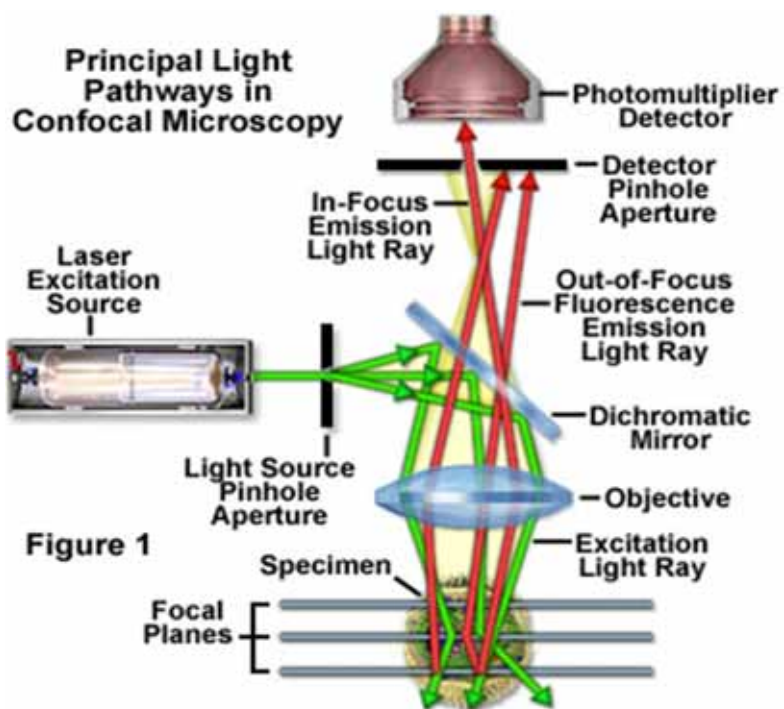


Figure 5



Figure 1

# Confocal



### Optical Section Z-Series

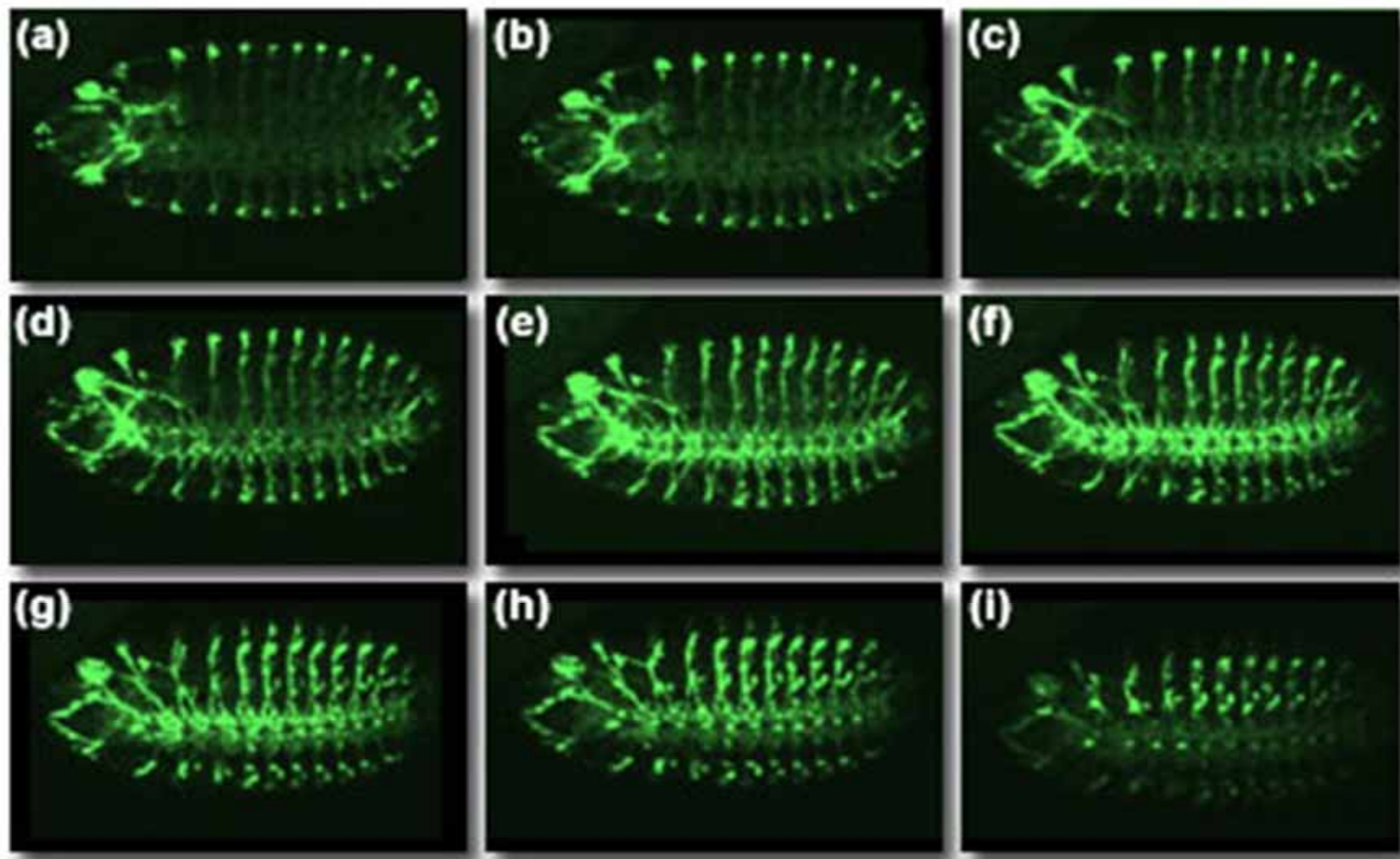
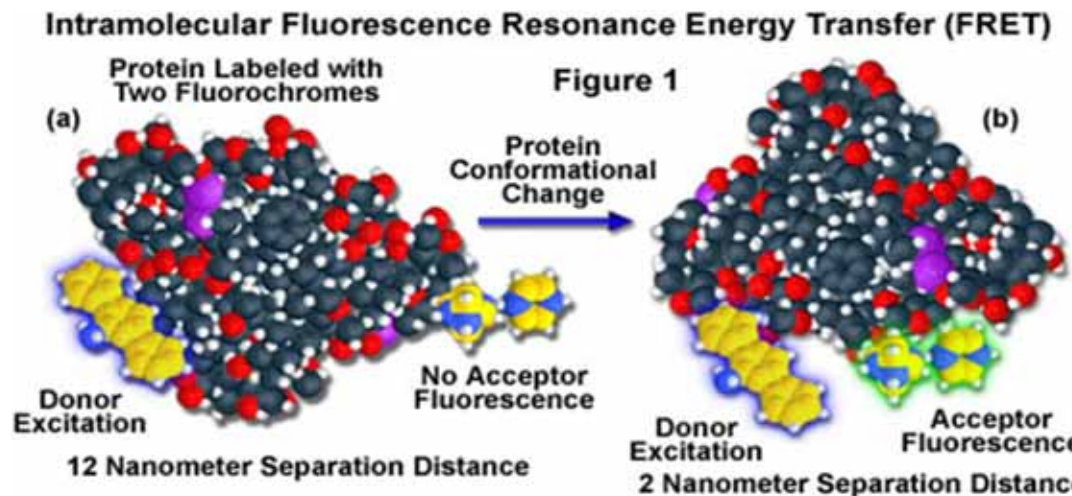


Figure 3

# Foster Resonance Energy Transfer (FRET)

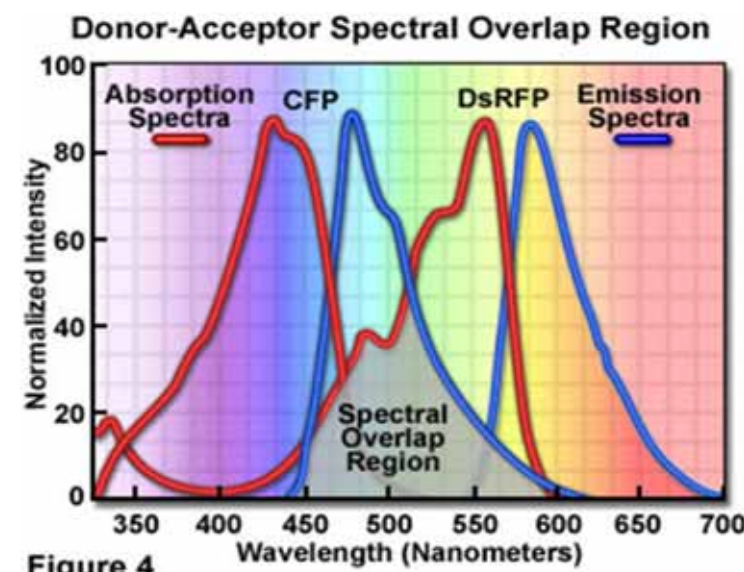
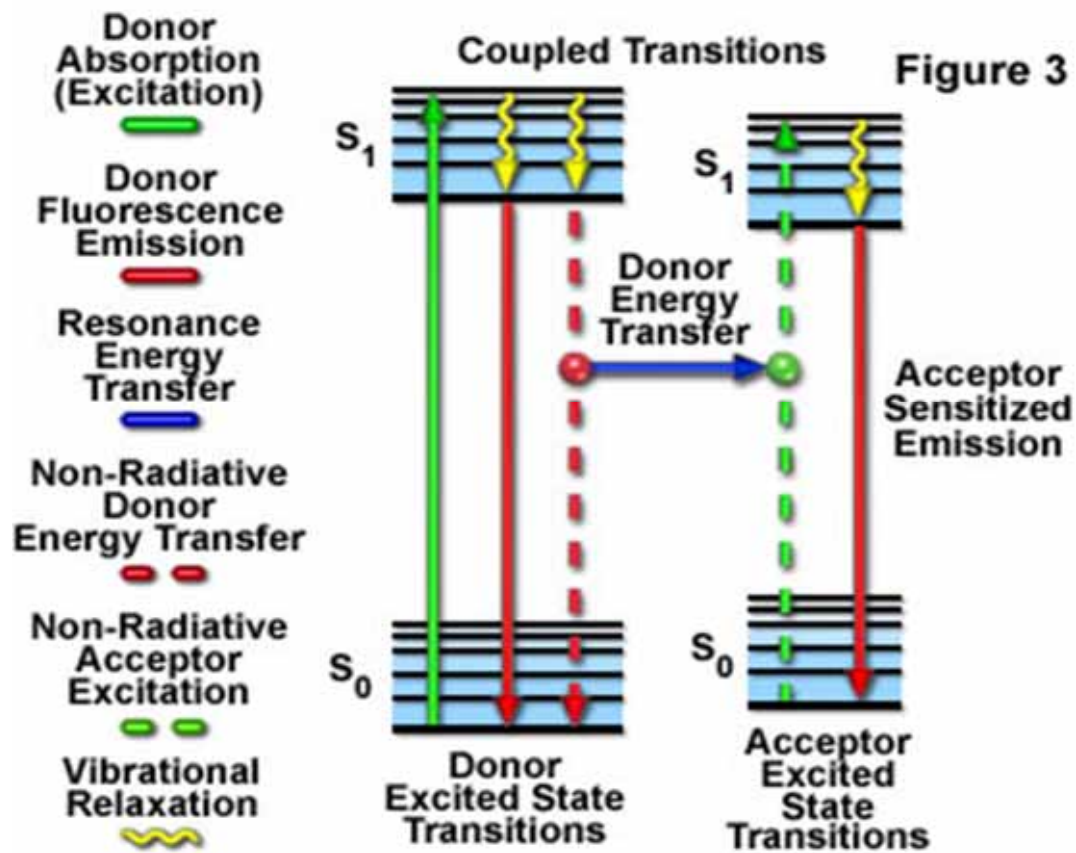


$$E = \frac{k_{ET}}{k_f + k_{ET} + \sum k_i}$$

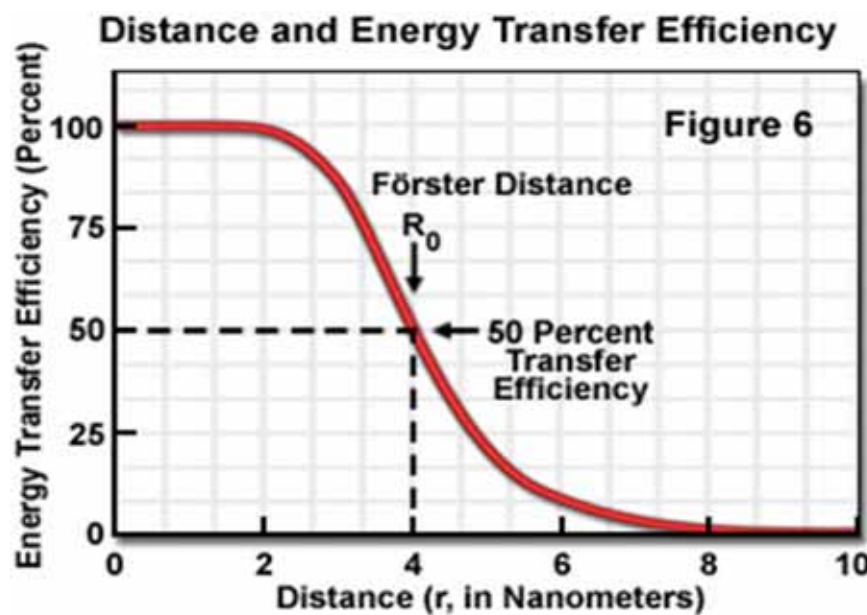
$$E = \frac{1}{1 + (r/R_0)^6}$$

# FRET

## Resonance Energy Transfer Jablonski Diagram

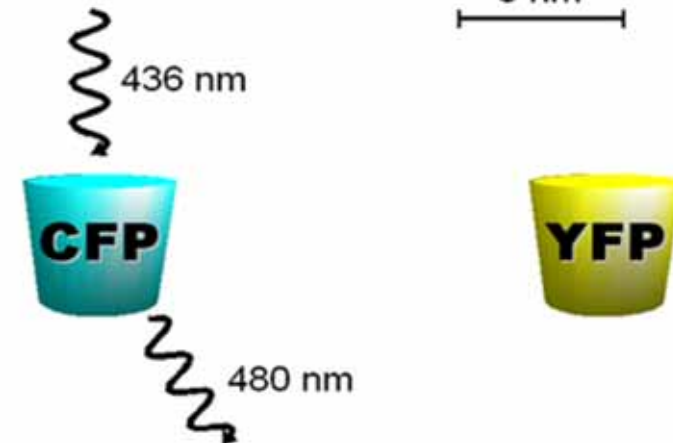


# FRET

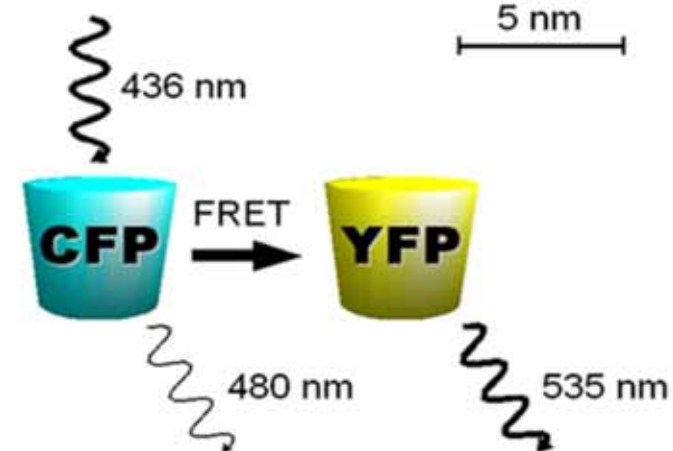


2-8 nm

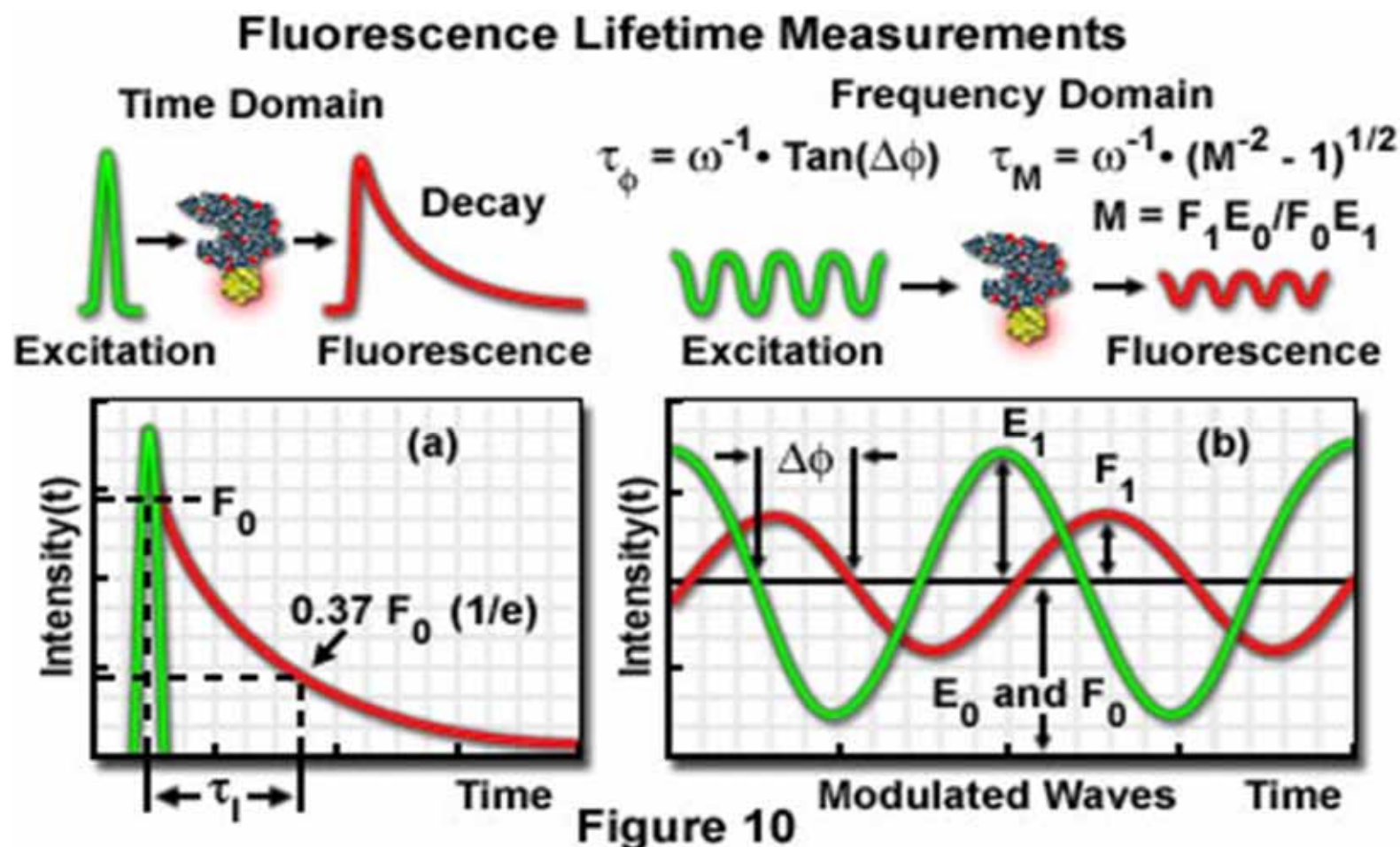
Nessun segnale FRET



Segnale FRET



# FRET



# Applications

## Biomolecular Fluorescence Resonance Energy Transfer Applications

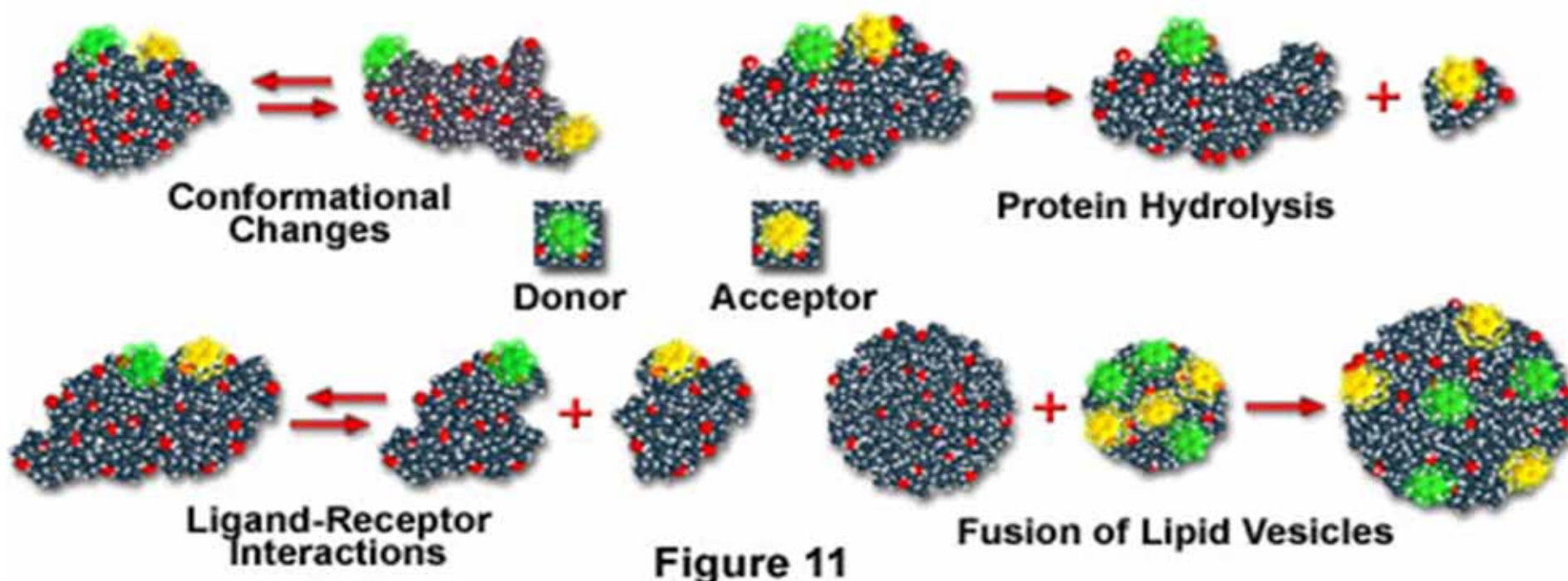


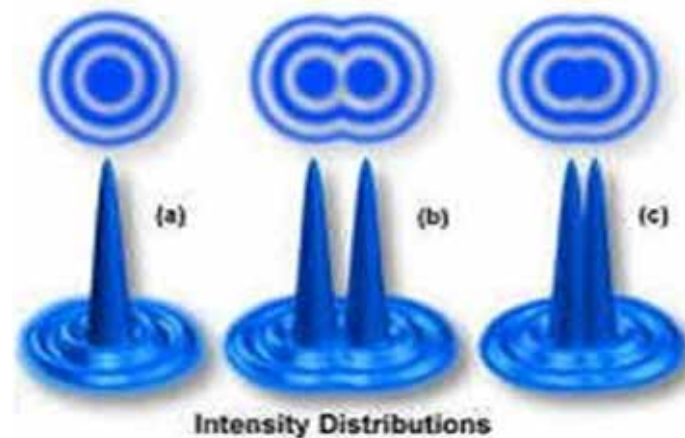
Figure 11

# Diffraction Limit



$$d = \lambda / (2n \sin \alpha)$$

$$, k_0 = 2NA/\lambda_{\text{em}}$$



# Localization

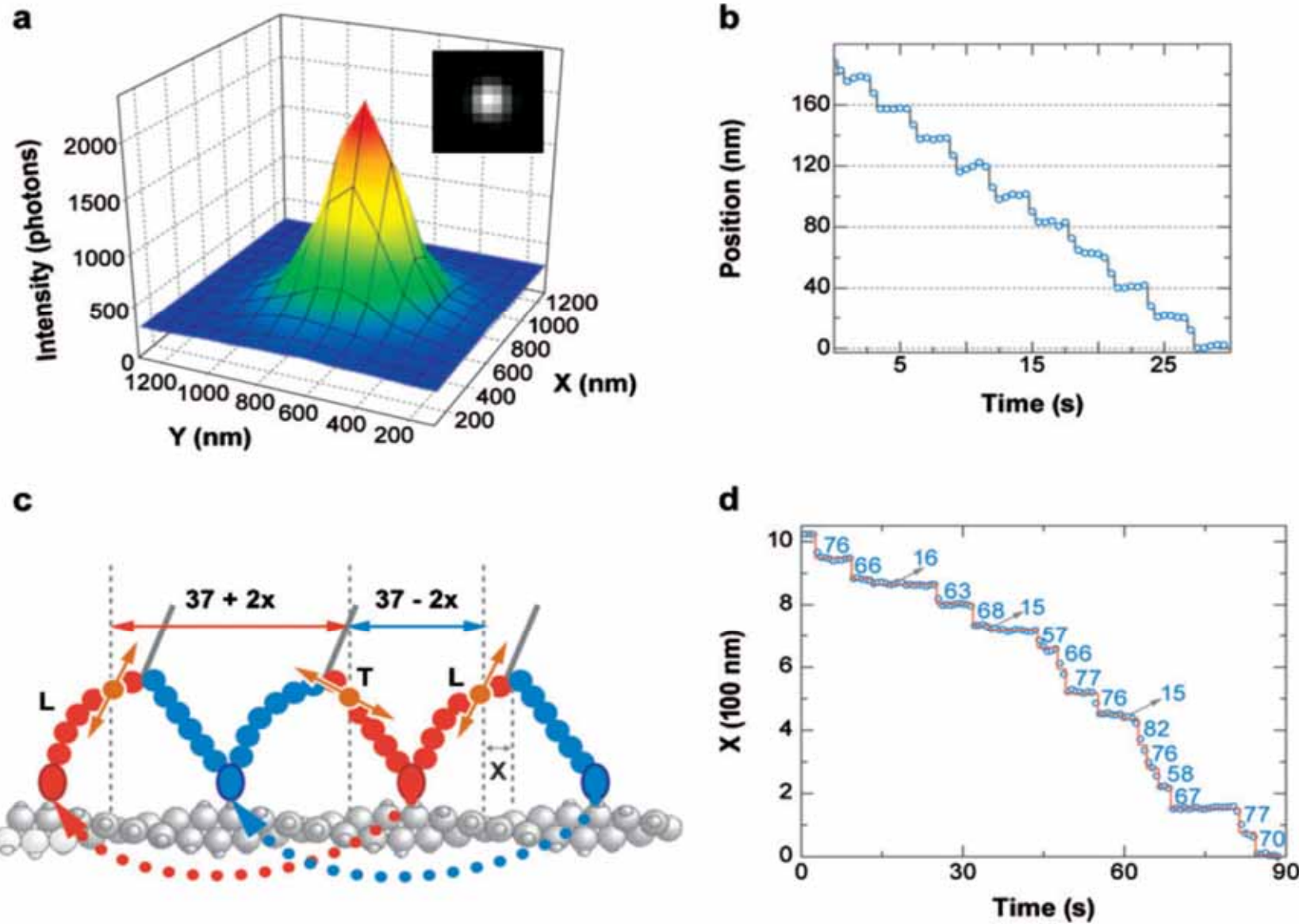
$$I(x, y) = I_{\text{background}} + A.$$

$$\exp \left\{ -1/2 \left[ \left( \frac{x - x_0}{s_x} \right)^2 + \left( \frac{y - y_0}{s_y} \right)^2 \right] \right\},$$

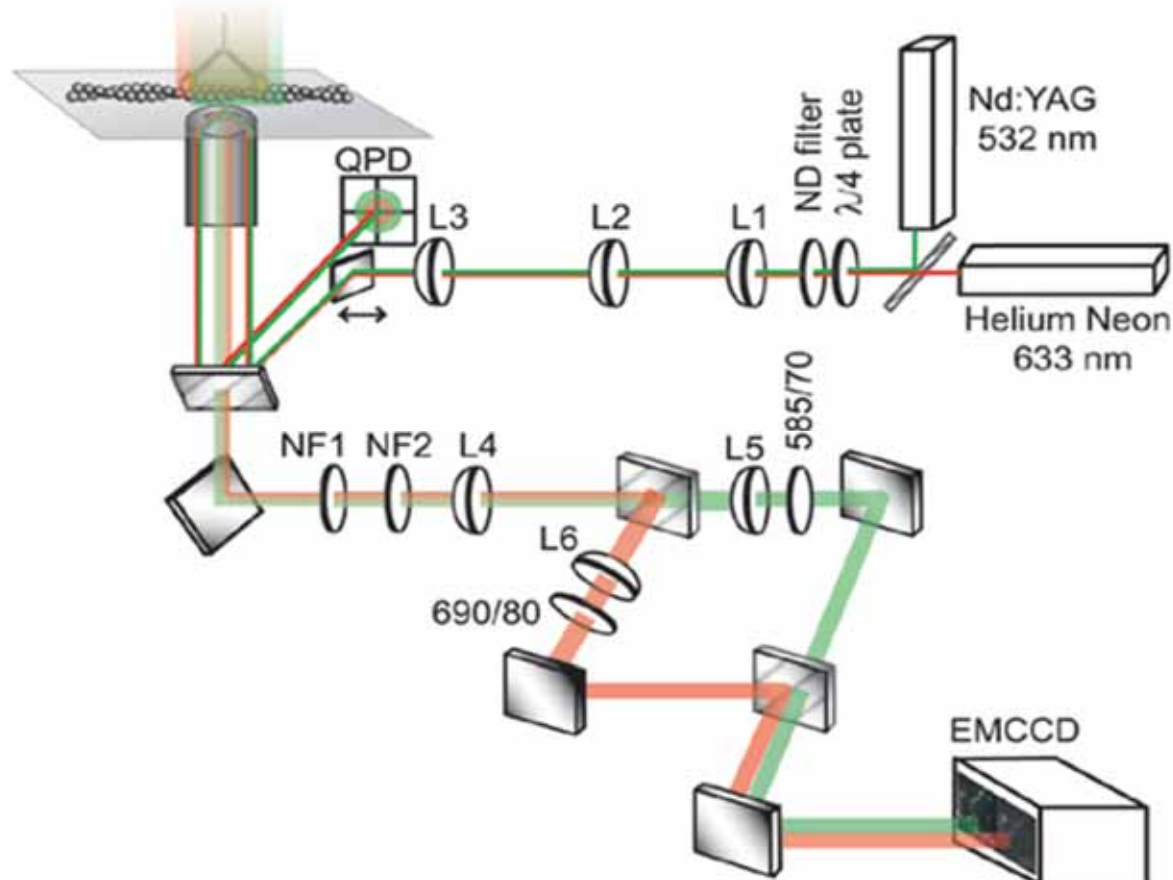
$$\sigma_{x,y}^{\mu}$$

$$= \sqrt{\frac{s_{x,y}^2}{N_{\text{photons}}} + \frac{a^2}{12.N_{\text{photons}}} + \frac{8.\pi.s_{x,y}^4.b^2}{a^2.N_{\text{photons}}}},$$

# Fluorescence Imaging with One Nanometer Accuracy (FIONA)

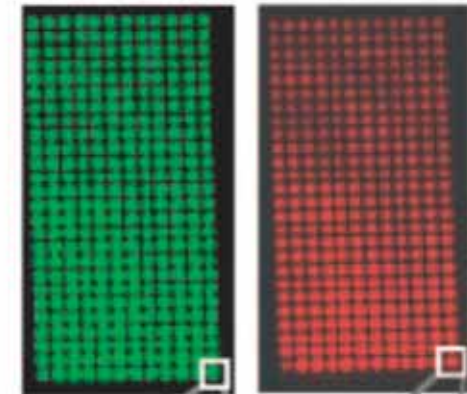


# Fluorescence Imaging with One-Nanometer Accuracy (FIONA)



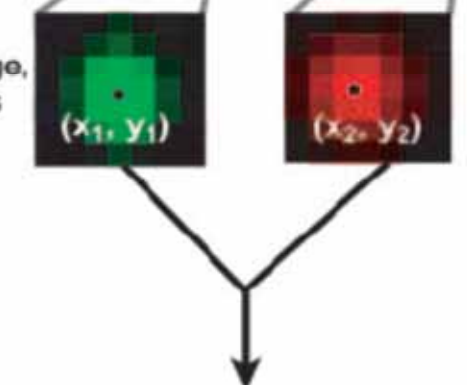
a

Cy3 Channel Cy5 Channel



b

For each bead image, a center is found



c

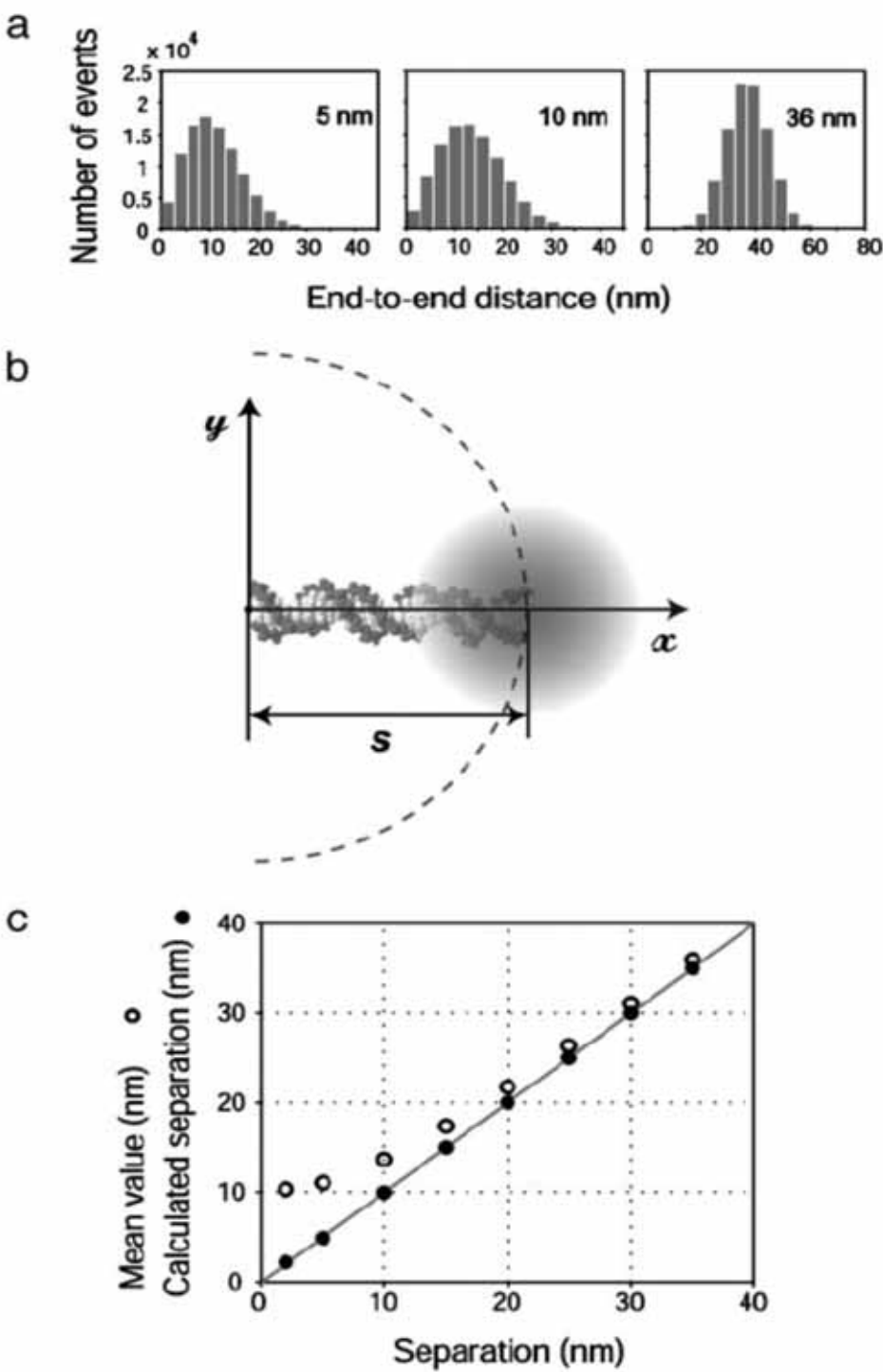
Combining all the locations, a local weighted mean transformation is calculated which maps any point in the Cy5 channel precisely onto the Cy3 channel

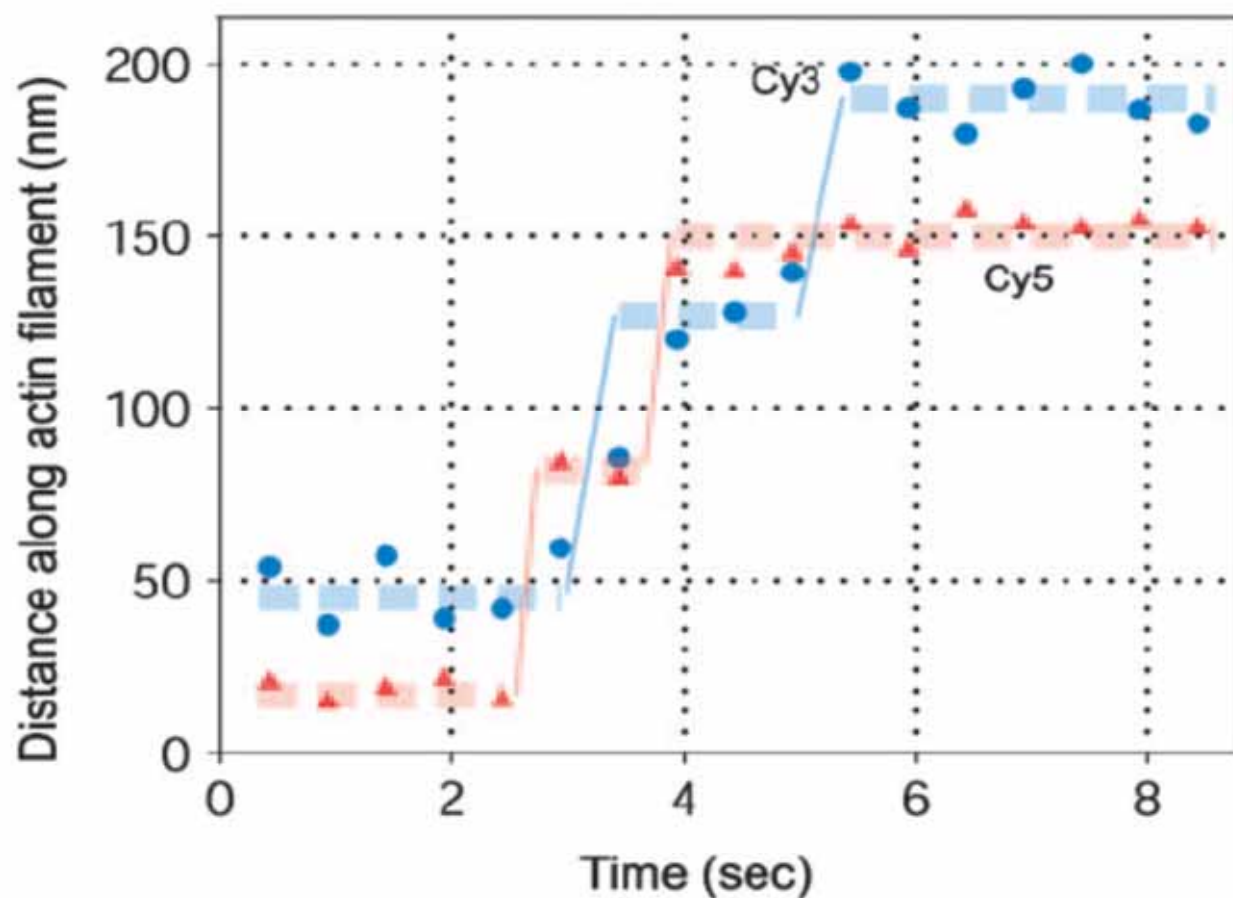
$$f(x_2, y_2) \longrightarrow (x_1, y_1)$$

$$f(x, y) = z_0 + A \exp\left(\frac{1}{2}\left[\left(\frac{x - \mu_x}{\sigma_x}\right)^2 + \left(\frac{y - \mu_y}{\sigma_y}\right)^2\right]\right)$$

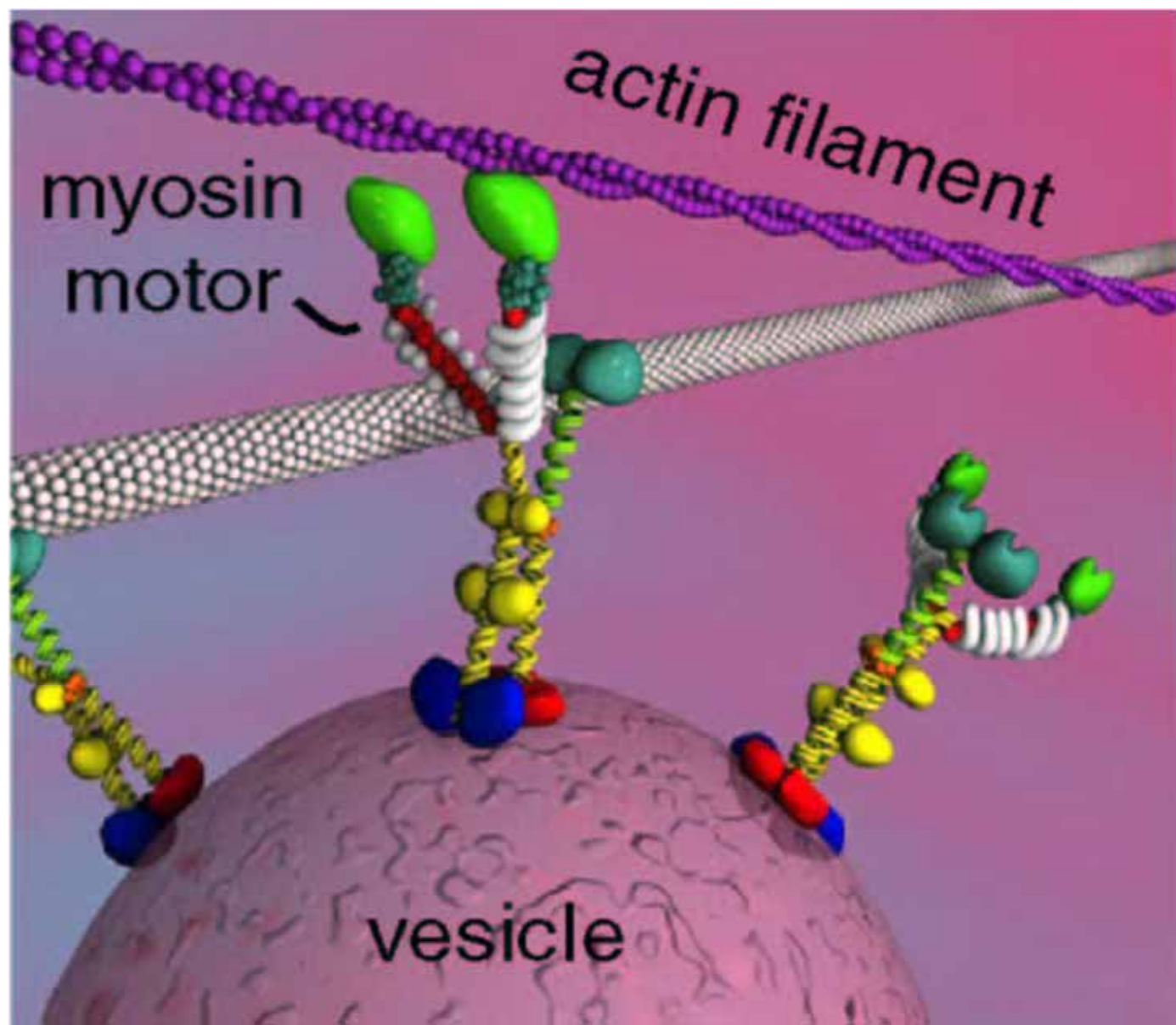
$$\sigma_\mu = \sqrt{(\sigma_x^2 + \sigma_y^2)} / \sqrt{N_\gamma - 1}.$$

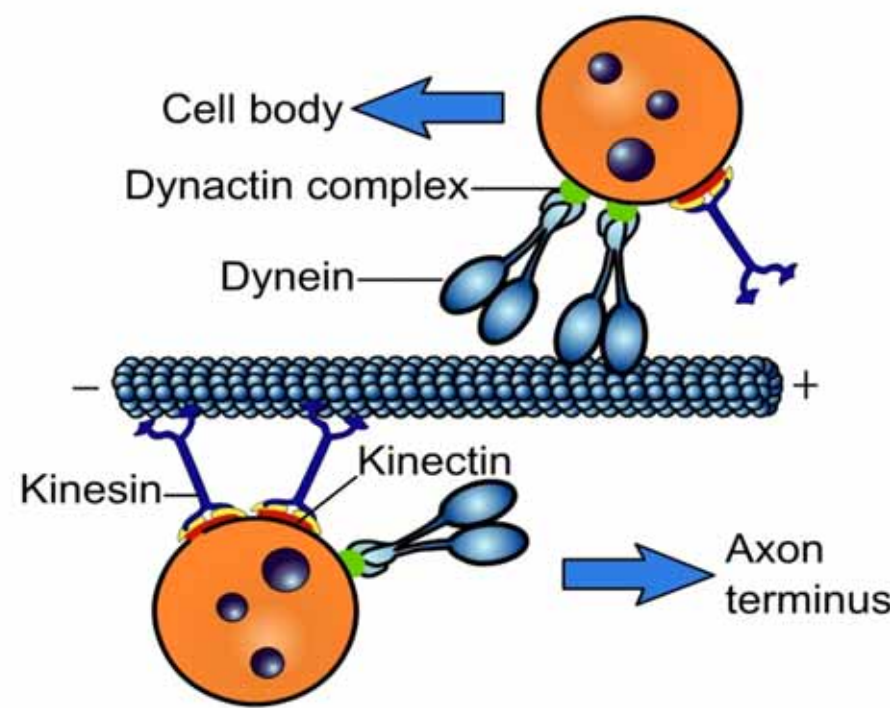
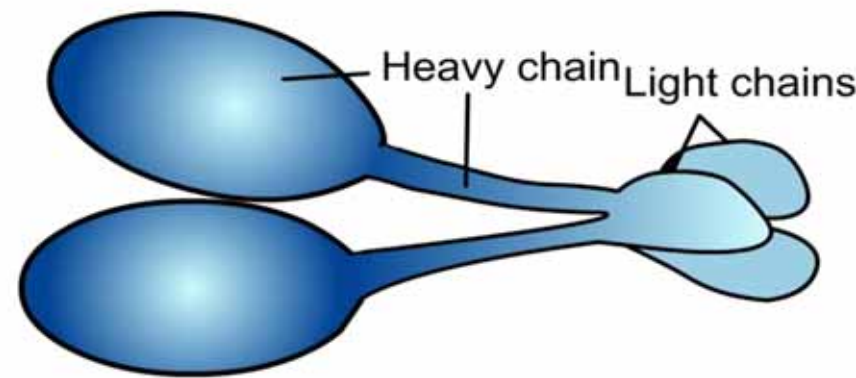
**Fig. 2.** Determining the accurate end-to-end distance from the skewed distribution of distance measurements. (a) The distance probability distribution was calculated by means of Monte Carlo simulations. (b) The skew in the histograms toward large values can be understood from a geometric argument. If one end of the DNA molecule is measured to reside at the origin, then only points lying on the circumference of a circle with radius  $s$  and origin  $(0, 0)$  will yield the true end-to-end distance. It is more likely that a point will lie outside of the dashed-line semicircle than inside it, which gives the distance distribution a long tail. (c) Despite the non-Gaussian nature of the distance distribution, the end-to-end separation can be calculated using the geometric mean, variance, and localization errors.





**Fig. 4.** Time trace of a differentially labeled myosin V molecule walking along an actin filament. The labels (Cy3 and Cy5) are covalently attached to calmodulins that were exchanged onto the myosin V molecule. In this trace, both of the fluorescent probe's locations are taking 72-nm steps, indicating that the calmodulins were exchanged close to the motor domain. The alternating positions of the probes provide a direct observation of myosin V's hand-over-hand walking mechanism.





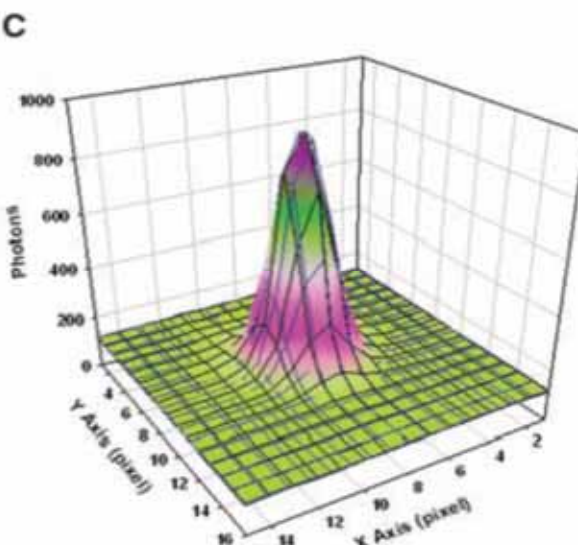
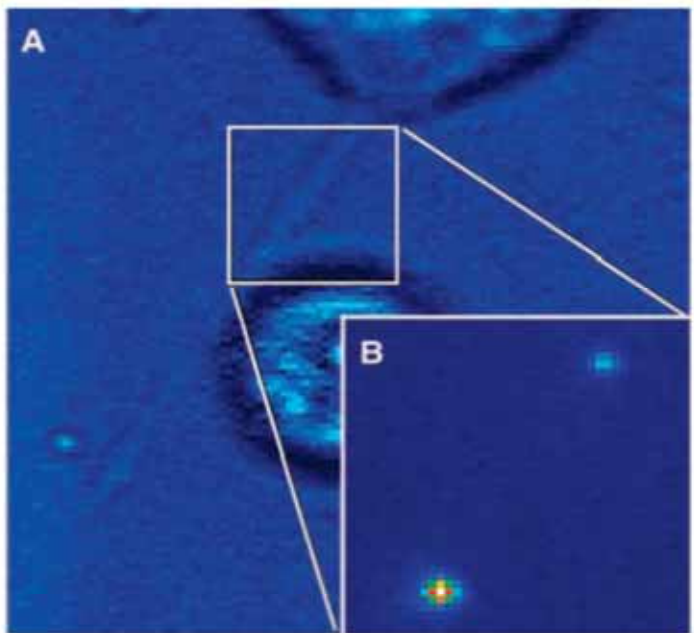
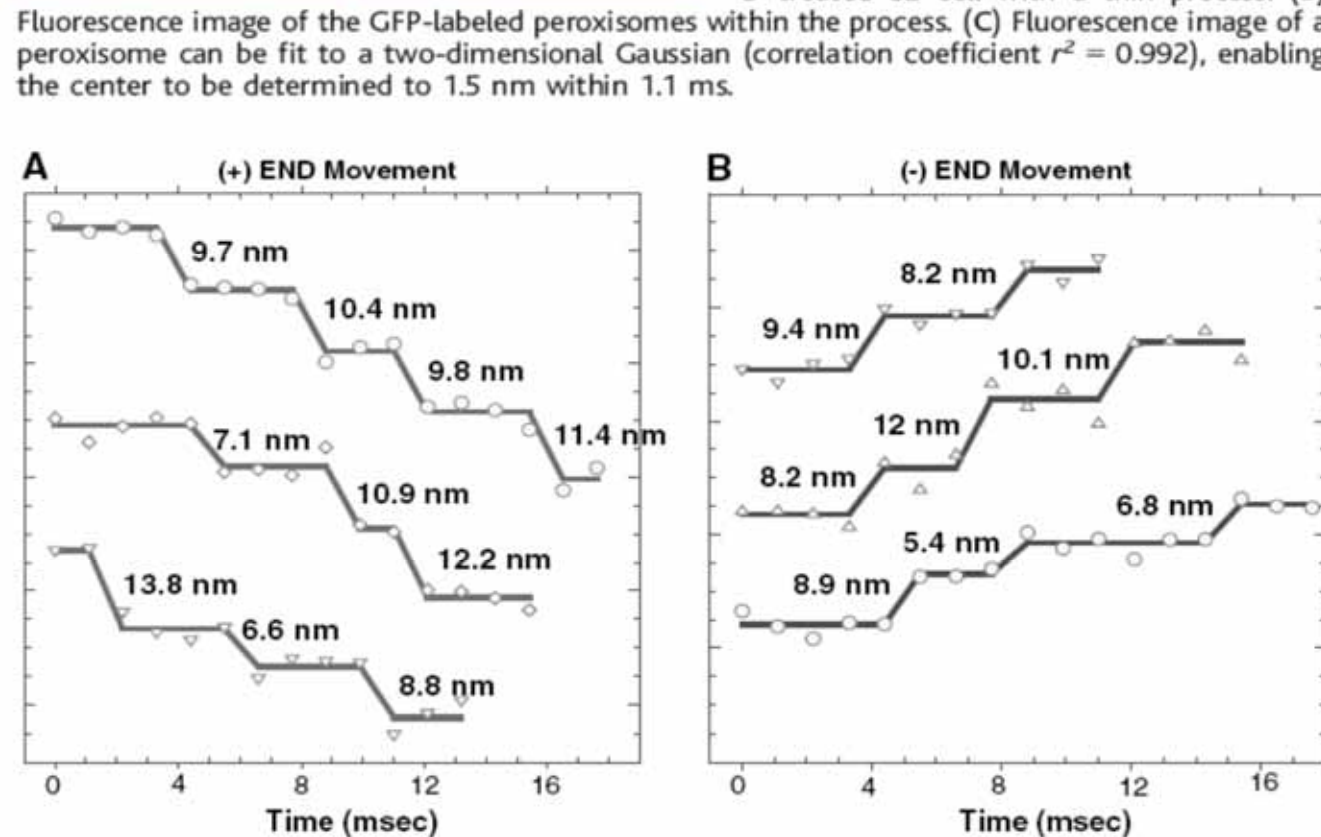


**Fig. 1.** (A) Bright-field image of a cytochalasin-D-treated S2 cell with a thin process. (B) Fluorescence image of a peroxisome can be fit to a two-dimensional Gaussian (correlation coefficient  $r^2 = 0.992$ ), enabling the center to be determined to 1.5 nm within 1.1 ms.



**Kinesin and Dynein Move a Peroxisome in Vivo: A Tug-of-War or Coordinated Movement?**

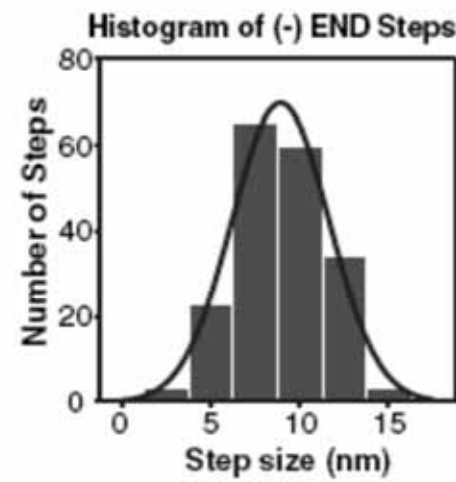
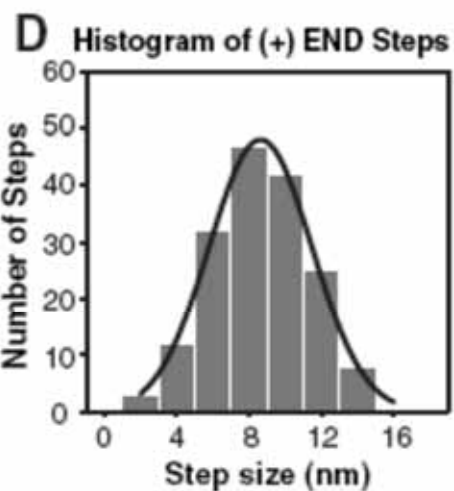
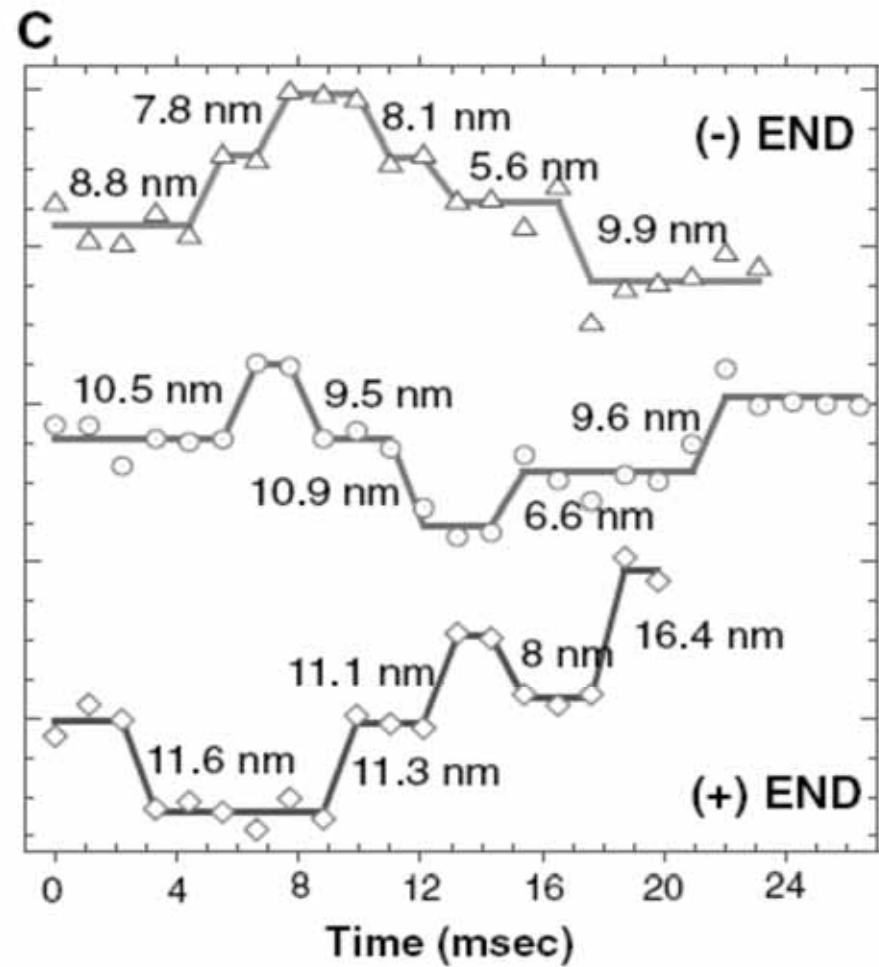
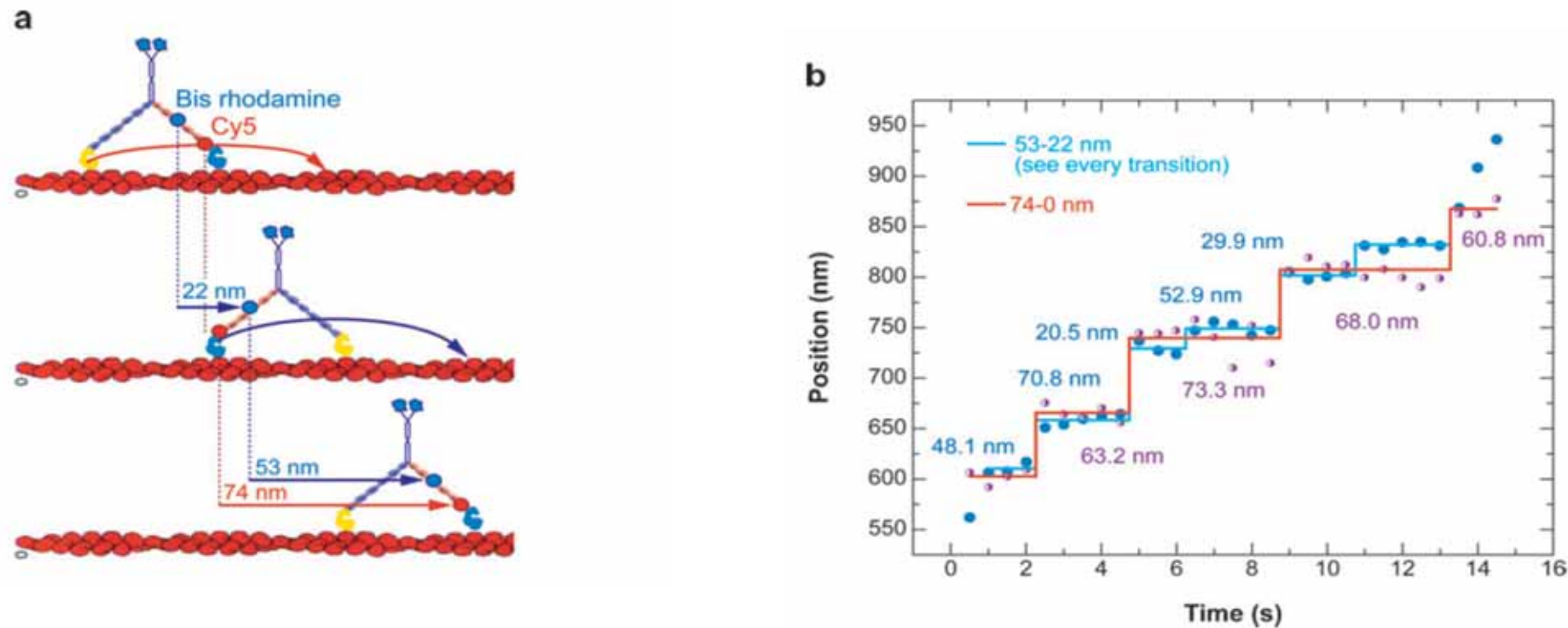
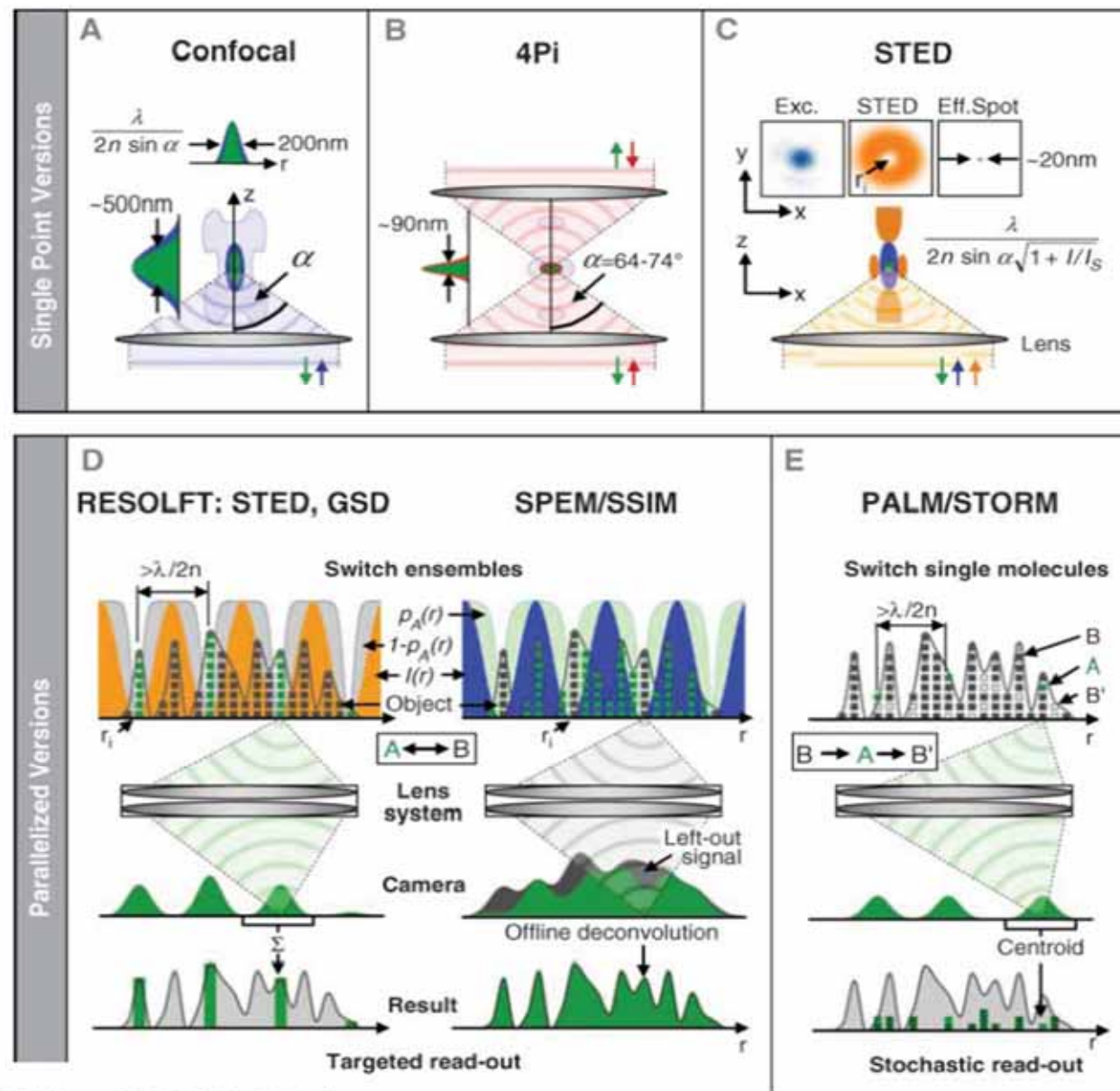


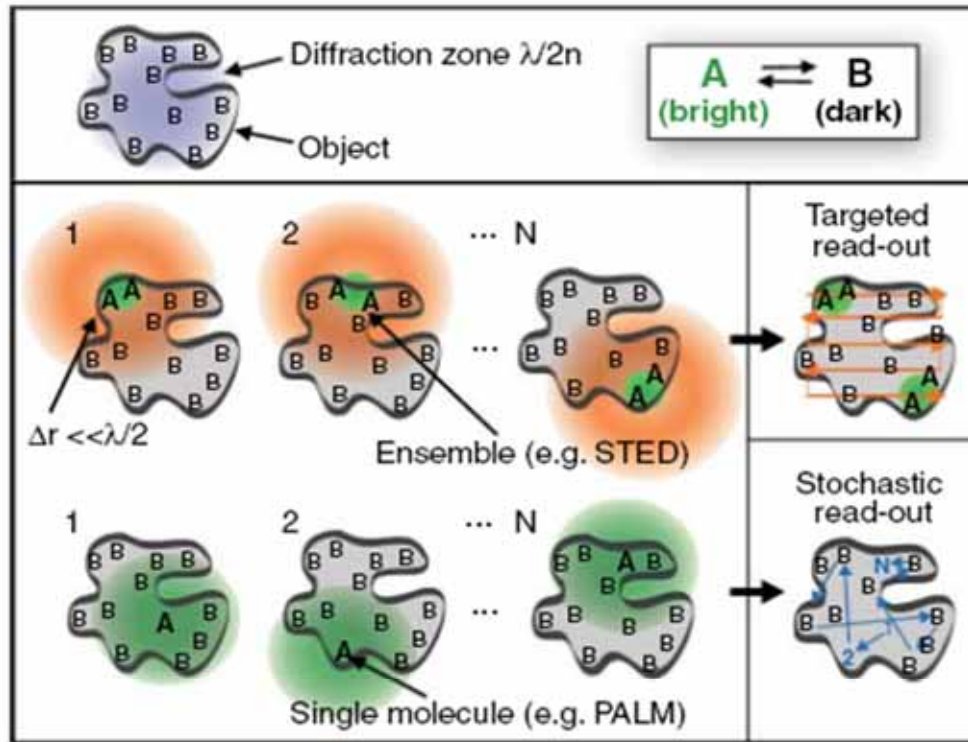
**Fig. 2.** Step-by-step movement of peroxisomes carried by (A) a single kinesin, (B) a single dynein, and (C) a coordination of kinesin and dynein. (D) Histograms of the individual steps of anterograde (kinesin) and retrograde (dynein) movement. A pairwise displacement of kinesin and dynein, showing the multiples of 8-nm displacement, is shown in fig. S6.

# Single-molecule High-Resolution Colocalization (SHREC)

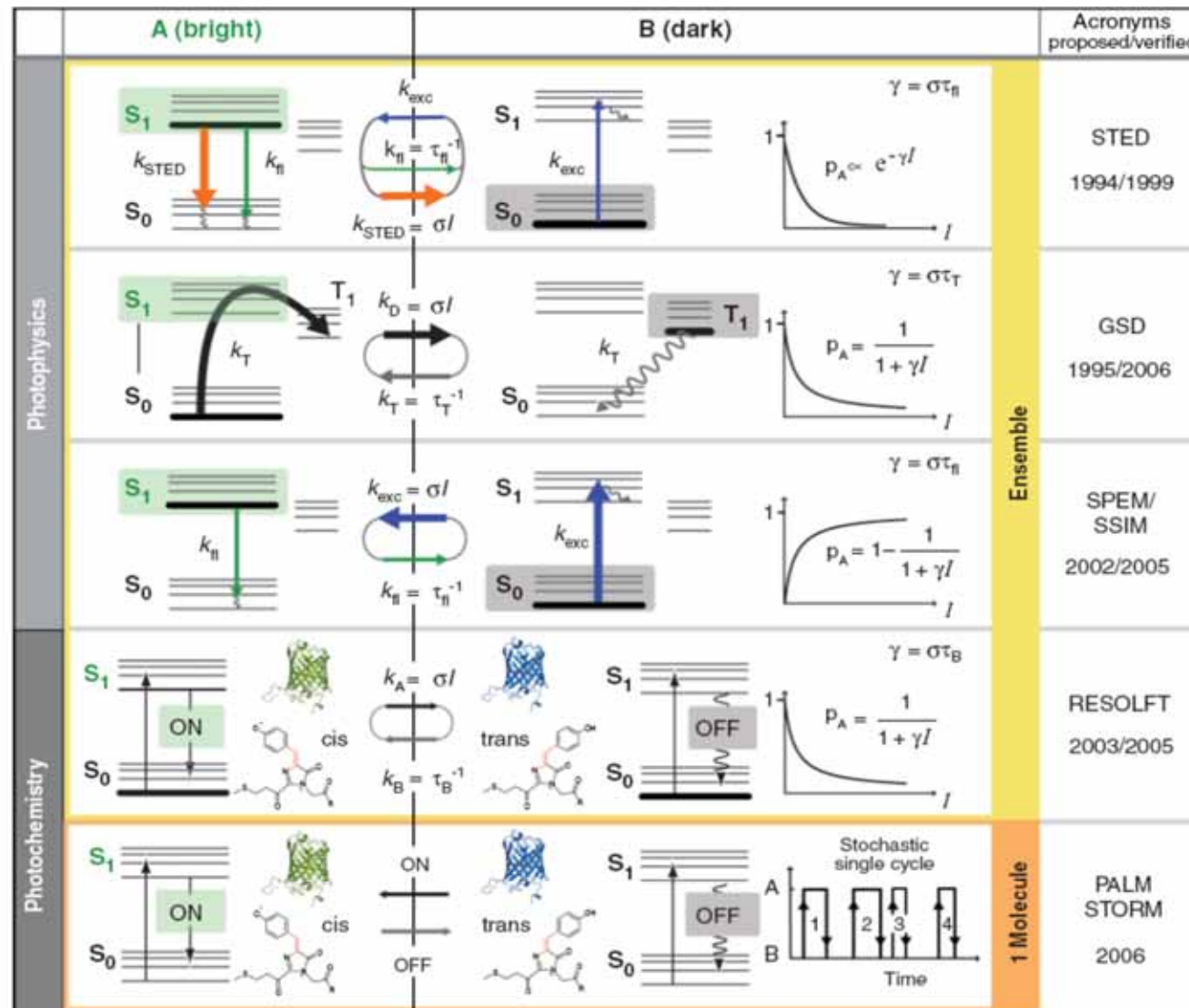


# Super-Resolution Microscopy

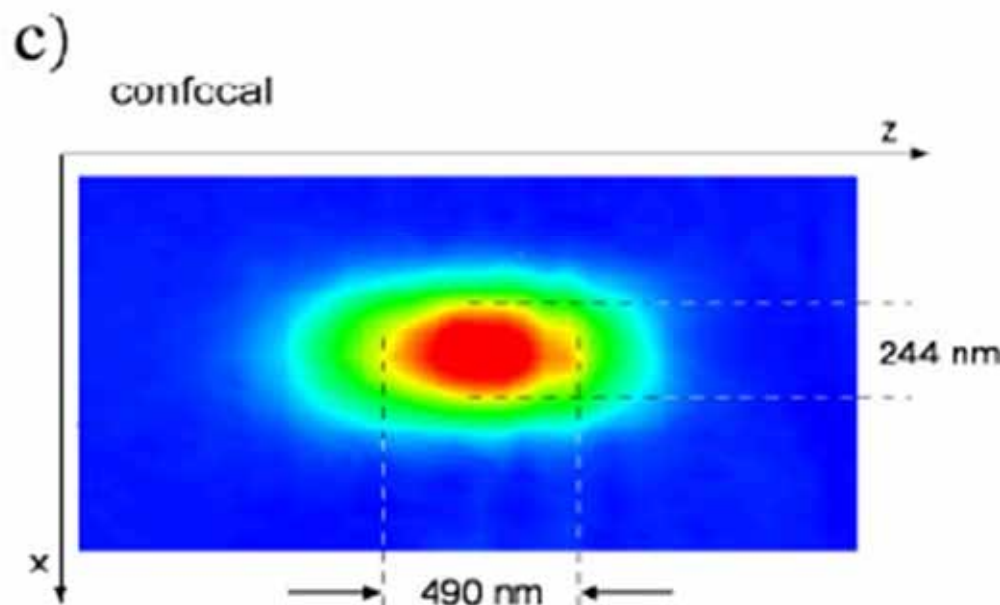
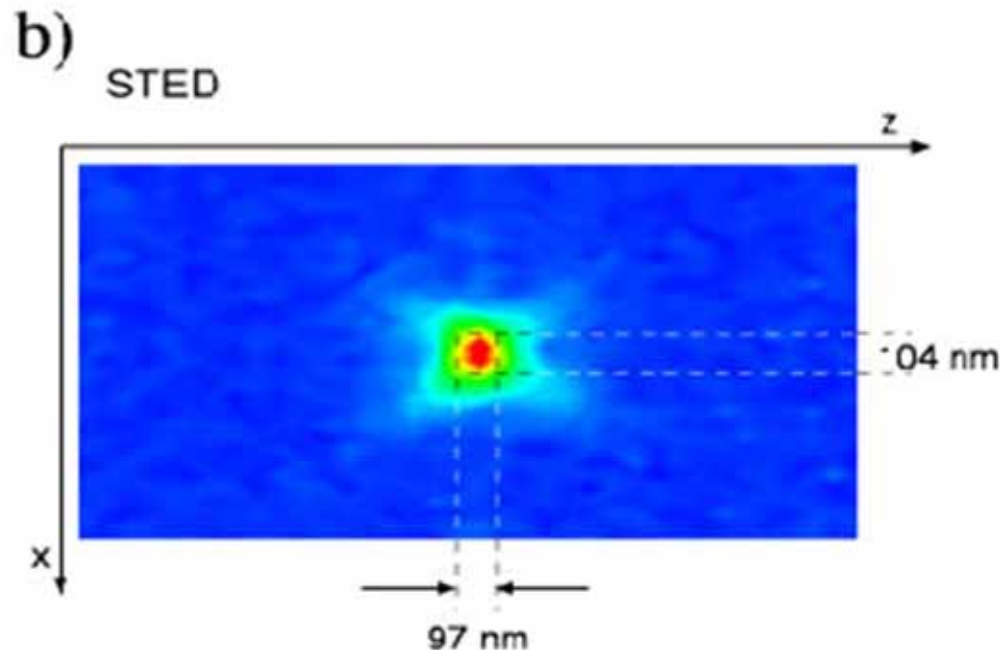
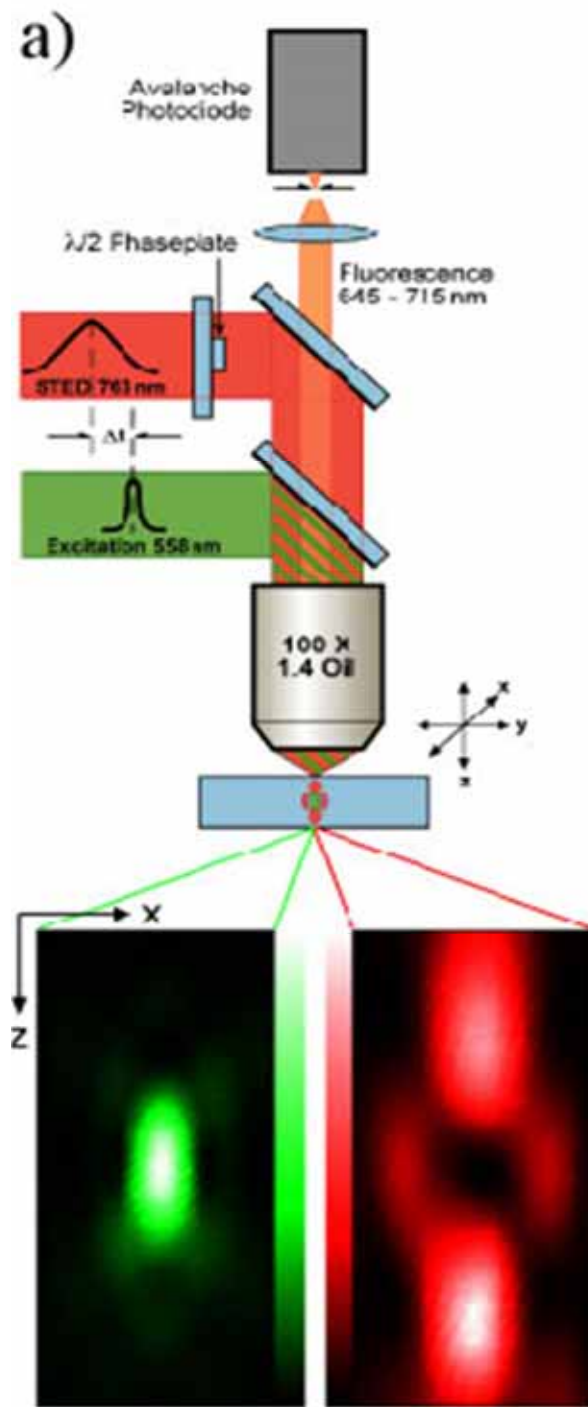


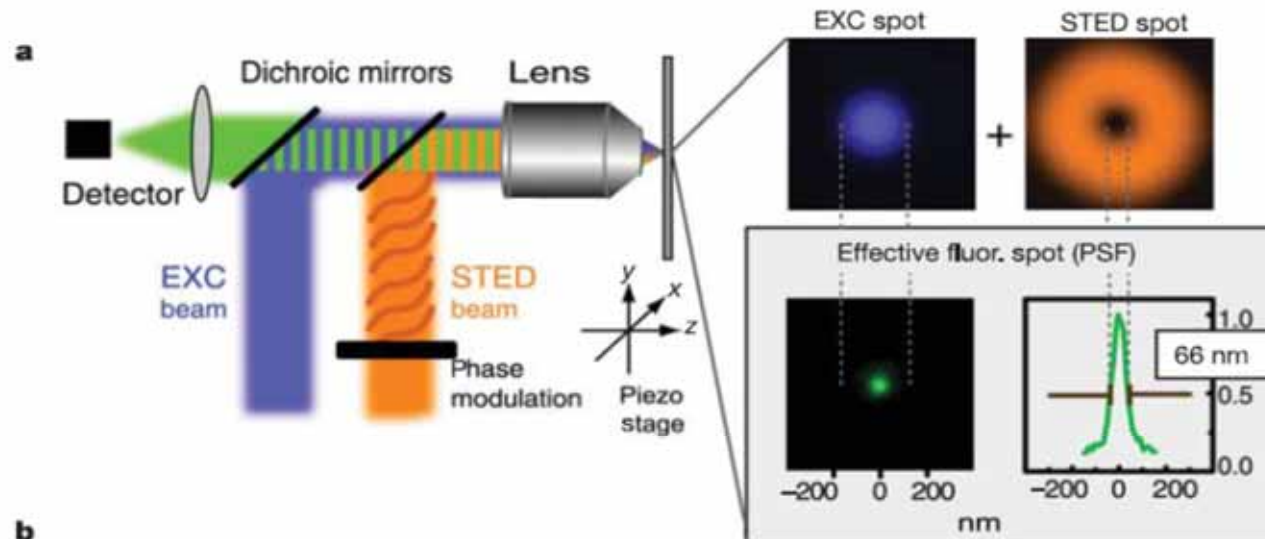
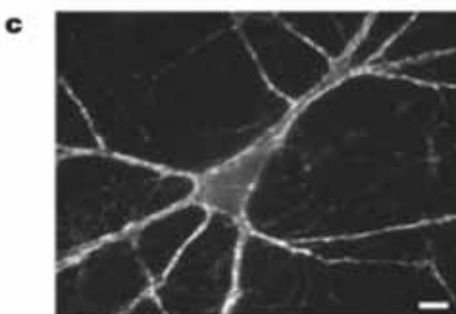
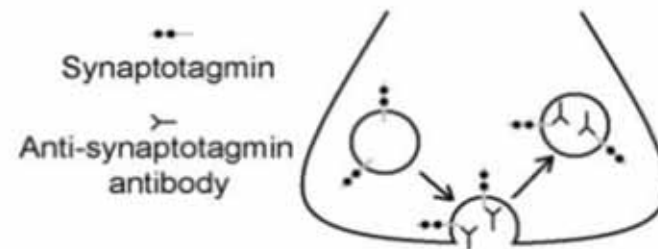
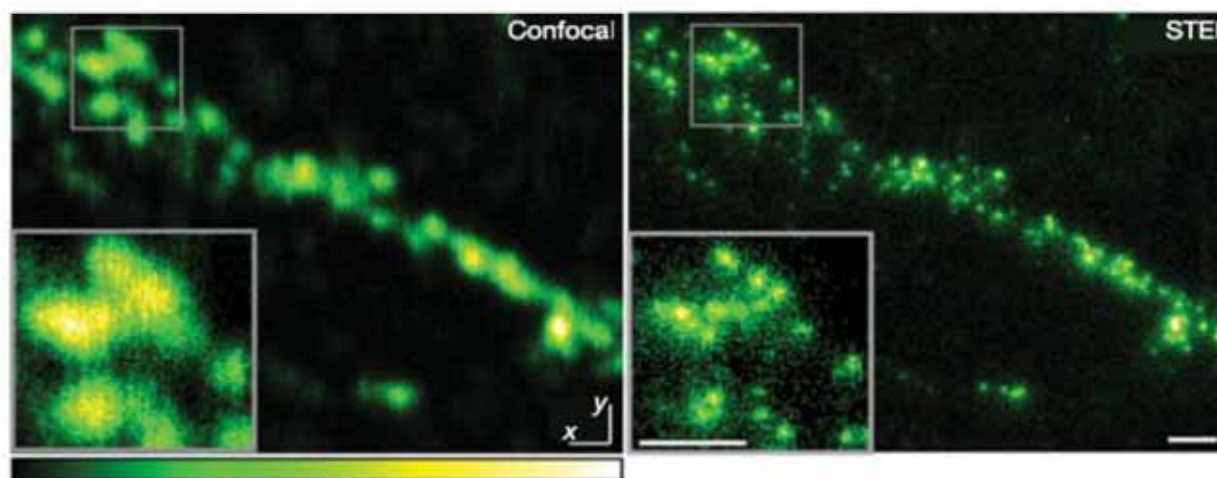


**Fig. 2.** Targeted versus stochastic time-sequential readout of fluorophore markers of a nanostructured object within the diffraction zone whose lower bound is given by  $\lambda/2n$ . A and B denote a bright and a dark state, respectively. In the targeted readout mode, one of the two states (here A) is established at a subdiffraction-sized spot at the position of a zero to read out an unknown number of fluorophore molecules. The image is assembled by deliberate translation of the zero. The zero can also be a groove. In the stochastic readout mode, a single switchable fluorophore from a random position within the diffraction zone is switched to a stable state A, while the other molecules remain in B. The coordinate is calculated from the centroid of the diffraction fluorescence spot measured by a pixelated detector. The coordinate pops up stochastically depending on where the interrogated marker molecule is located.

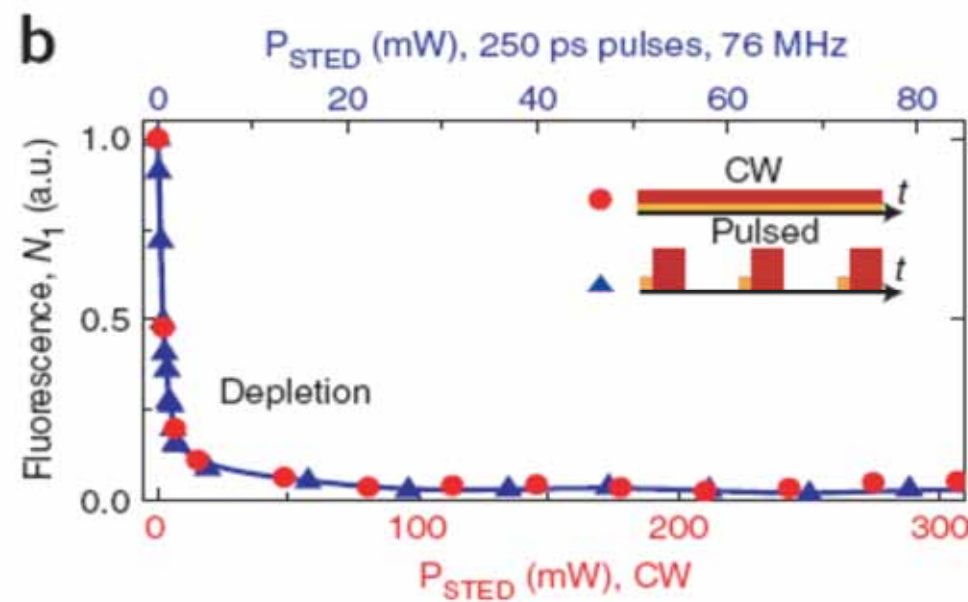
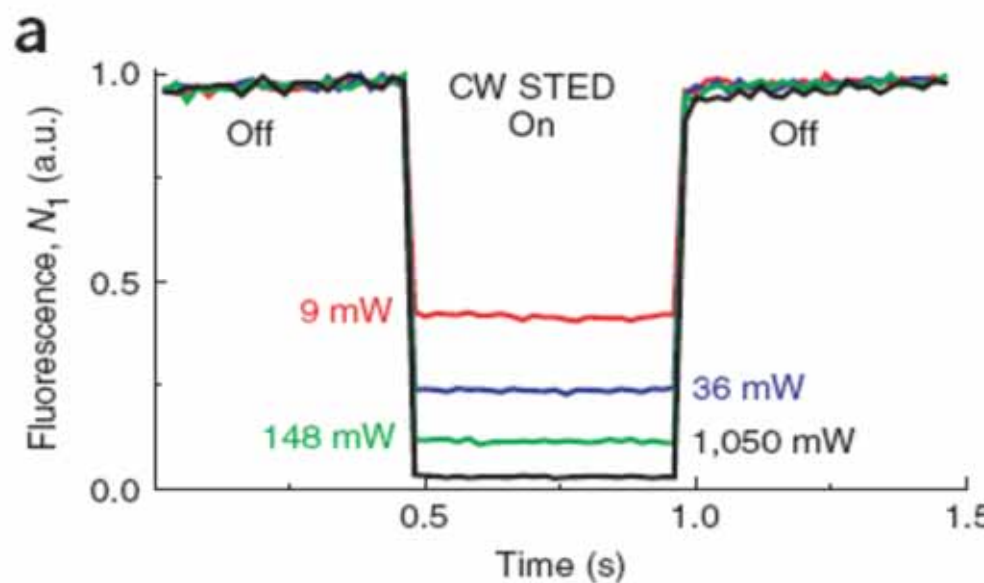


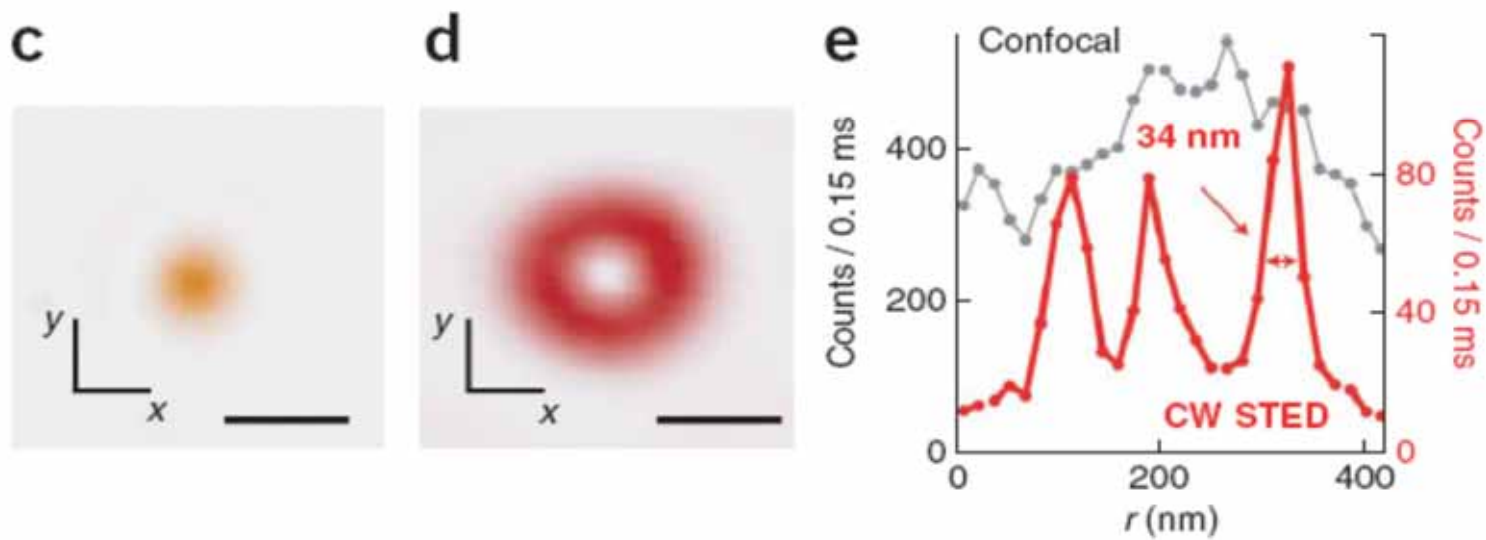
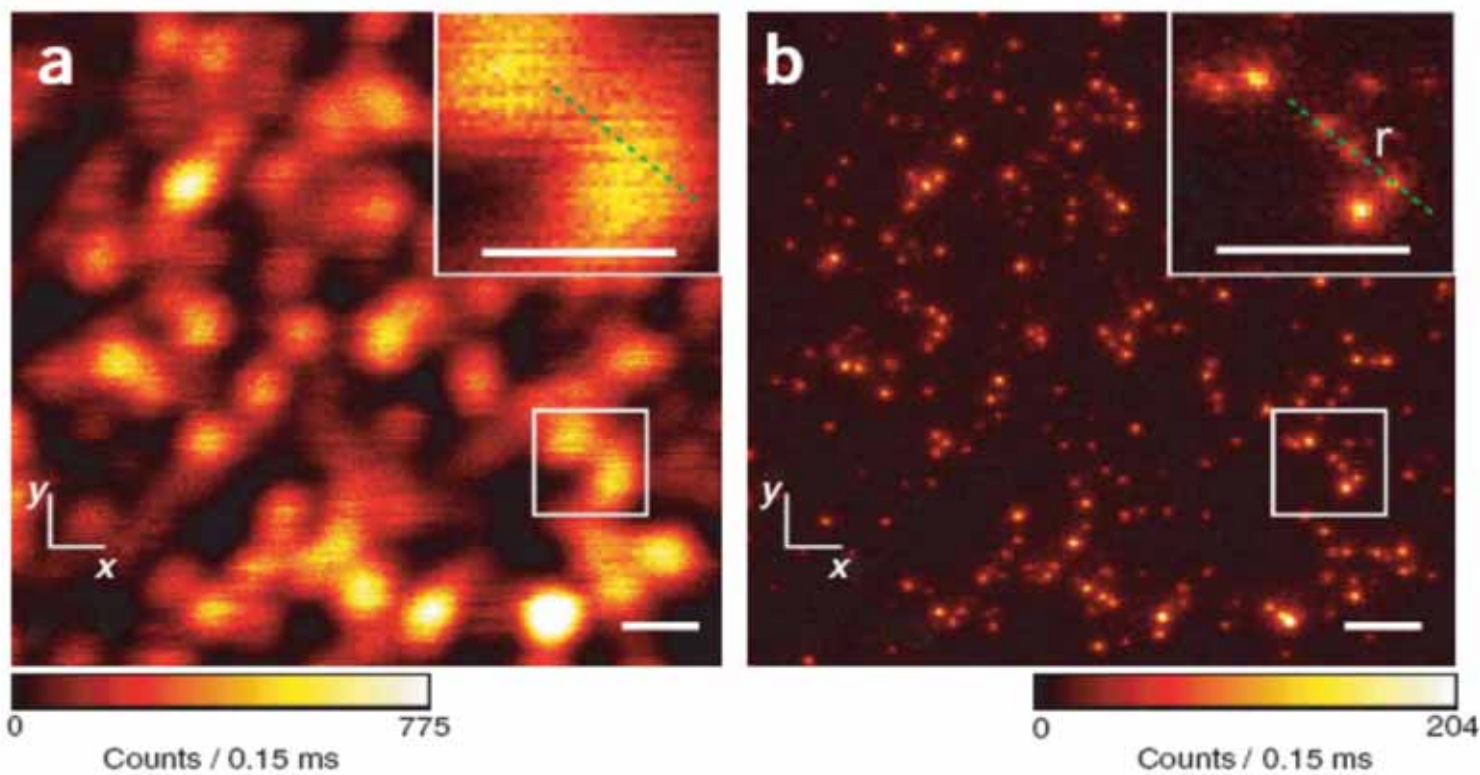
**Fig. 3.** Bright (A) and dark (B) molecular states used to break the diffraction barrier. Whereas STED, GSD, and SPEM utilize photophysical transitions, the photoswitching version of the RESOLFT scheme, as well as PALM and STORM, exploit photochemical transitions in which atoms are relocated or bonds formed and broken. PALM and STORM rely on measuring single (or at least identifiable) molecules at a time, whereas the other concepts, although compatible with single-molecule imaging, principally read out ensembles. Ensemble techniques rely on reversible transitions between A and B, as indicated by the rates  $k$ . The probability  $p_A$  of being in state A depends nonlinearly on the light intensity applied, as indicated by the equations, ensuring that either A or B is confined to a subdiffraction area at a targeted coordinate in space. The  $e^{-\gamma I}$  and the  $(1 + \gamma I)^{-1}$  dependence entail nonlinearities of infinite order ( $\gamma I^m$ ;  $m \rightarrow \infty$ ). By increasing the lifetime of the chosen states,  $\gamma$  strengthens the nonlinear dependence of  $p_A$ , thus enabling huge nonlinearities at low  $I$ . This is radically different from  $m$ -photon processes that, depending on the concomitant action of  $m$  photons and hence just on  $I^m$ , are firmly limited to order  $m$  (15), which in practice is only  $m < 4$ . Because it operates with single molecules in a known state, the probability concept breaks down in PALM and STORM, but reminiscent of nonlinearity is the optical switching.

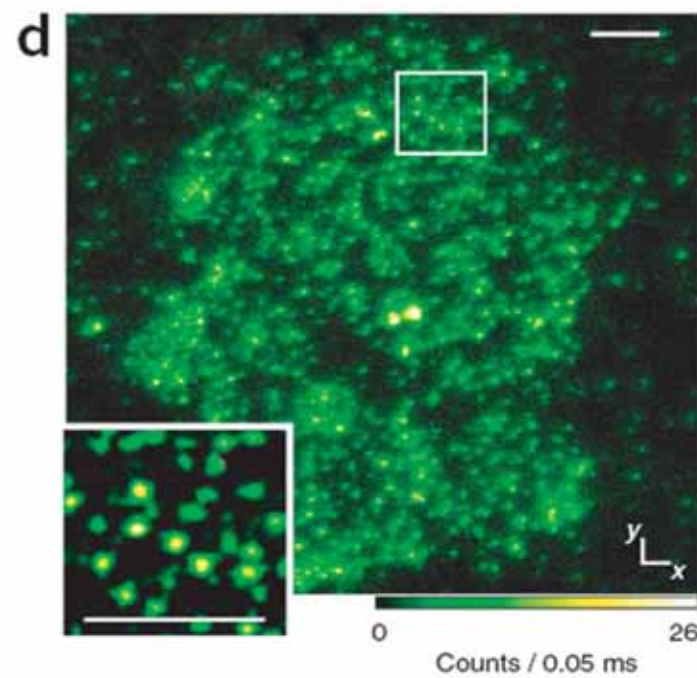
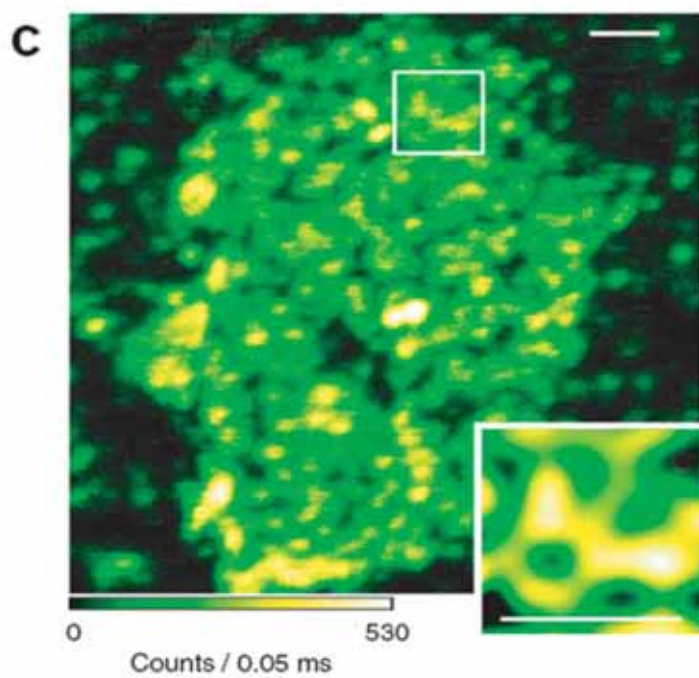
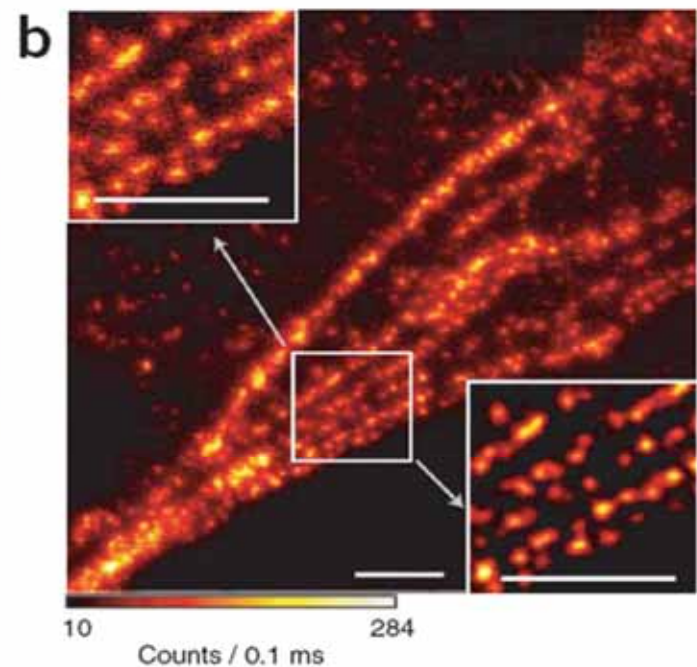
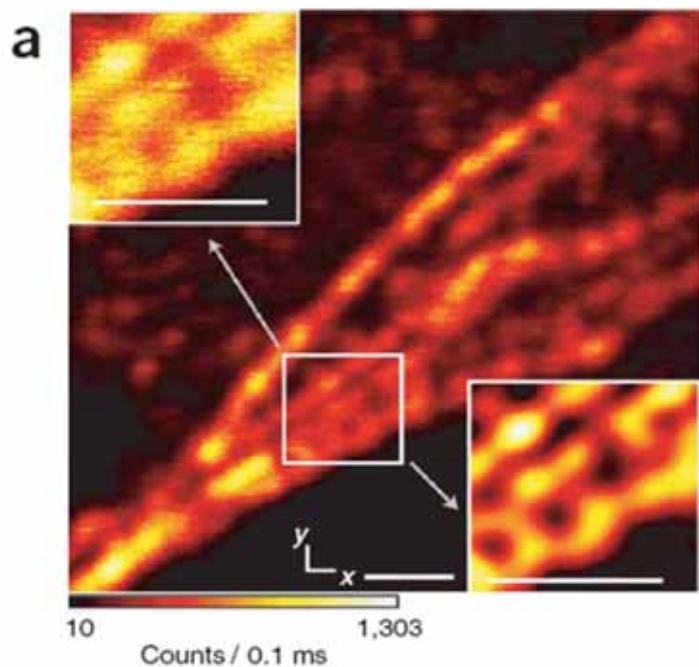


**b****d**

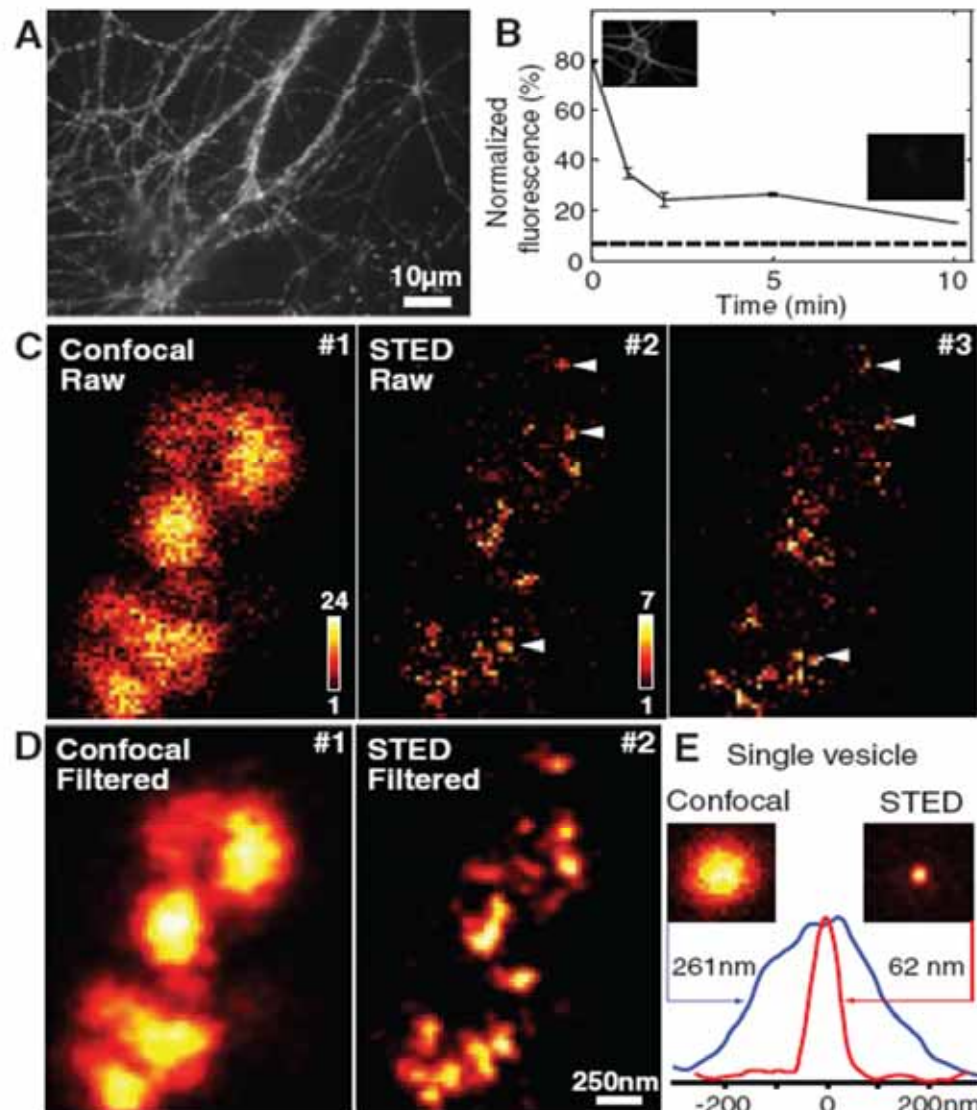
# STED microscopy with continuous wave beams







# Video-Rate Far-Field Optical Nanoscopy Dissects Synaptic Vesicle Movement



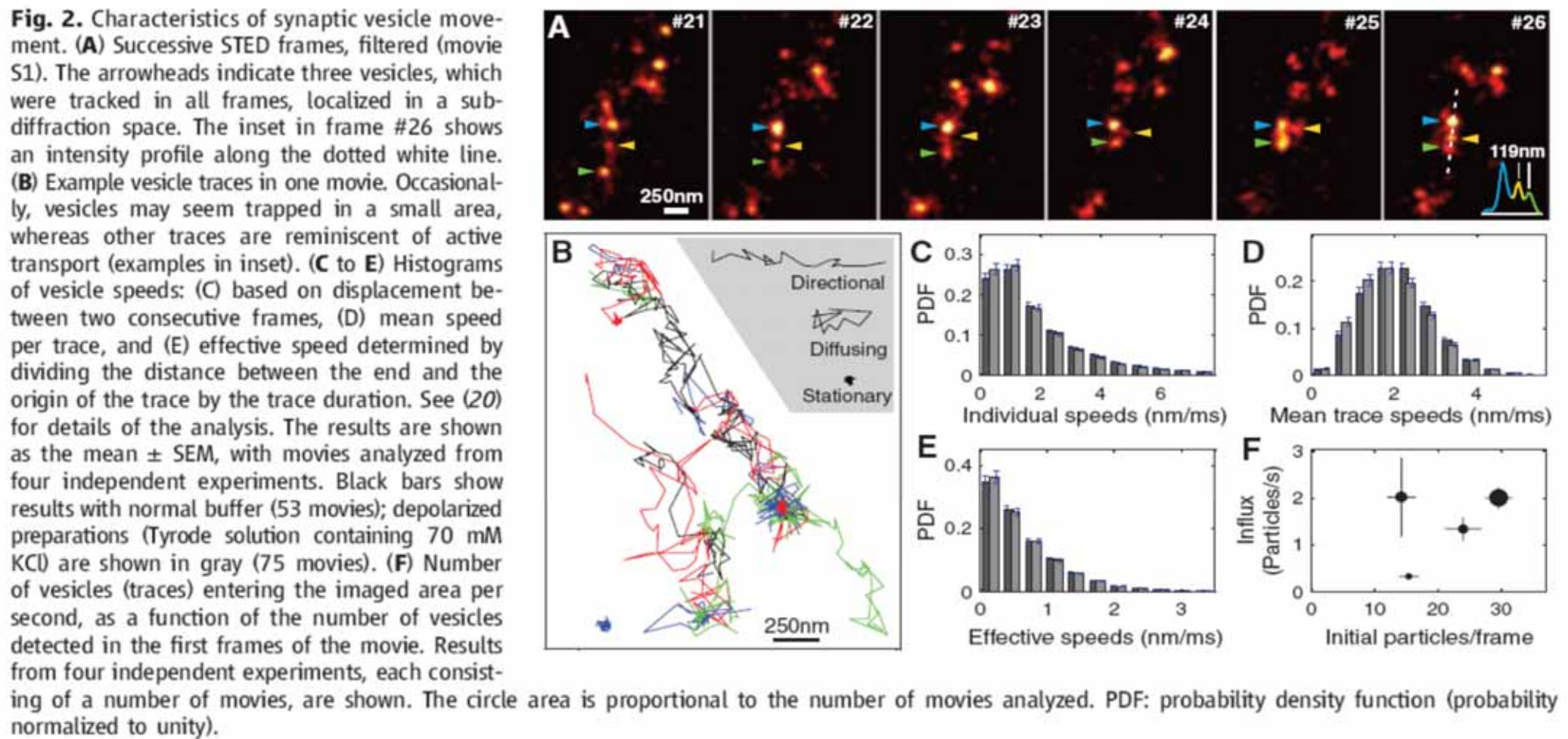
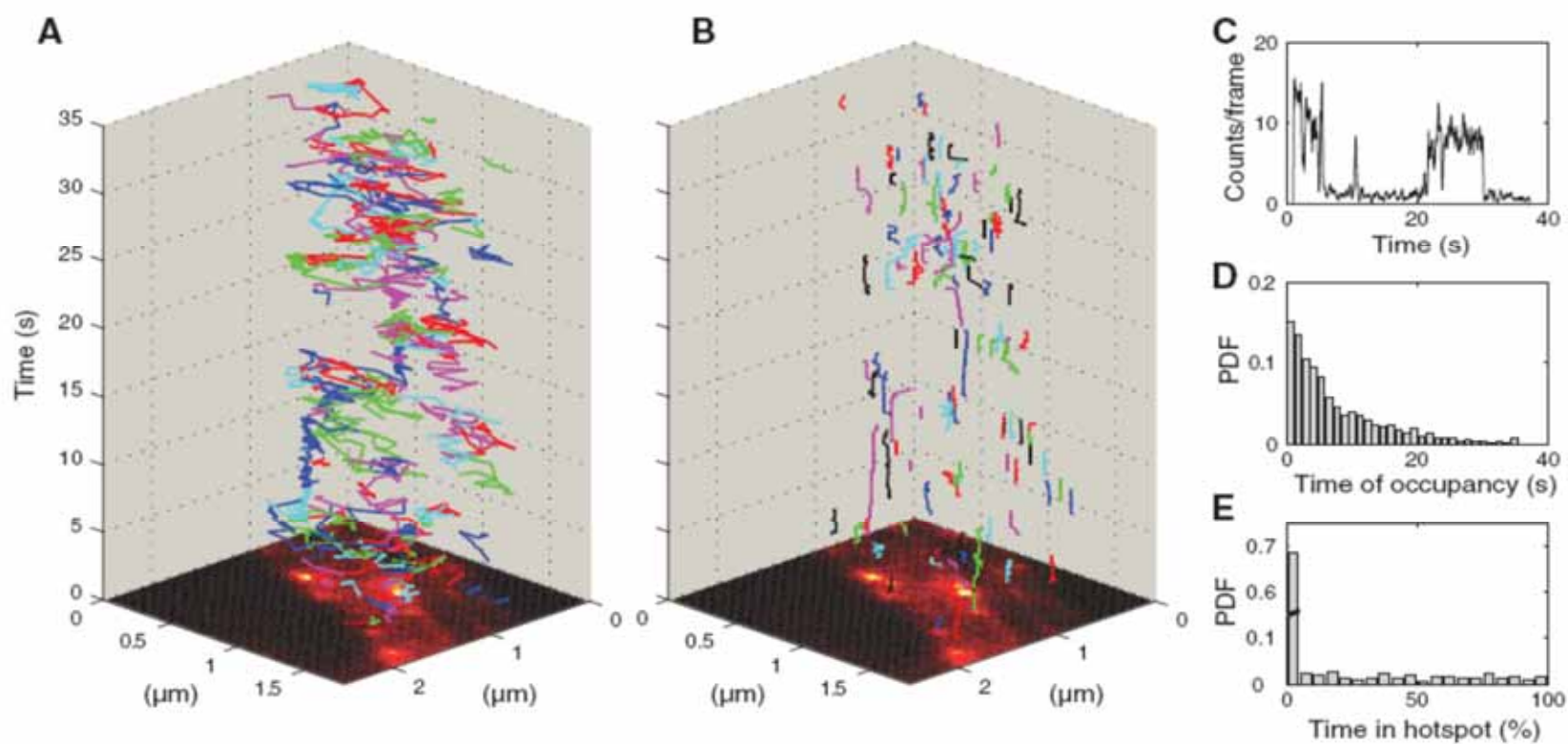
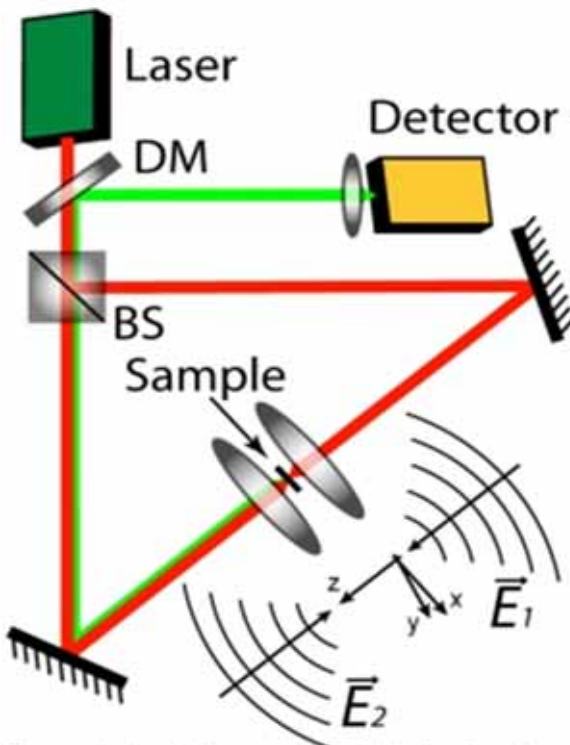


**Fig. 4.** Hot spots of vesicle localization. Comparison between synaptic vesicle traces (A) and hot spot traces (B). Hot spots were defined as pointlike objects appearing in a 50-frame moving average; they indicate small areas where fluorescence occurs over longer times (20). The average image of the complete movie is placed at the bottom. (C) Vesicles can move in and remain trapped in hot spots, as shown here by the strong signal fluctuation in a single hot spot. (D) Probability histogram of the occupancy time of the hot spots (the fraction of time they were filled by vesicles). (E) Histogram of the percentage of time each vesicle spent in a hot spot.

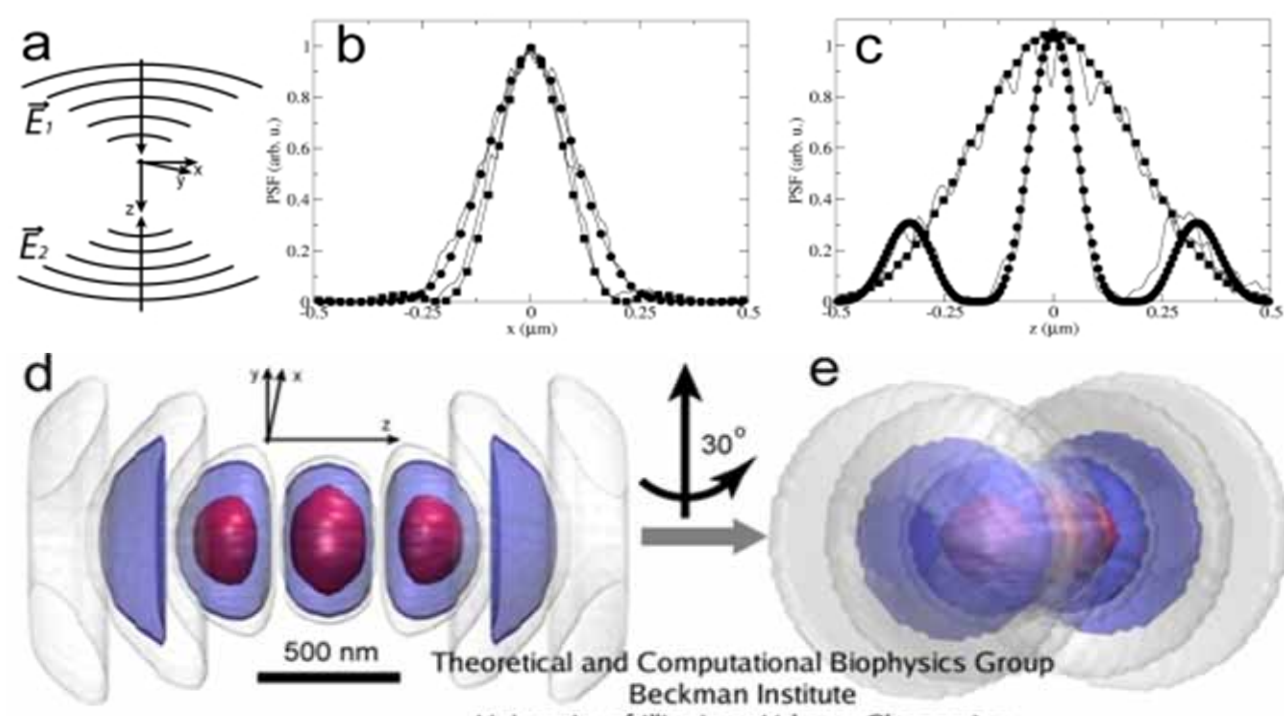


# 4 Pi

Schematic of the 4Pi microscope



Theoretical and Computational Biophysics Group  
Beckman Institute  
University of Illinois at Urbana-Champaign



Theoretical and Computational Biophysics Group  
Beckman Institute  
University of Illinois at Urbana-Champaign

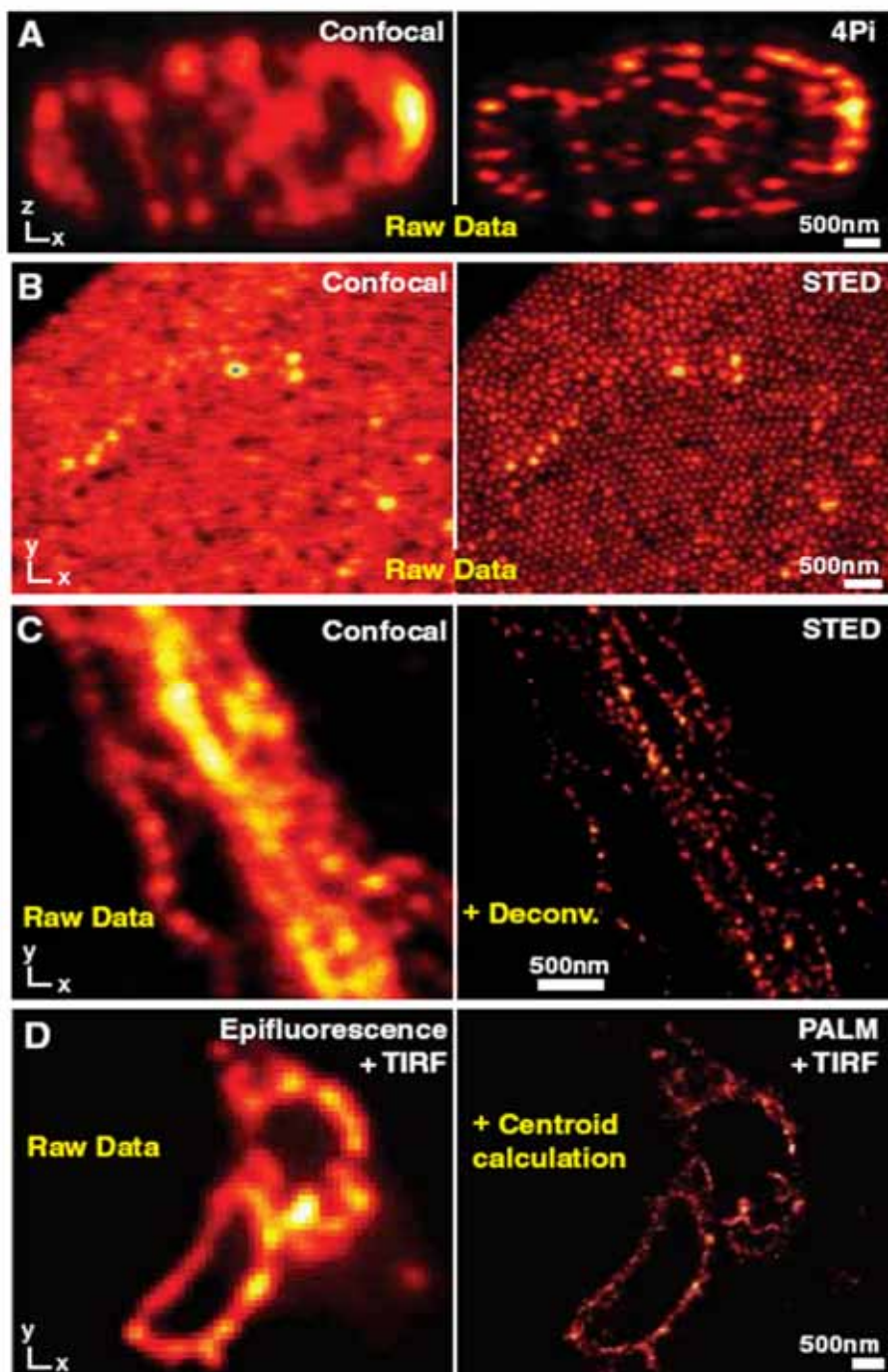
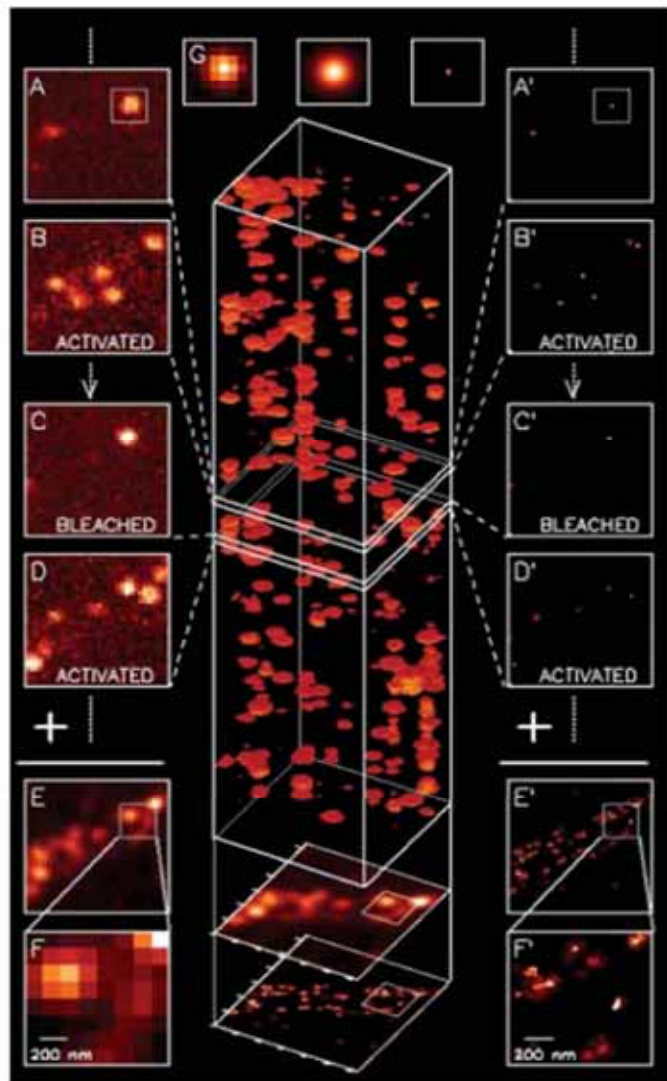


**Fig. 4.** Side-by-side comparisons. **(A)** Confocal versus 4Pi axial (xz) image of microtubules in a neuron: 4Pi image displays 140-nm *z* resolution; lens of  $\alpha = 74^\circ$  and with two-photon excitation at 800 nm. The plain 4Pi image is due to a narrow solitary peak without lobes; mathematical lobe-removal is not required. **(B)** Unlike the confocal reference, the STED image reveals the spatial order of self-assembled fused silica nanobeads containing a fluorescence core (45). **(C)** Neurofilaments in human neuroblastoma recorded in the confocal mode (left) and with STED after nonlinear deconvolution (right) displaying a focal plane resolution of 20 to 30 nm (39). **(D)** Epifluorescence versus PALM recording of a cryoprepared section from a mammalian cell expressing a lysosomal transmembrane protein tagged with a photoswitchable protein; both images were recorded with a TIRF setup. PALM resolution ranges between 20 and 60 nm, whereas individual protein localizations can be 2 nm (12).

# Imaging Intracellular Fluorescent Proteins at Nanometer Resolution



$$(\sigma_{x,y}^2)_m \approx \frac{s^2 + a^2/12}{N_m} + \frac{4\sqrt{\pi}s^3b_m^2}{aN_m^2}$$

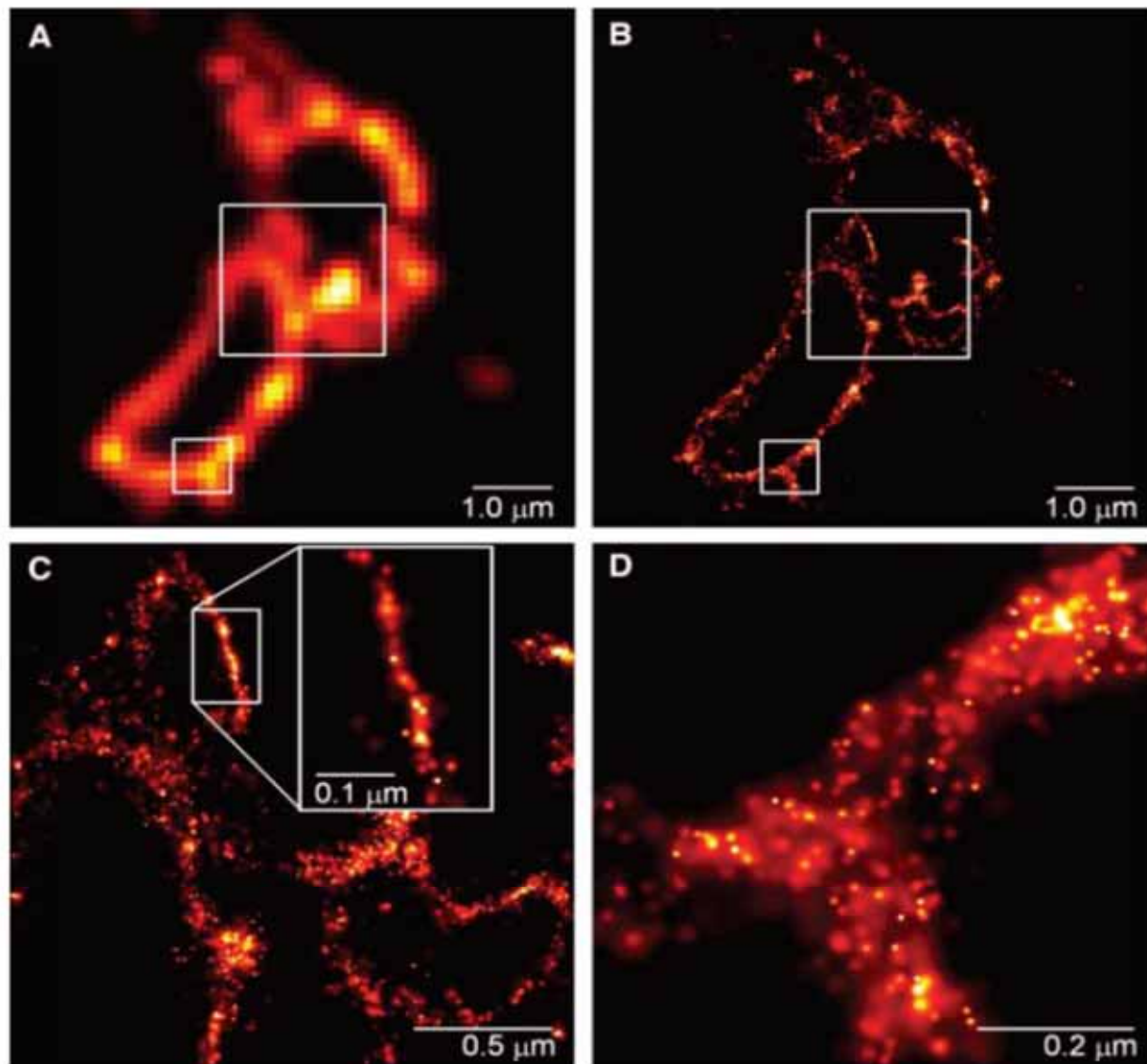


**Fig. 2.** Comparative summed-molecule TIRF (**A**) and PALM (**B**) images of the same region within a cryo-prepared thin section from a COS-7 cell expressing the lysosomal transmembrane protein CD63 tagged with the PA-FP Kaede. The larger boxed region in (**B**), when viewed at higher magnification (**C**) reveals smaller associated membranes that may represent interacting lysosomes or late endosomes that are not resolvable by TIRF. In a region where the section is nearly orthogonal to the lysosomal membrane, the most highly localized molecules fall on a line of width  $\sim 10$  nm (inset). In an obliquely cut region [(**D**), from the smaller boxed region in (**B**)], the distribution of CD63 within the membrane plane can be discerned.

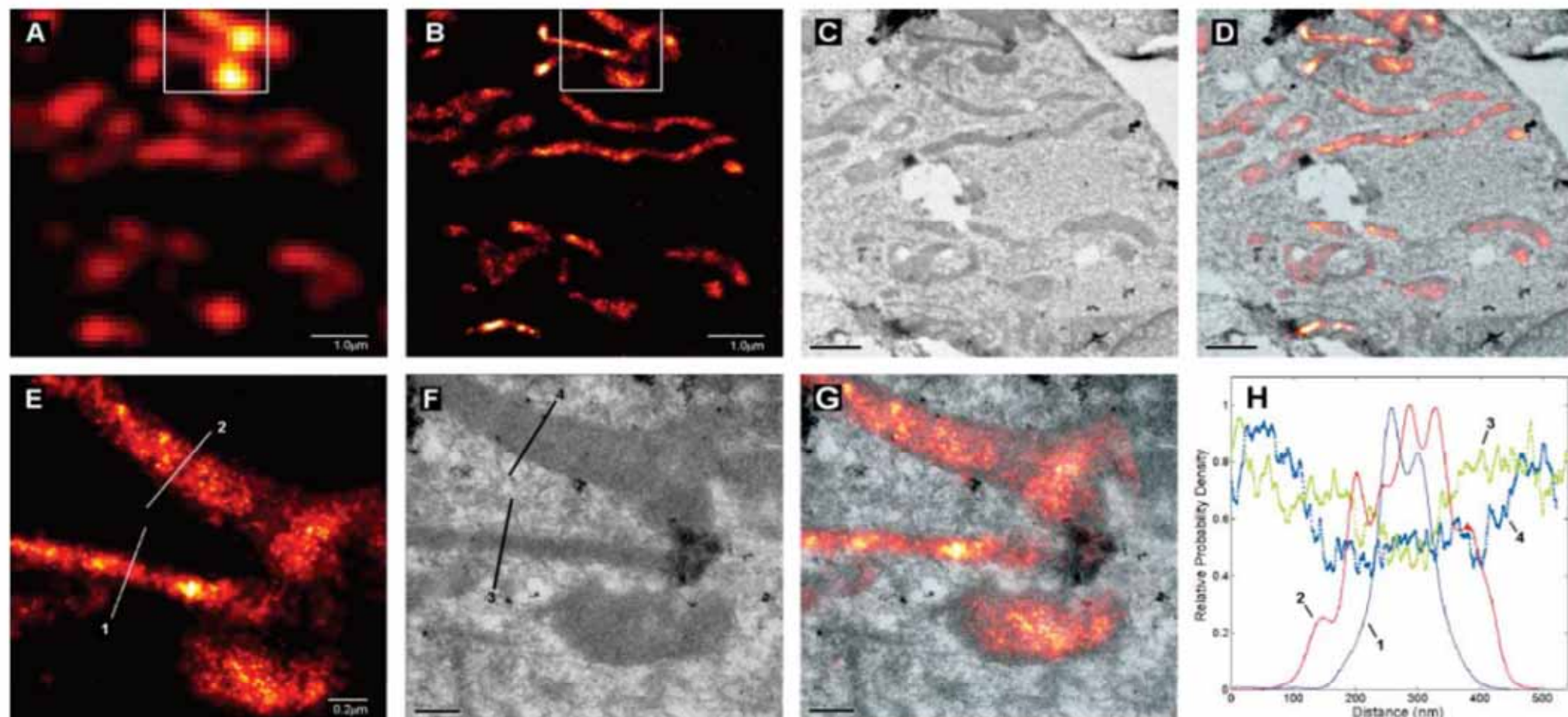


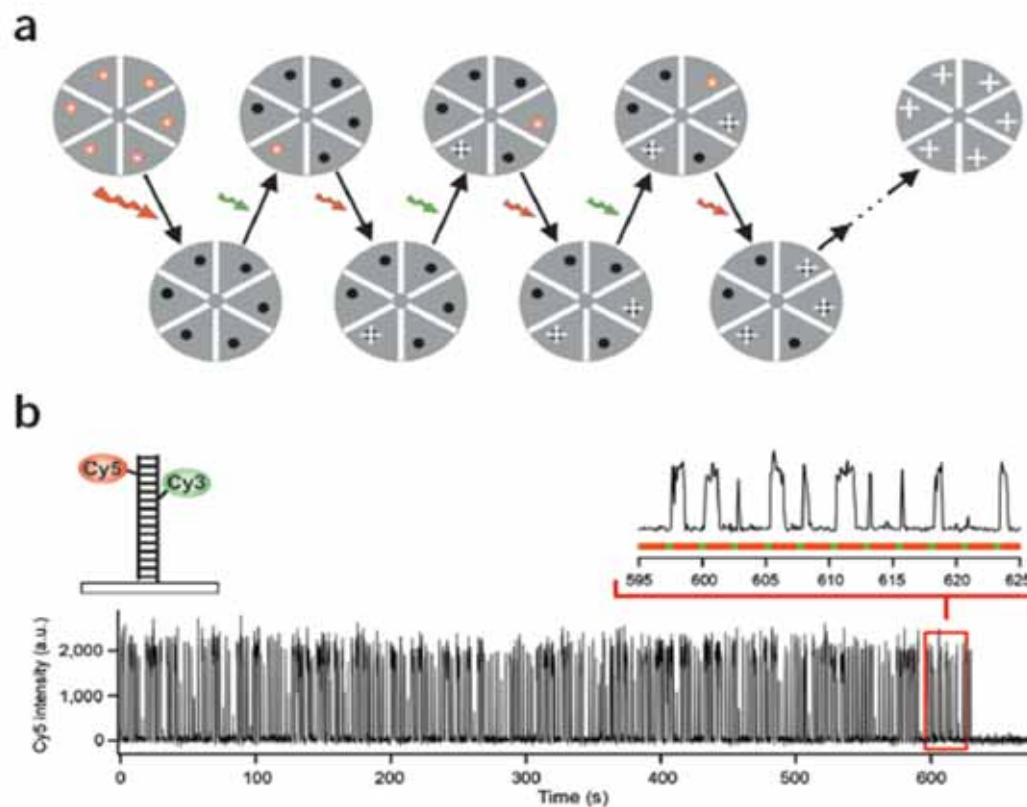
**Fig. 3.** Comparative summed-molecule TIRF (A), PALM (B), TEM (C), and PALM/TEM overlay (D) images of mitochondria in a cryo-prepared thin section from a COS-7 cell expressing dEosFP-tagged cytochrome-C oxidase import sequence. Higher magnification PALM (E), TEM (F), and overlay (G) images within the box in (B) reveal that these matrix re-

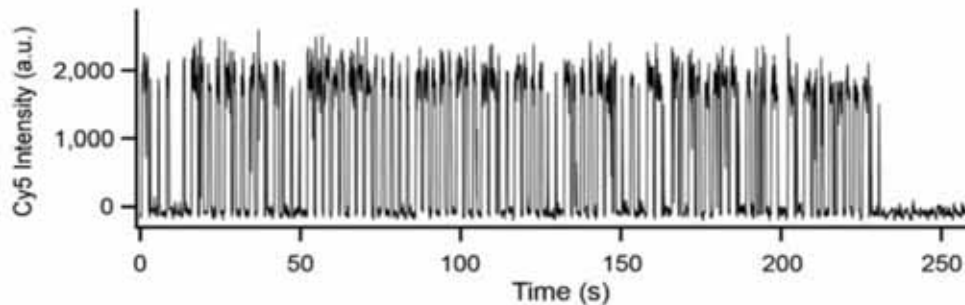
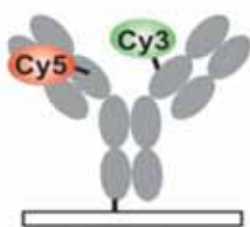
porter molecules extend up to, but not into, the ~20-nm outer mitochondrial membrane. The molecular distribution across two mitochondria along lines 1 and 2 in PALM image (E) are compared in (H) to the TEM signal along lines 3 and 4 in (F) across the same mitochondria. Scale bars: 1.0  $\mu$ m in (A) to (D); 0.2  $\mu$ m in (E) to (G).

# Sub-diffraction-limit imaging by stochastic optical reconstruction microscopy (STORM)

Michael J Rust<sup>1,5</sup>, Mark Bates<sup>2,5</sup> & Xiaowei Zhuang<sup>1,3,4</sup>

NATURE METHODS





• 2.2 : 1 for Cy3 and 0.1 : 1 for Cy5

Goat anti-mouse secondary antibody labeled with the cyanine switch exhibits photoswitching behavior similar to switch-labeled DNA. The antibody was labeled with Cy3 and Cy5 (as described in **Supplementary Methods** online) and bound to a quartz slide coated with unlabeled mouse anti-transferrin primary antibody. The trace shows the Cy5 fluorescence intensity detected from a single labeled antibody as it switches on and off until permanent photobleaching occurs after 230 seconds. A red laser (633 nm, 30 W/cm<sup>2</sup>) is used to excite fluorescence from Cy5 and to switch Cy5 to the dark state. A green laser (532 nm, 1 W/cm<sup>2</sup>) is used to switch the Cy5 back to the fluorescent state. The sample was excited with a sequence of alternating green and red laser pulses (0.5 s green followed by 2 s red).

$$I(x, y) = A + I_0 e^{[-(x'/a)^2 - (y'/b)^2]/2}$$

$$\begin{aligned}x' &= (x - x_0) \cos \theta - (y - y_0) \sin \theta \\y' &= (x - x_0) \sin \theta + (y - y_0) \cos \theta\end{aligned}$$

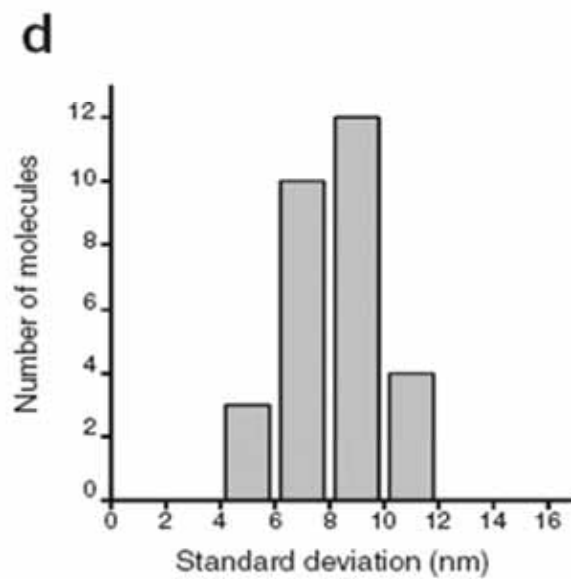
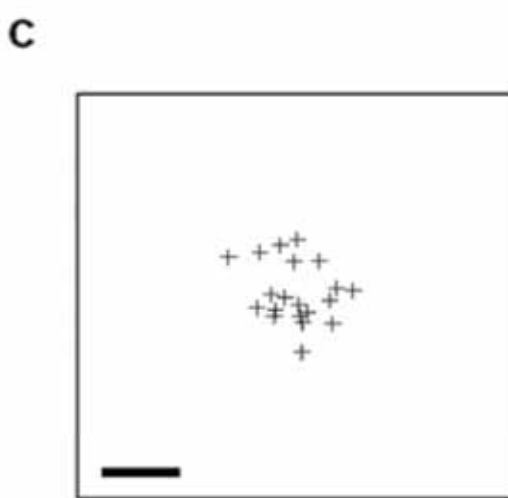
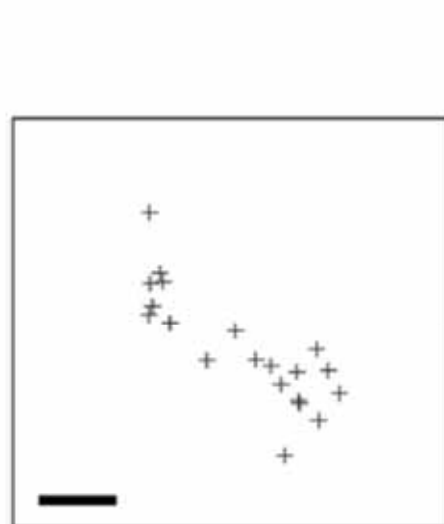
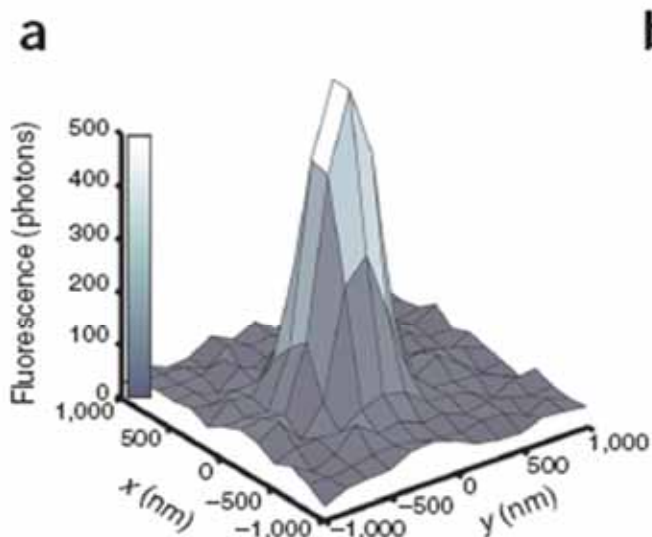


**Figure 2 |** The high localization accuracy of individual switches during each switching cycle defines the intrinsic resolution of STORM. (a) The point spread function (PSF) of the emission from a single switch on DNA during a single switching cycle. Fitting the PSF to a two-dimensional Gaussian (not shown) gives the centroid position of the PSF. (b,c) The centroid positions of an individual switch determined in 20 successive imaging cycles before (b) and after (c) correction for sample drift. Scale bars, 20 nm. (d) A histogram of the standard deviation of centroid positions. The standard deviation is determined as  $(\sigma_x + \sigma_y) / 2$  for each switch using 20 imaging cycles, where  $\sigma_x$  and  $\sigma_y$  are the standard deviations of the centroid positions in the  $x$  and  $y$  dimensions. This histogram was constructed from 29 switches.

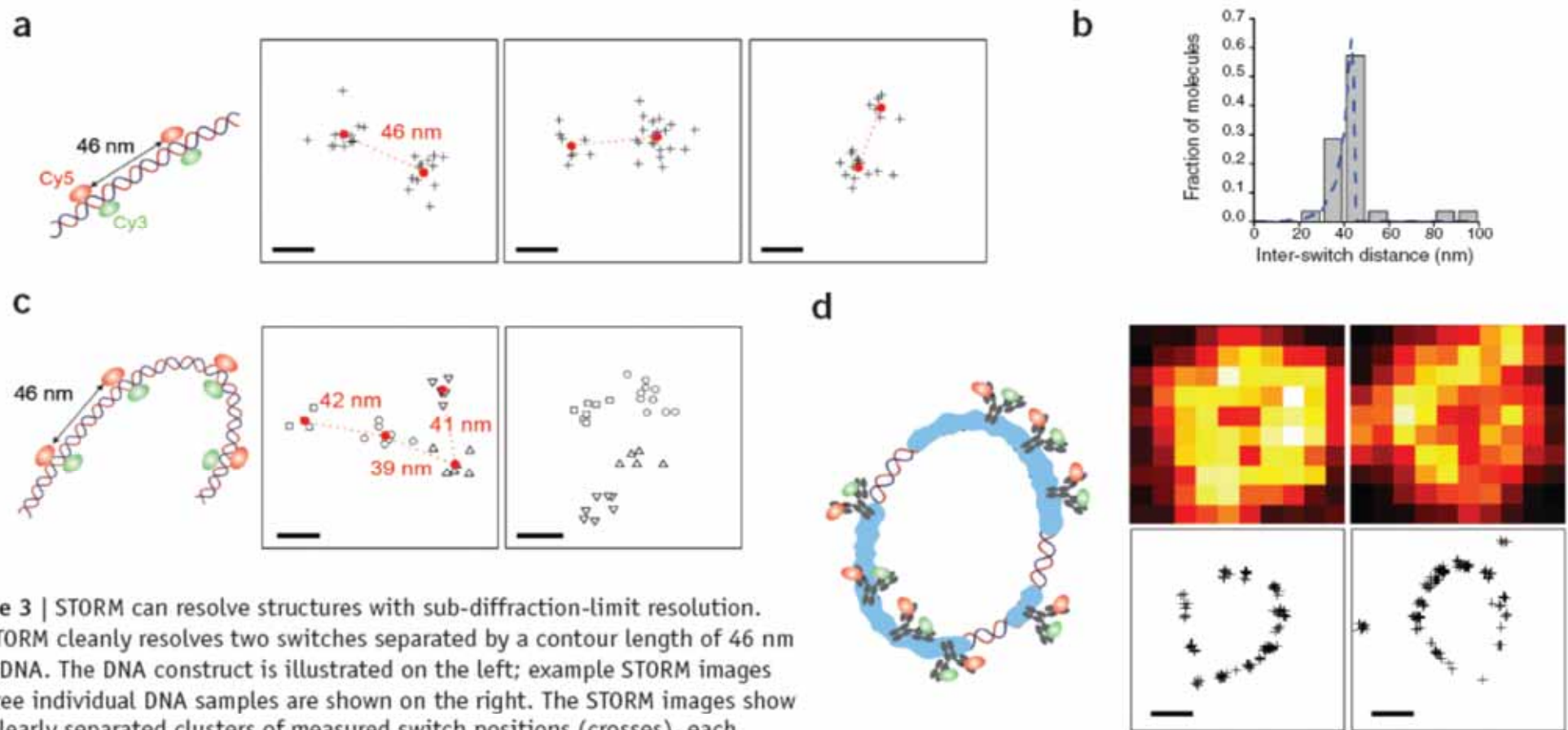


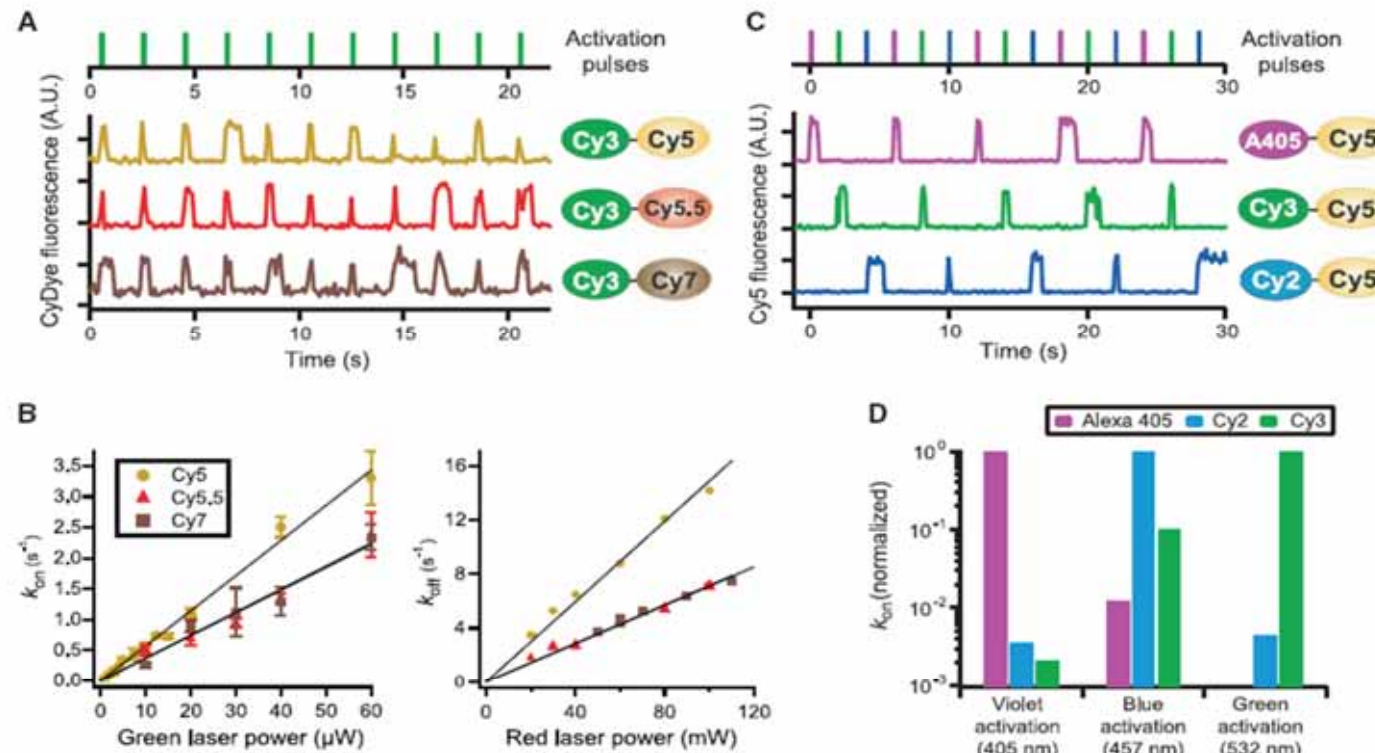
**Figure 3 |** STORM can resolve structures with sub-diffraction-limit resolution.

(a) STORM cleanly resolves two switches separated by a contour length of 46 nm on dsDNA. The DNA construct is illustrated on the left; example STORM images of three individual DNA samples are shown on the right. The STORM images show two clearly separated clusters of measured switch positions (crosses), each corresponding to a single switch. The center-of-mass position of each cluster is marked by a red dot. The inter-switch distances are 46 nm, 44 nm and 34 nm for these three examples. Scale bars, 20 nm. (b) Comparison between the inter-switch distances measured using STORM (columns) and the predicted distance distribution considering the flexibility of DNA (dashed line). (c) STORM images of four switches attached to a dsDNA, pair-wise separated by a contour length of 46 nm. The measured switch positions are clustered by an automated algorithm and different clusters are indicated by different symbols. Scale bars, 20 nm. (d) STORM images of RecA-coated circular plasmid DNA. Indirect immunofluorescence images with switch-labeled secondary antibody taken by a total internal reflection microscope (top); the reconstructed STORM images of the same filaments (bottom). Scale bars, 300 nm.

# Multicolor Super-Resolution Imaging with Photo-Switchable Fluorescent Probes

SCIENCE VOL 317 21 SEPTEMBER 2007

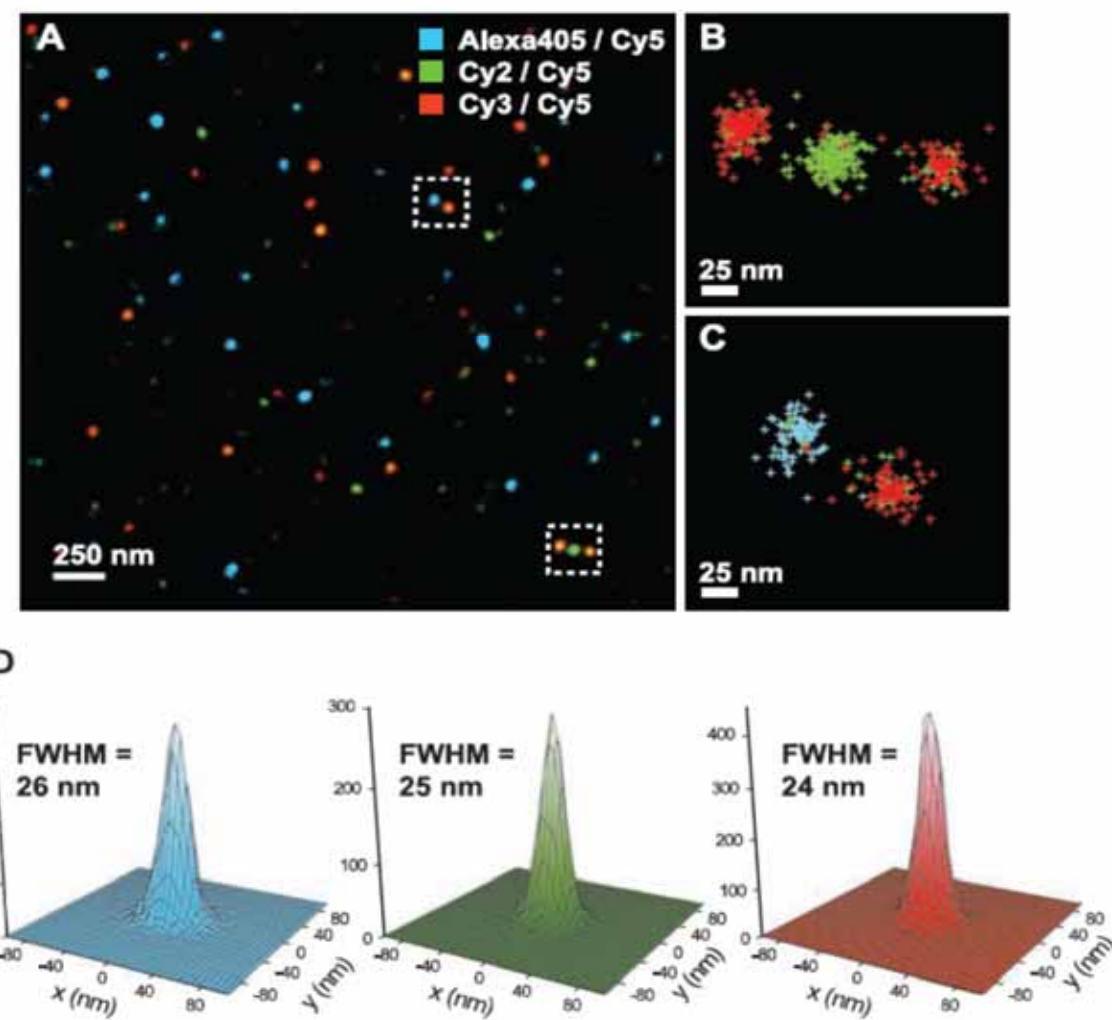
**Fig. 1.** Photo-switchable probes constructed from activator-reporter pairs. (A) Spectrally distinct reporters exhibit photo-switching behavior. The lower panel shows the fluorescence time traces of three photo-switchable reporters Cy5 (dark yellow line), Cy5.5 (red line), and Cy7 (brown line), each paired with a Cy3 dye as the activator on a DNA construct. The upper panel shows the green laser pulses (532 nm) used to activate the reporters. The red laser (657 nm) was continuously on, serving to excite fluorescence from the reporters and to switch them to the dark state. Traces were shifted relative to each other for clarity. (B) Switching rate constants  $k_{on}$  and  $k_{off}$  of the Cy3-Cy5, Cy3-Cy5.5, and Cy3-Cy7 pairs as a function of green and red laser power. Error bars indicate SEM from about three data sets. The laser power to intensity calibration may vary between different samples because of moderate differences in the laser spot size at the sample. (C) The same reporter can be activated by spectrally distinct activators. The lower panel shows the fluorescence time traces of Cy5 paired with three different activators, Alexa 405 (magenta line), Cy2 (blue line), and Cy3 (green line). The upper panel shows the violet (405 nm, magenta line), blue (457 nm, blue line), and green (532 nm, green line) activation pulses. (D)



indicate SEM from about three data sets. The laser power to intensity calibration may vary between different samples because of moderate differences in the laser spot size at the sample. (C) The same reporter can be activated by spectrally distinct activators. The lower panel shows the fluorescence time traces of Cy5 paired with three different activators, Alexa 405 (magenta line), Cy2 (blue line), and Cy3 (green line). The upper panel shows the violet (405 nm, magenta line), blue (457 nm, blue line), and green (532 nm, green line) activation pulses. (D)

Normalized activation rate constants of the three dye pairs at three activation wavelengths: 405, 457, and 532 nm. The  $k_{on}$  values of Alexa 405-Cy5, Cy2-Cy5, and Cy3-Cy5 were used for normalization at 405, 457, and 532 nm, respectively. The absolute activation rates were rapid for each pair at its corresponding optimal wavelength, with values of  $10 \text{ s}^{-1}$  or greater at only a few hundred  $\mu\text{W}$  of laser power. The activation rate of the Alexa 405-Cy5 pair by the 532-nm laser was too small to be measured reliably.

**Fig. 2.** Three-color STORM imaging of a model DNA sample. **(A)** Three-color STORM image of three different DNA constructs labeled with Alexa 405-Cy5, Cy2-Cy5, or Cy3-Cy5 mixed at a high surface density on a microscope slide. The image was plotted by rendering each localization as a Gaussian peak, the width of which was scaled with the theoretical localization accuracy given by the number of photons detected (26). Each colored spot in this image represents a cluster of localizations from a single DNA molecule. A conventional fluorescence image of the same area is shown in fig. S3 for comparison. **(B and C)** Higher-magnification views of the boxed regions in (A) show several examples of closely spaced DNA molecules. Each localization was plotted as a cross, colored according to the following code: If the molecule was activated by a 405-, 457-, or 532-nm laser pulse, the color of the cross was assigned as blue, green, or red, respectively. **(D)** The localization distributions of the blue, green, or red clusters. The two-dimensional histograms of localizations were generated by aligning multiple (50 to 60) clusters by their center of mass. The histograms were fit to a Gaussian profile to determine their FWHM.



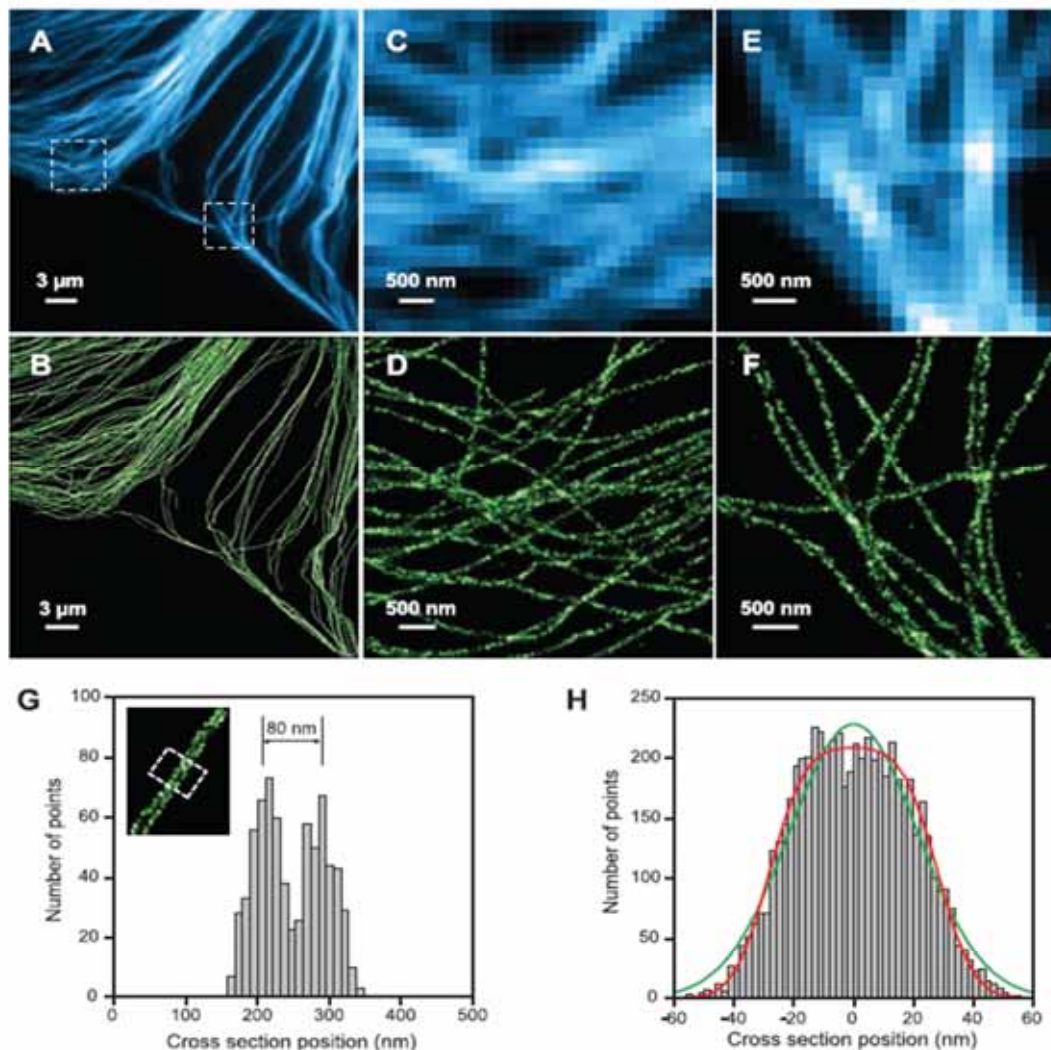


**Fig. 3.** STORM imaging of microtubules in a mammalian cell. **(A)** Conventional immunofluorescence image of microtubules in a large area of a BS-C-1 cell. **(B)** STORM image of the same area. **(C and E)** Conventional and **(D and F)** STORM images corresponding to the boxed regions in **(A)**. **(G)** Cross-sectional profiles of two nearby microtubule filaments in the cell. The inset shows the STORM image, and the histogram shows the cross-sectional distribution of localizations within the small regions specified by the white box. **(H)** Cross-sectional profile of a microtubule segment determined from the STORM image. A relatively long segment ( $\sim 7 \mu\text{m}$ ) was chosen to obtain good statistics. The histogram shows the cross-sectional distribution of localizations. The green line is a single Gaussian fit with  $\text{FWHM} = 51 \text{ nm}$ . The red line shows the fit obtained by convolving a rectangular function of width =  $d$  with a Gaussian function of  $\text{FWHM} = r$ . The fit yields  $d = 56 \text{ nm}$  and  $r = 22 \text{ nm}$ , corresponding to the antibody-coated microtubule width and the imaging resolution, respectively.

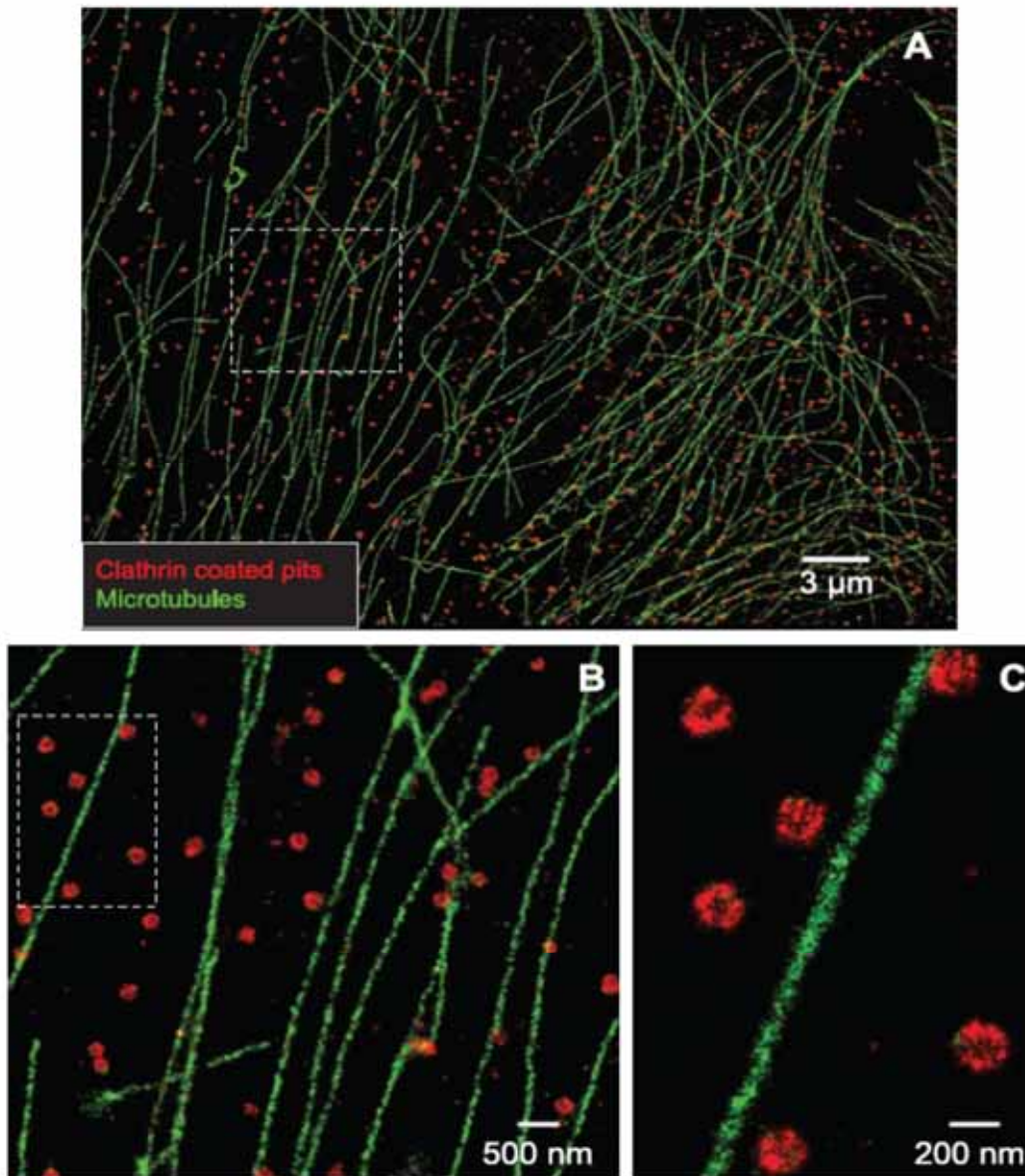
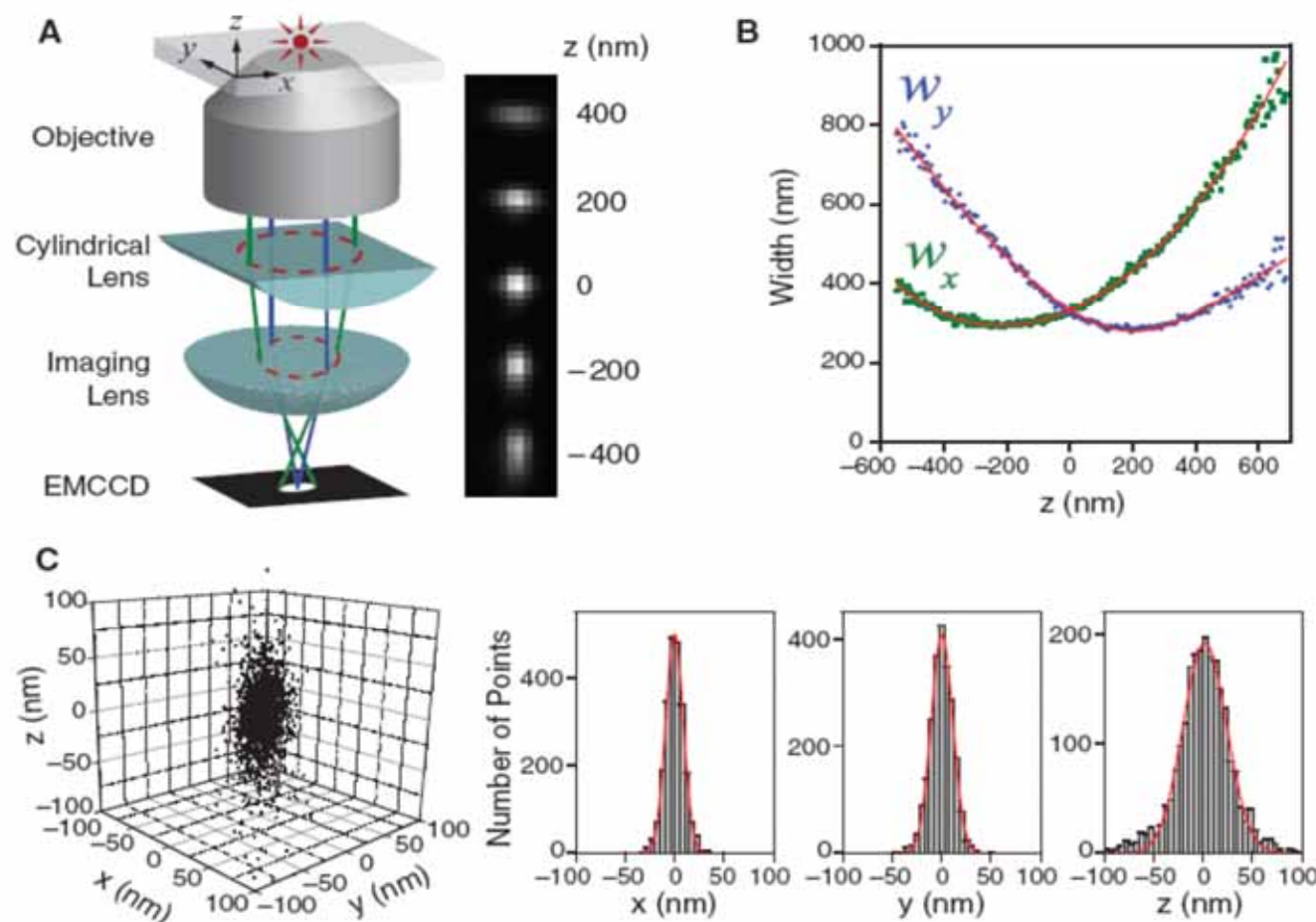


**Fig. 4.** Two-color STORM imaging of microtubules and CCPs in a mammalian cell. **(A)** STORM image of a large area of a BS-C-1 cell. The secondary antibodies used for microtubule staining were labeled with Cy2 and Alexa 647, and those for clathrin were labeled with Cy3 and Alexa 647. The 457- and 532-nm laser pulses were used to selectively activate the two pairs. Each localization was false colored according to the following code: green for 457-nm activation and red for 532-nm activation. **(B)** STORM image corresponding to the boxed region in (A) shown at a higher magnification. **(C)** Further magnified view of the boxed region in (B).

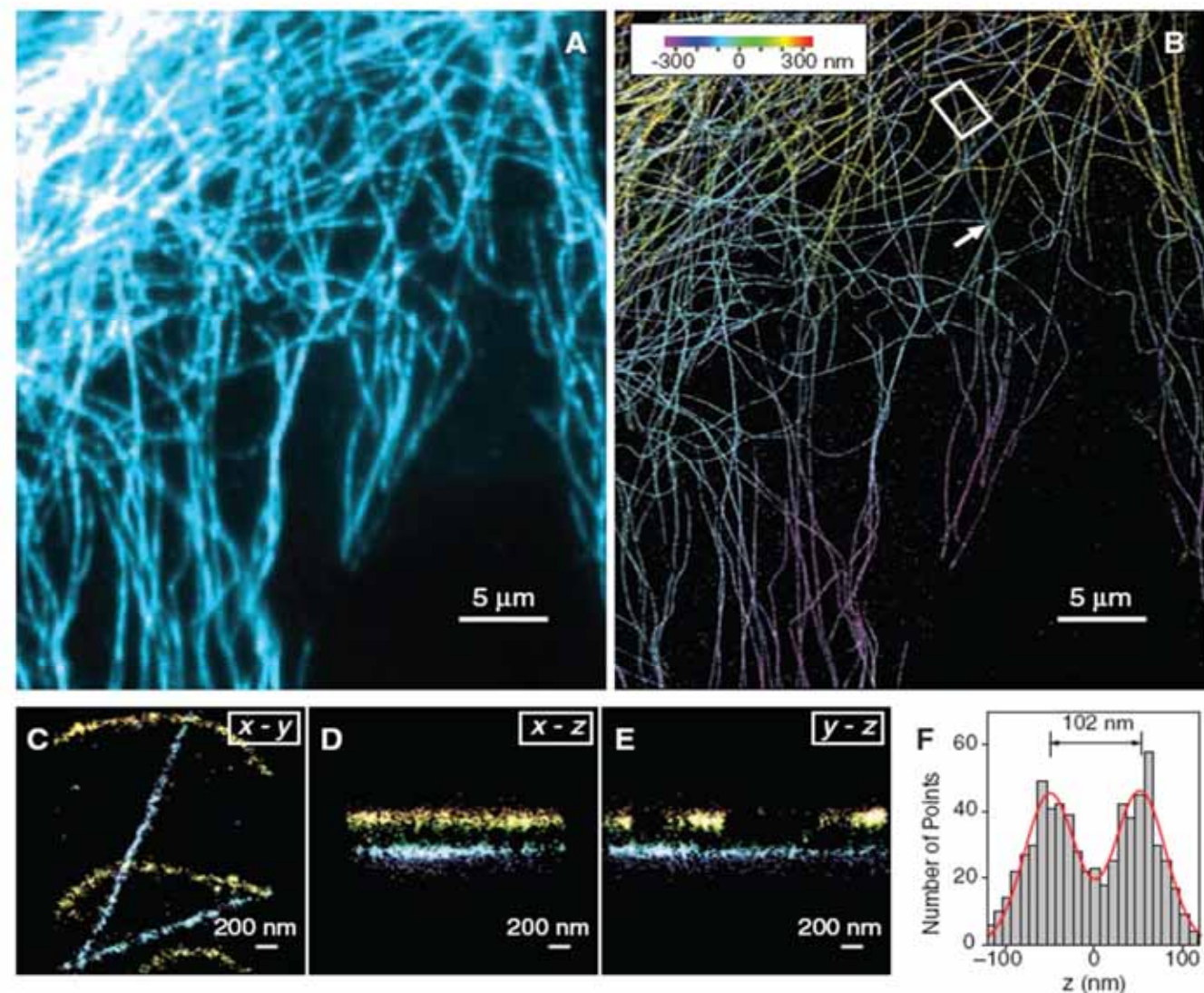
# Three-Dimensional Super-Resolution Imaging by Stochastic Optical Reconstruction Microscopy

8 FEBRUARY 2008 VOL 319 SCIENCE

**Fig. 1.** The scheme of 3D STORM. **(A)** Three-dimensional localization of individual fluorophores. The simplified optical diagram illustrates the principle of determining the  $z$  coordinate of a fluorescent object from the ellipticity of its image by introducing a cylindrical lens into the imaging path. The right panel shows images of a fluorophore at various  $z$  positions. EMCCD, electron-multiplying charge-coupled device. **(B)** Calibration curve of image widths  $w_x$  and  $w_y$  as a function of  $z$  obtained from single Alexa 647 molecules. Each data point represents the average value obtained from six molecules. The data were fit to a defocusing function (red curve) as described in (27). **(C)** Three-dimensional localization distribution of single molecules. Each molecule gives a cluster of localizations due to repetitive activation of the same molecule. Localizations from 145 clusters were aligned by their center of mass to generate the overall 3D presentation of the localization distribution (left panel). Histograms of the distribution in  $x$ ,  $y$ , and  $z$  (right panels) were fit to a Gaussian function, yielding standard deviations of 9 nm in  $x$ , 11 nm in  $y$ , and 22 nm in  $z$ .



**Fig. 2.** Three-dimensional STORM imaging of microtubules in a cell. **(A)** Conventional indirect immunofluorescence image of microtubules in a large area of a BS-C-1 cell. **(B)** The 3D STORM image of the same area, with the *z*-position information color-coded according to the color scale bar. Each localization is depicted in the STORM image as a Gaussian peak, the width of which is determined by the number of photons detected (5). **(C to E)** The *x*-*y*, *x*-*z*, and *y*-*z* cross sections of a small region of the cell outlined by the white box in (B), showing five microtubule filaments. Movie S1 shows the 3D representation of this region, with the viewing angle rotated to show different perspectives (27). **(F)** The *z* profile of two microtubules crossing in the *x*-*y* projection but separated by 102 nm in *z*, from a region indicated by the arrow in (B). The histogram shows the distribution of *z* coordinates of the localizations, fit to two Gaussians with identical widths (FWHM = 66 nm) and a separation of 102 nm (red curve). The apparent width of 66 nm agrees quantitatively with the convolution of our imaging resolution in *z* (represented by a Gaussian function with FWHM of 55 nm) and the previously measured width of antibody-coated microtubules (represented by a uniform distribution with a width of 56 nm) (5).



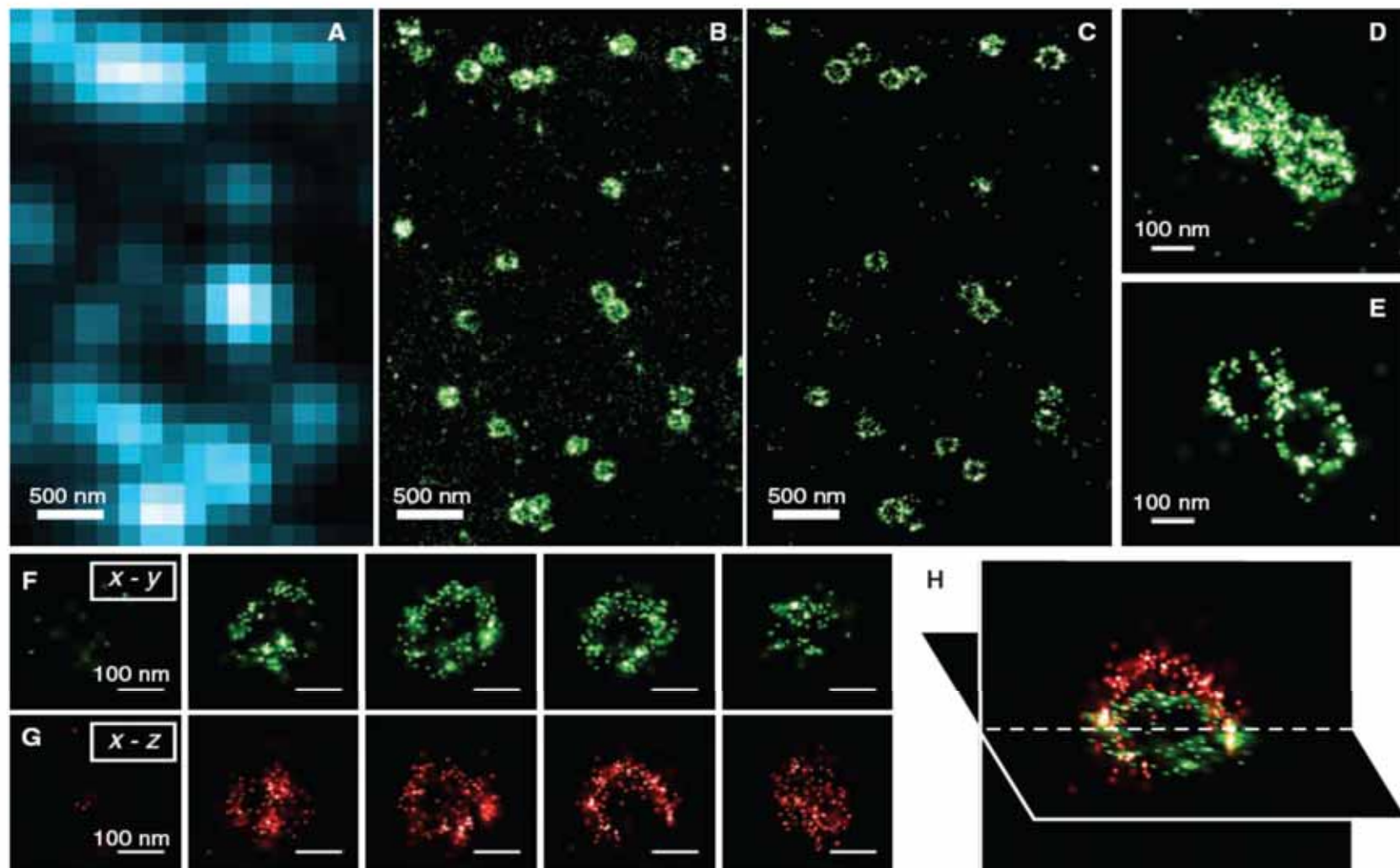
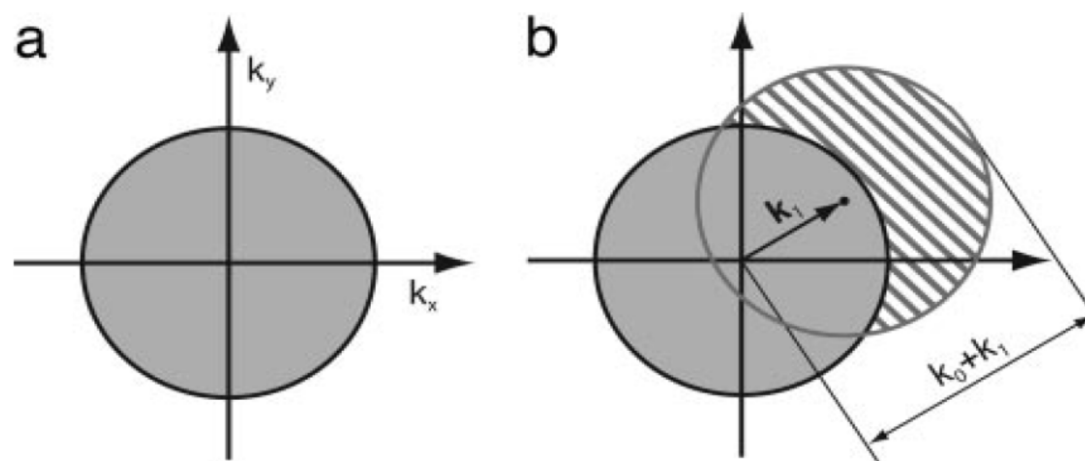
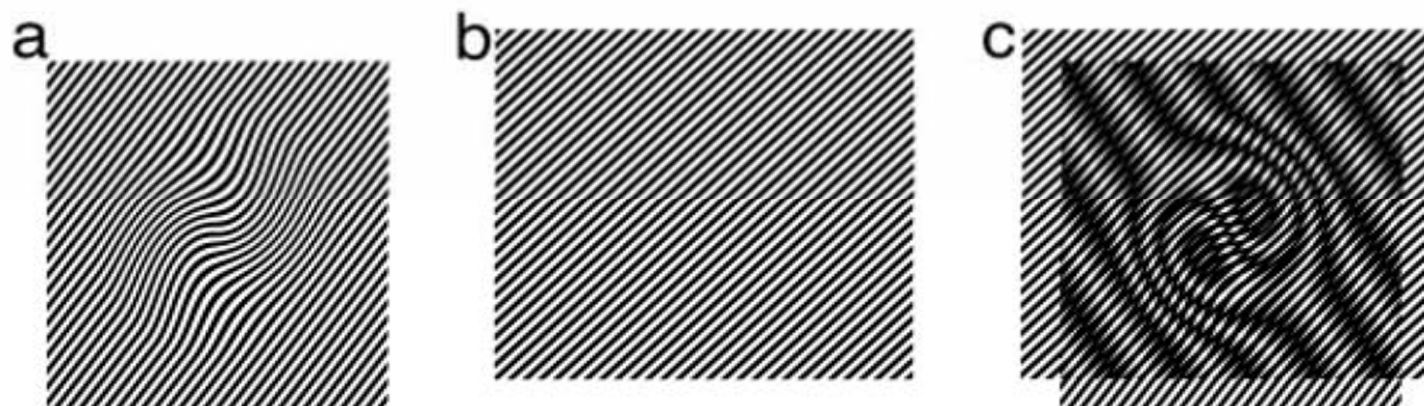


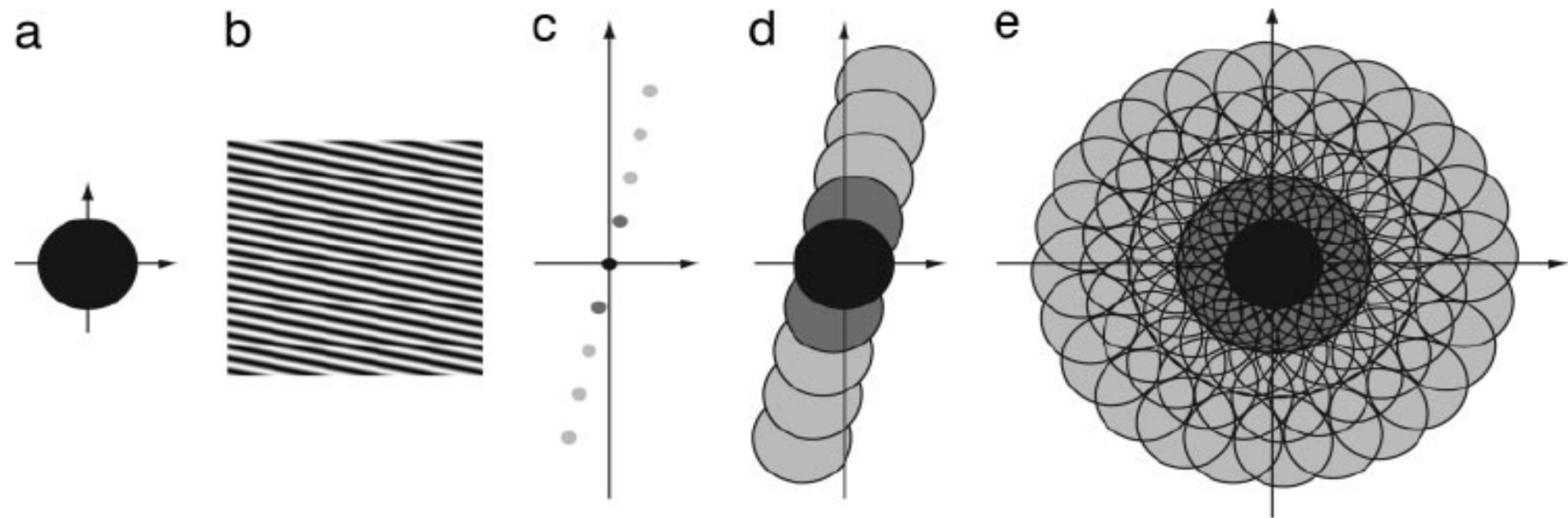
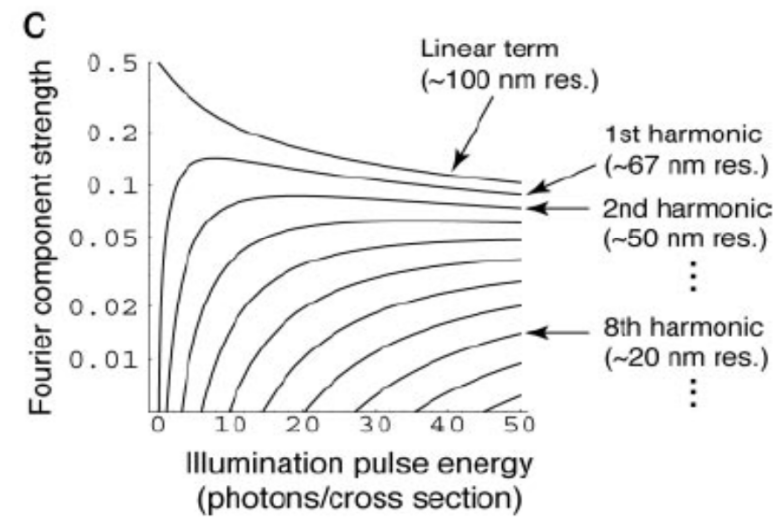
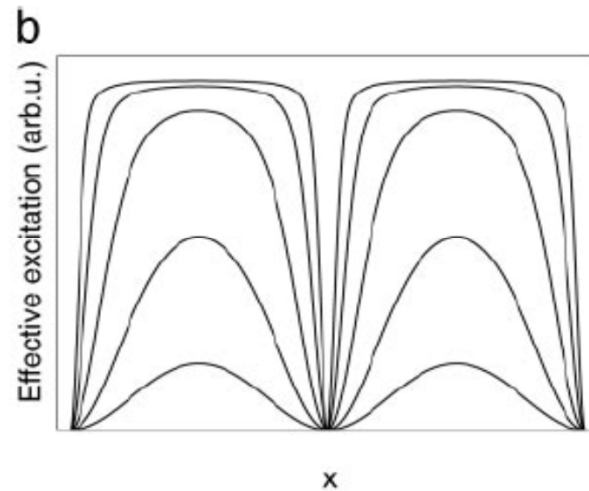
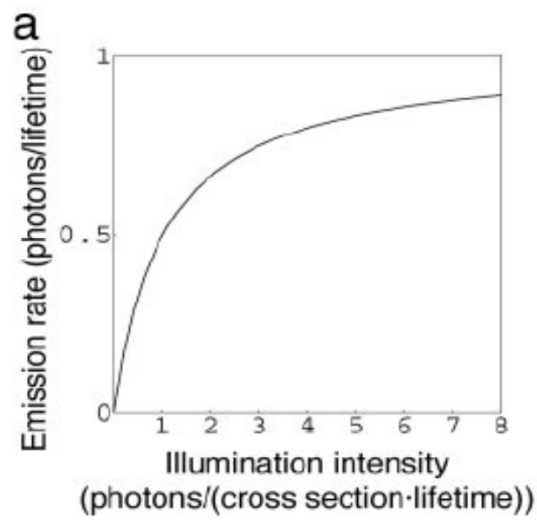
**Fig. 3.** Three-dimensional STORM imaging of clathrin-coated pits in a cell. **(A)** Conventional direct immunofluorescence image of clathrin in a region of a BS-C-1 cell. **(B)** The 2D STORM image of the same area, with all localizations at different  $z$  positions included. **(C)** An  $x$ - $y$  cross section (50 nm thick in  $z$ ) of the same area, showing the ring-like structure of the periphery of the CCPs at the

plasma membrane. **(D and E)** Magnified view of two nearby CCPs in 2D STORM (D) and their  $x$ - $y$  cross section (100 nm thick) in the 3D image (E). **(F to H)** Serial  $x$ - $y$  cross sections (each 50 nm thick in  $z$ ) (F) and  $x$ - $z$  cross sections (each 50 nm thick in  $y$ ) (G) of a CCP, and an  $x$ - $y$  and  $x$ - $z$  cross section presented in 3D perspective (H), showing the half-spherical cage-like structure of the pit.

# Nonlinear structured-illumination microscopy: Wide-field fluorescence imaging with theoretically unlimited resolution

PNAS | September 13, 2005 | vol. 102 | no. 37 | 13081–13086



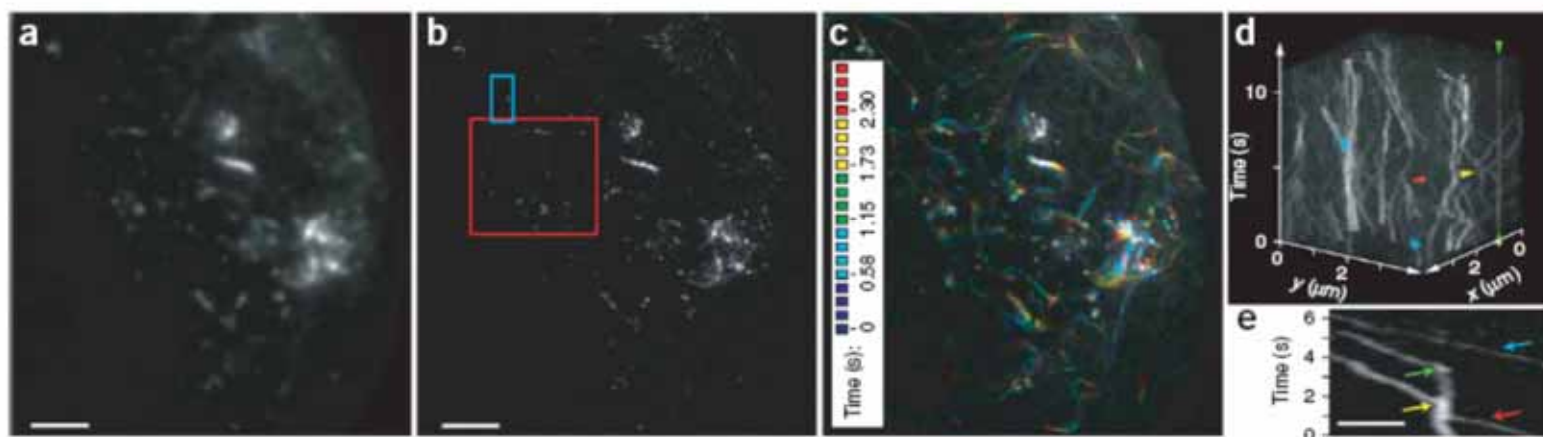
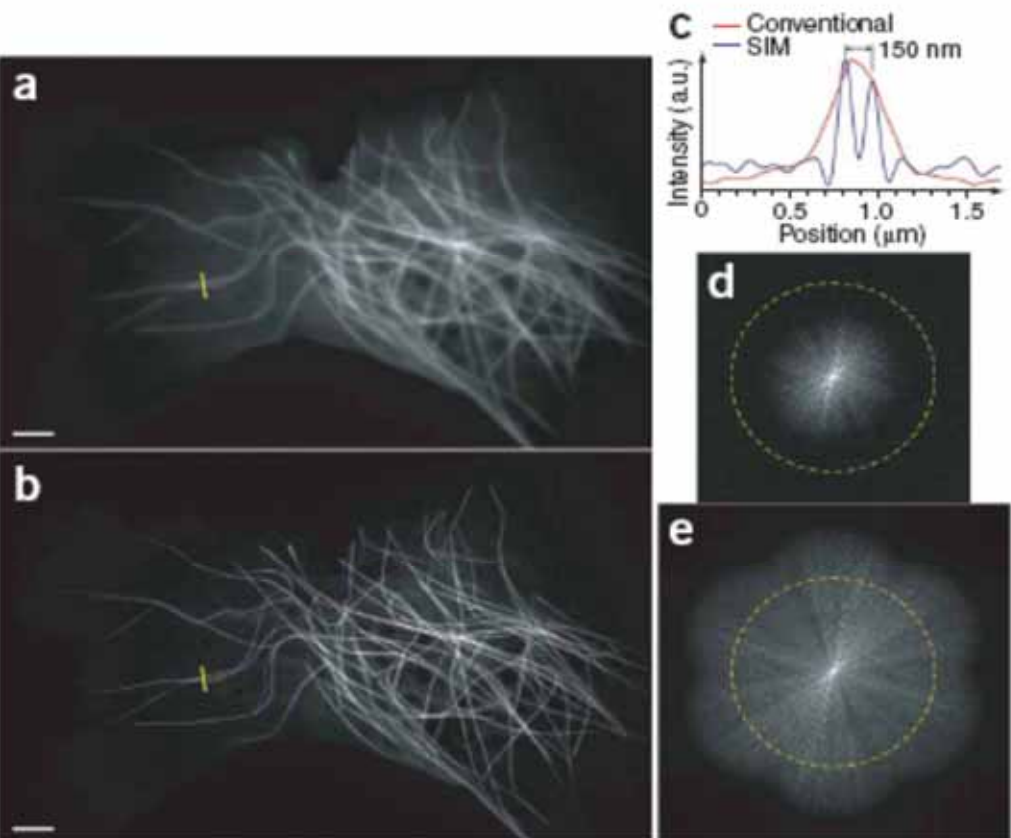


# Super-resolution video microscopy of live cells by structured illumination

Peter Kner<sup>1,2,7,8</sup>, Bryant B Chhun<sup>1,8</sup>, Eric R Griffis<sup>3,4</sup>,  
Lukman Winoto<sup>5</sup> & Mats G L Gustafsson<sup>5,6</sup>

NATURE METHODS | VOL.6 NO.5 | MAY 2009 | 339

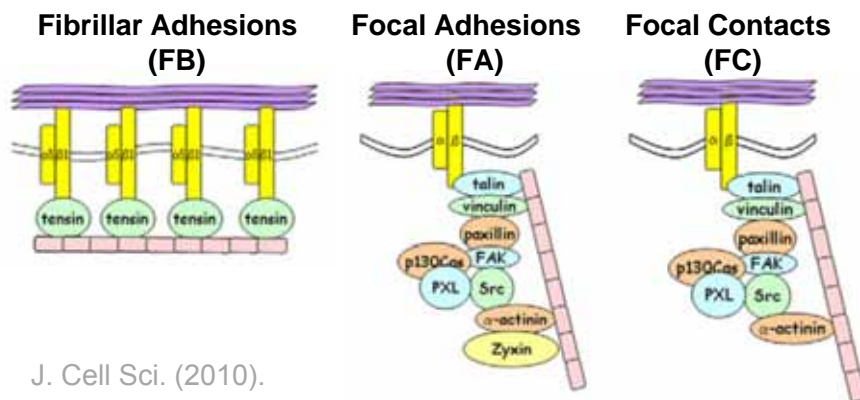
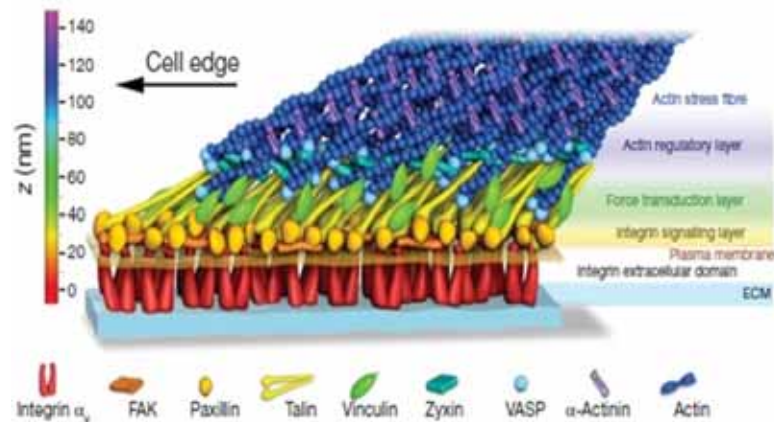
Structured-illumination microscopy can double the resolution of the widefield fluorescence microscope but has previously been too slow for dynamic live imaging. Here we demonstrate a high-speed structured-illumination microscope that is capable of 100-nm resolution at frame rates up to 11 Hz for several hundred time points. We demonstrate the microscope by video imaging of tubulin and kinesin dynamics in living *Drosophila melanogaster* S2 cells in the total internal reflection mode.



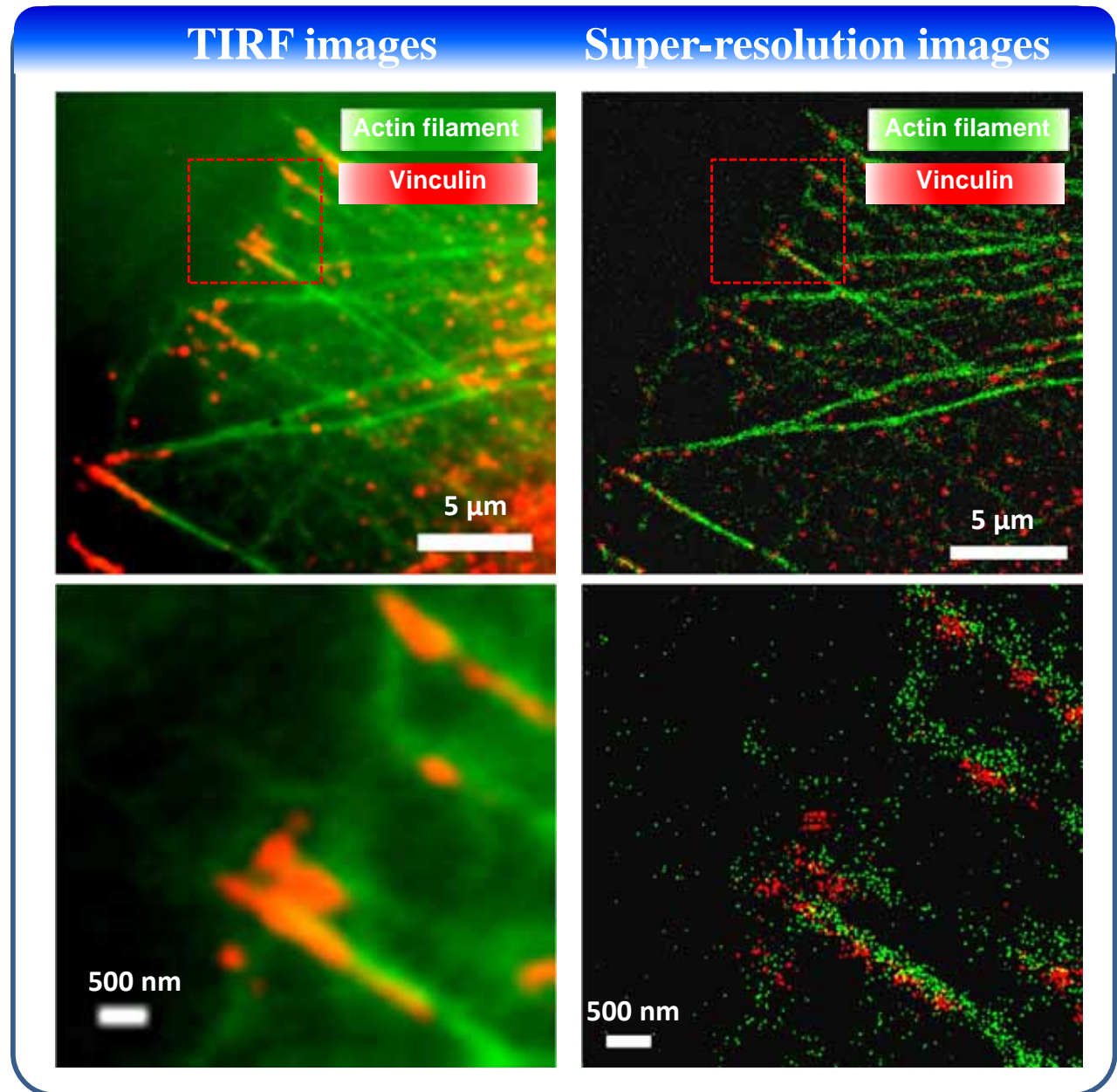
# Multicolor superresolution fluorescence imaging

## Objective

1. Characteristic distance between focal adhesion complexes.
2. Cross-correlation between different focal adhesion complexes.
3. Number of focal adhesion complexes at different adhesion types.

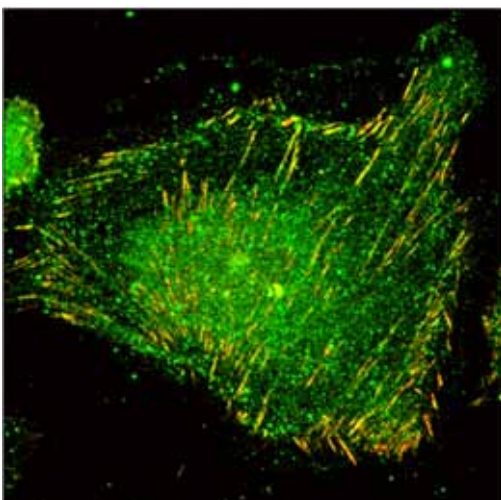
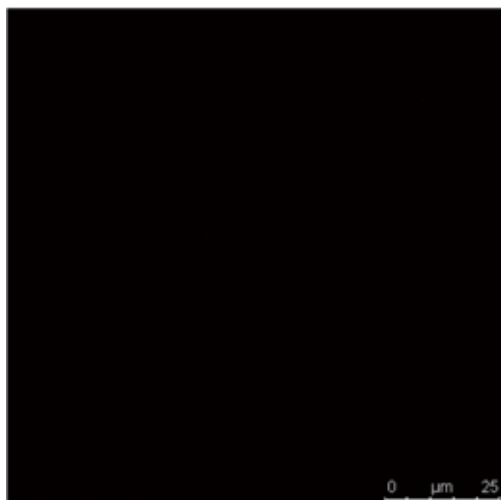


J. Cell Sci. (2010).

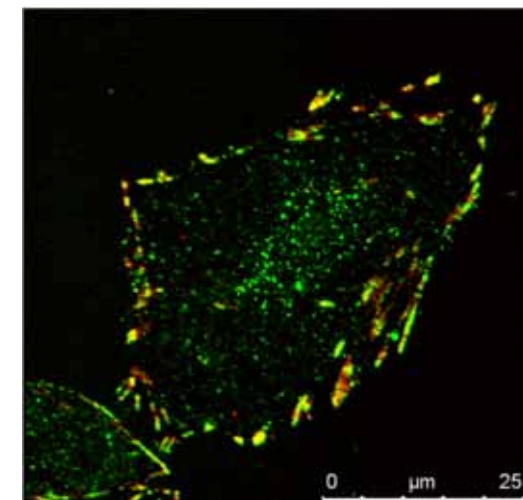
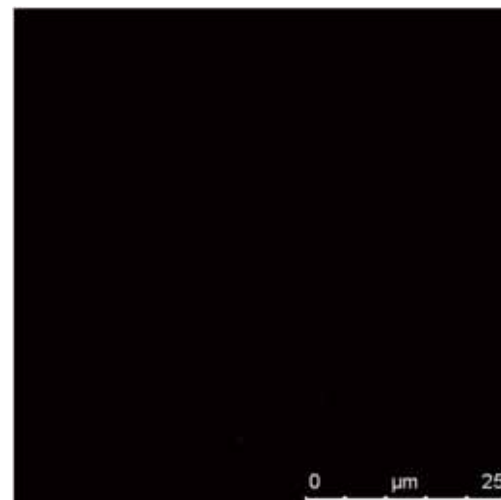


# Focal adhesion complexes

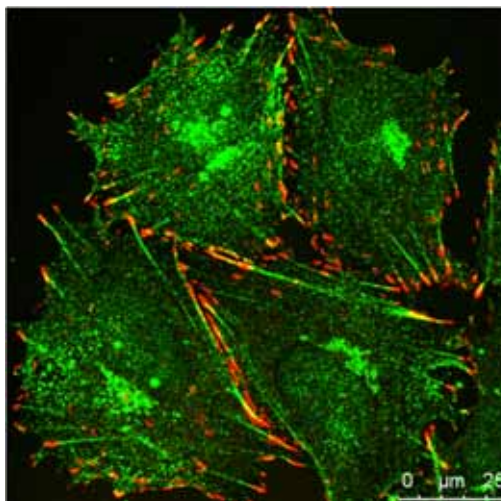
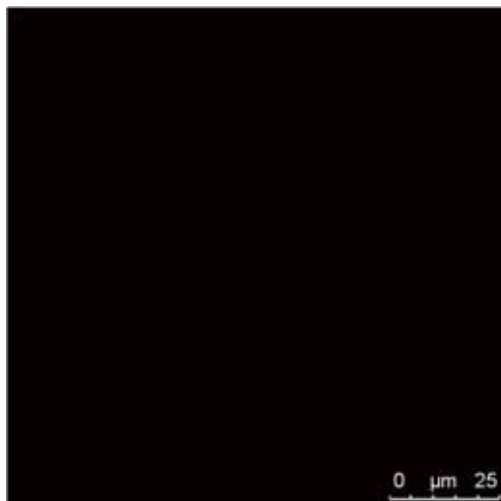
FAK & Vinculin



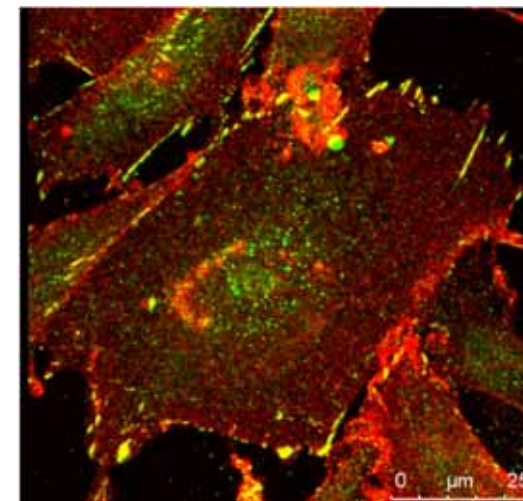
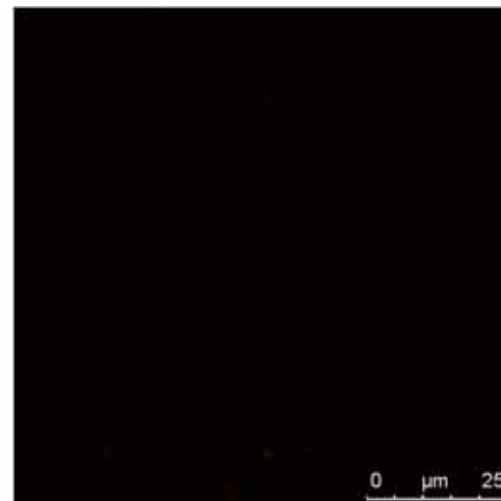
Paxillin & Vinculin



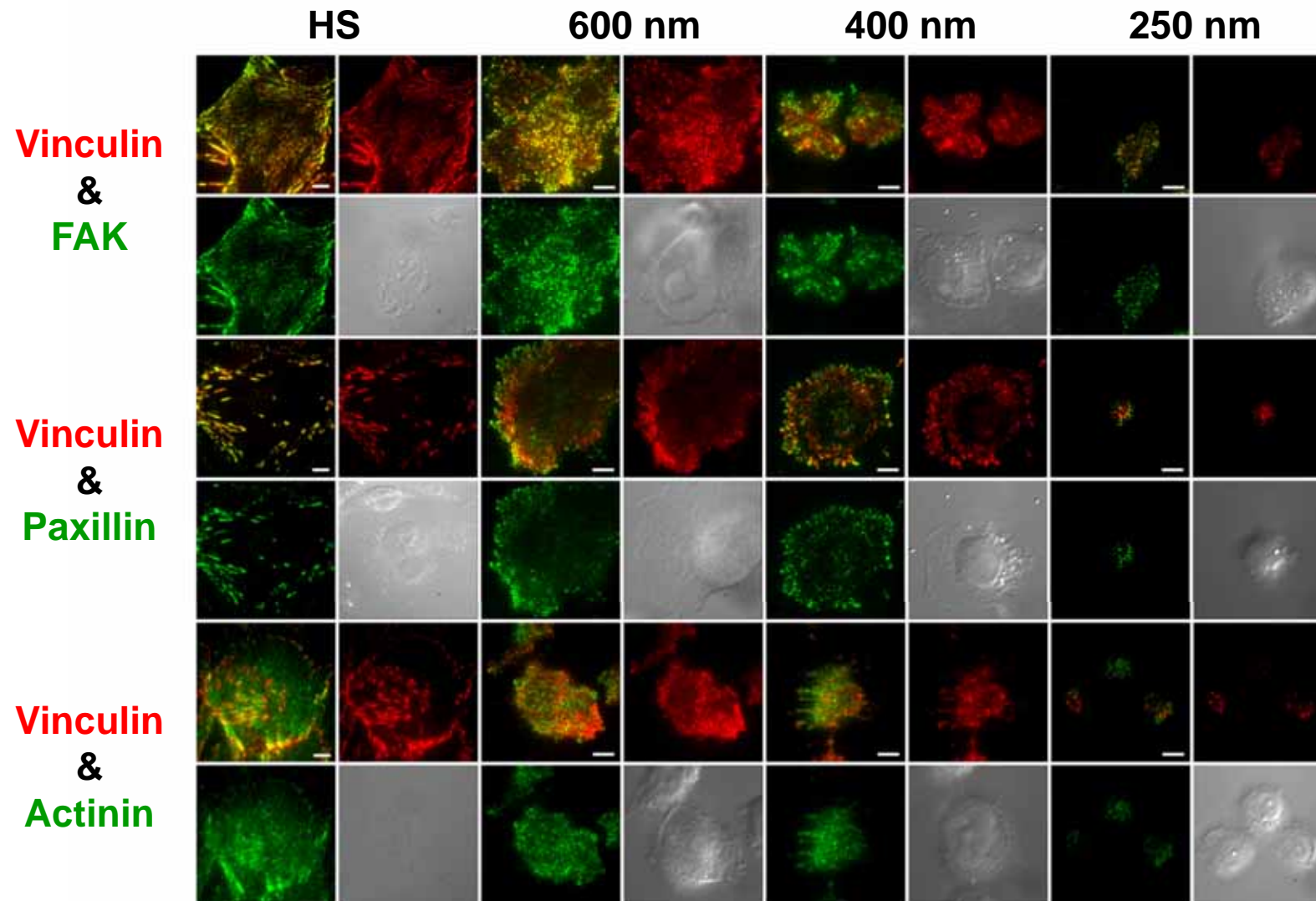
Actinin & Vinculin



FAK & Integrin  $\alpha 5$

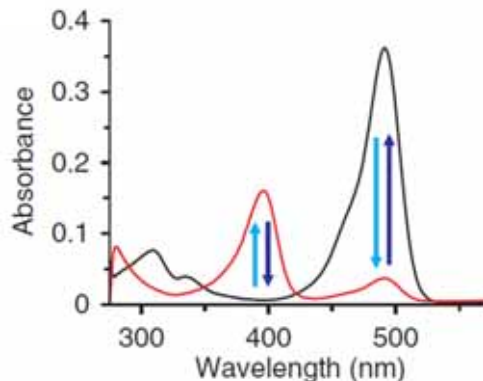
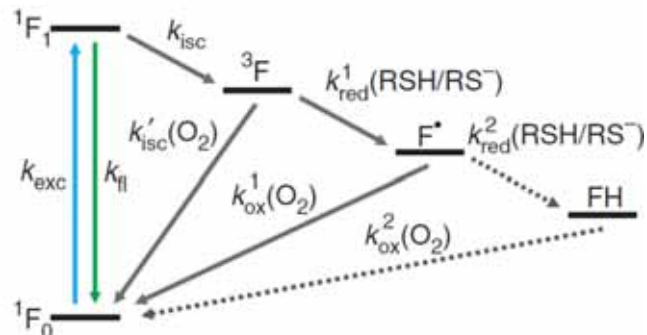


# Focal adhesion complexes on HS and pattern ECM surface

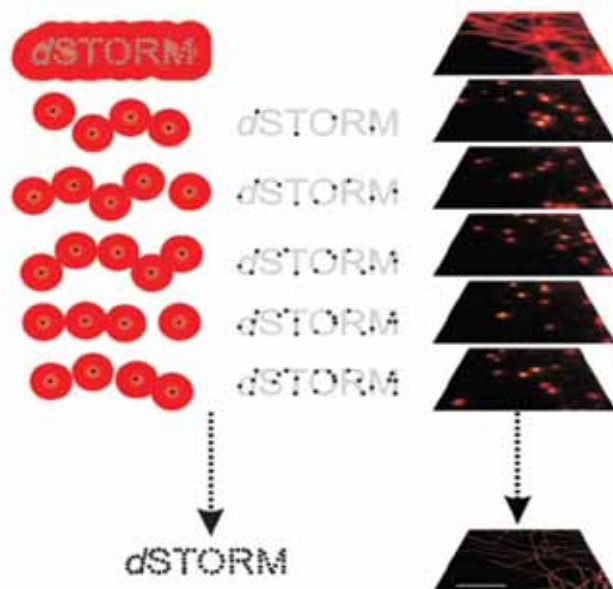


# Direct stochastic optical reconstruction microscopy (dSTORM)

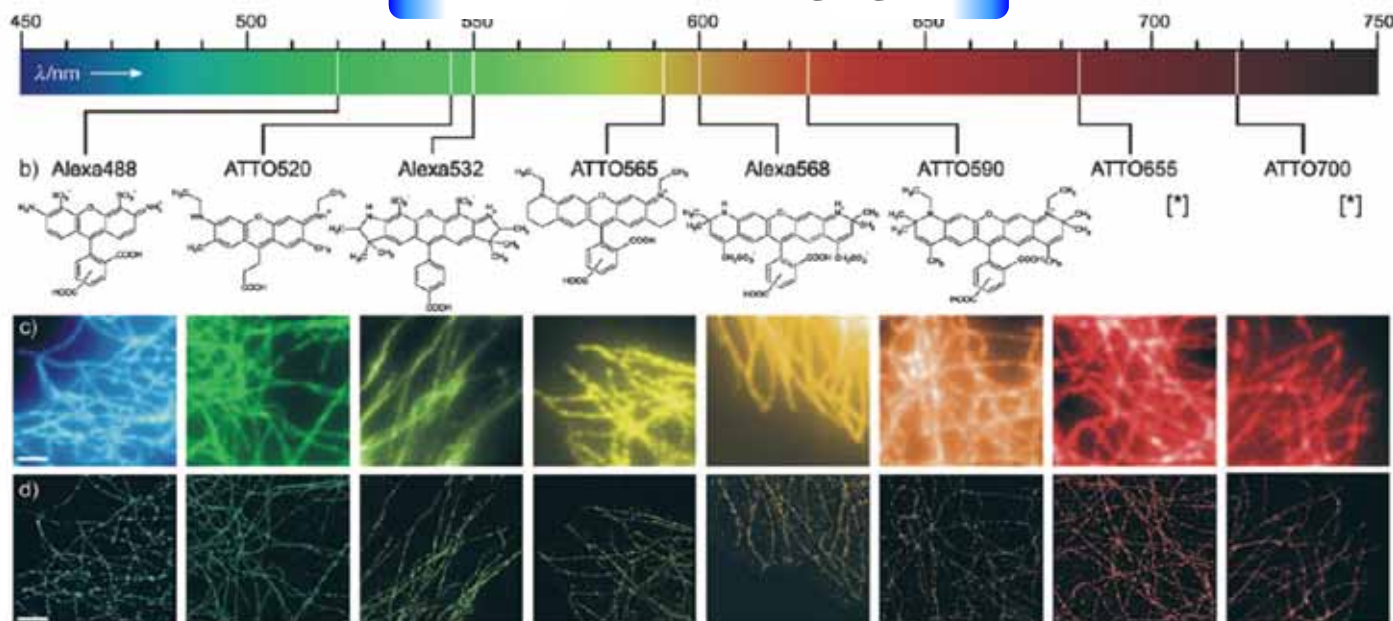
## Reversible photoswitching mechanism of standard fluorophores



### Localization imaging concept



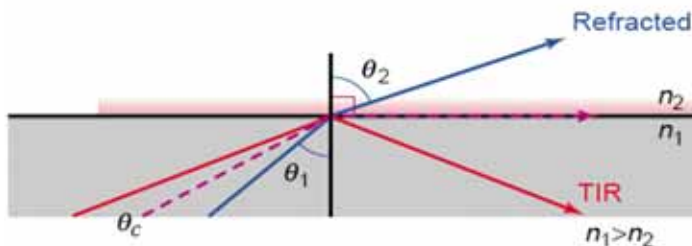
### Multicolor imaging



# Multicolor super-resolution fluorescence microscopy

## Multicolor localization imaging system

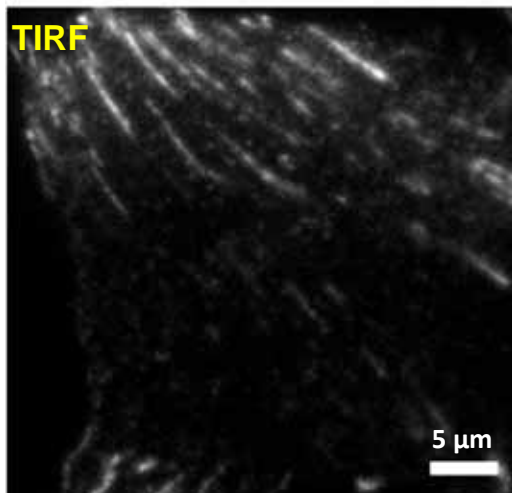
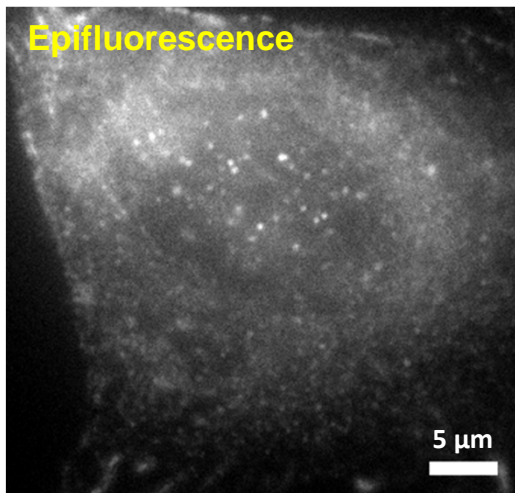
### Total internal reflection (TIR) concept



Penetration depth of evanescent wave:

$$I_z = I_0 e^{(-z/d_p)}$$

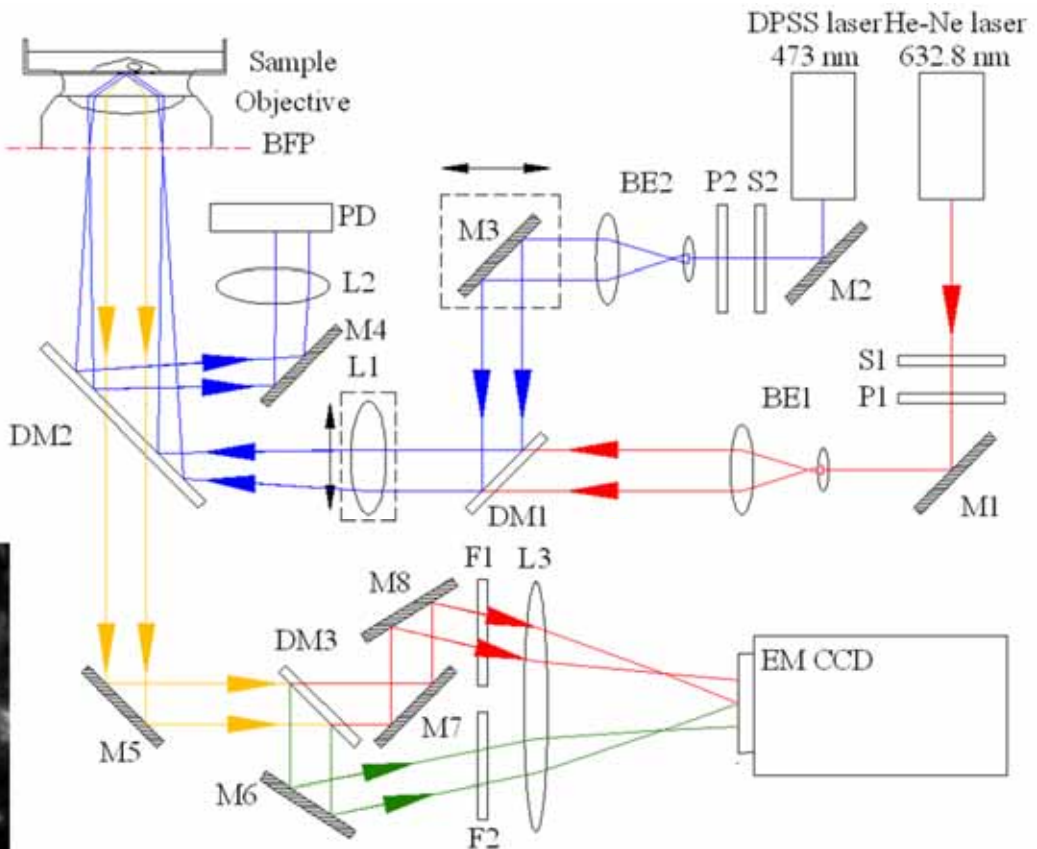
$$d_p = \lambda / 4\pi \sqrt{n_1^2 \sin^2 \theta_1 - n_2^2}$$



5  $\mu\text{m}$

5  $\mu\text{m}$

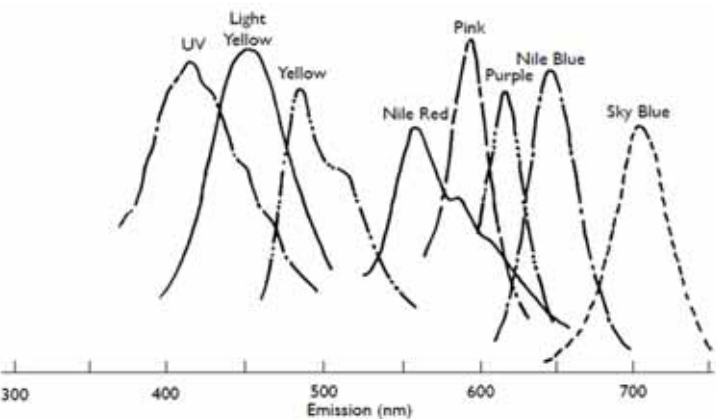
### TIRF microscope with dual-view configuration:



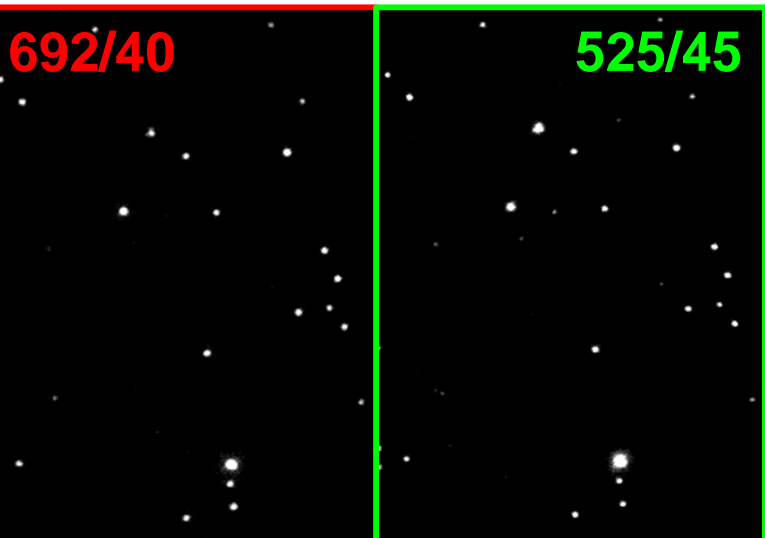
S: shutter, P: polarizer, M: mirror, BE: beam expander, DM: dichroic mirror, L: lens, BFP: back focal plane, F: filter, PD: photodiode

# Distance alignment of dual color imaging

## Multi fluorescence sphere

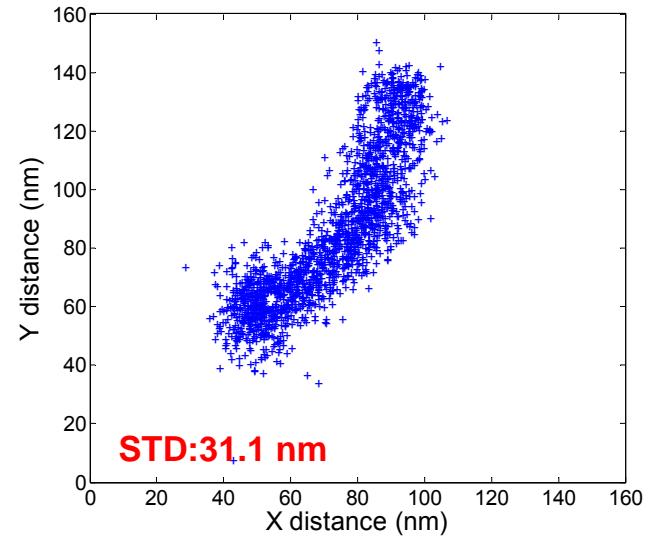


## TIRF images with dual-view system

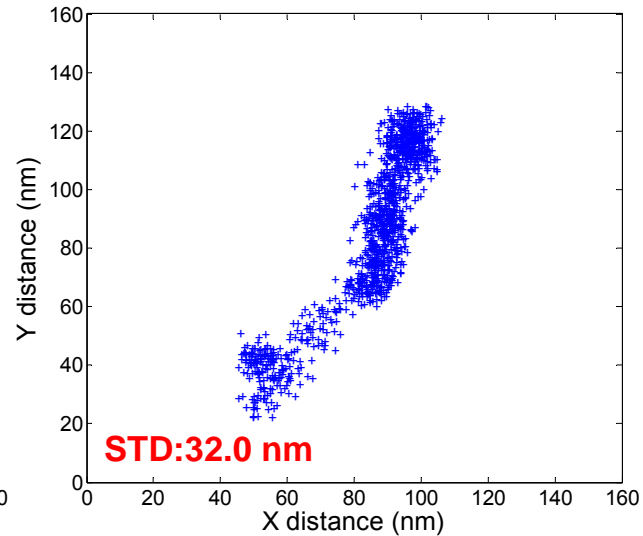


## Spatial localization

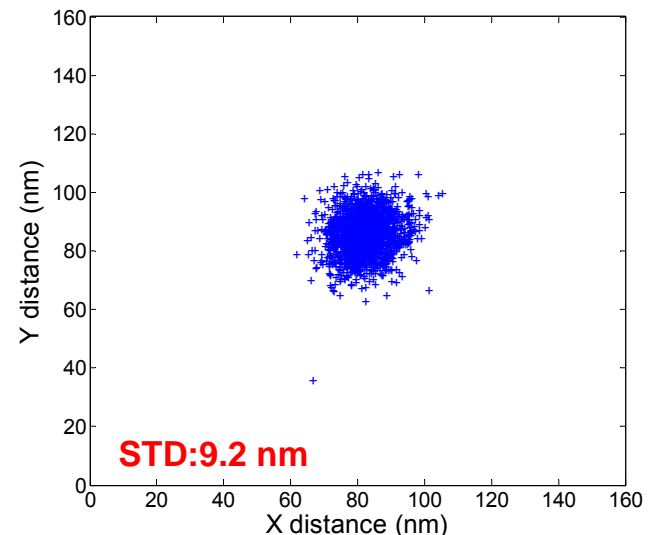
692/40



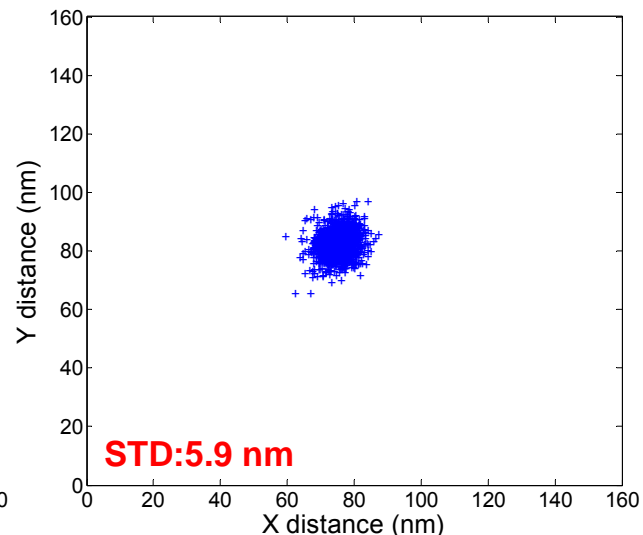
525/45



STD:9.2 nm



STD:5.9 nm



# Distance alignment of dual color imaging

Coordinates transformation matrix in long term measurement

Image 1

$$T_1 = \begin{bmatrix} t_{11} & t_{12} & t_{13} \\ t_{21} & t_{22} & t_{23} \\ t_{31} & t_{32} & t_{33} \end{bmatrix}$$

TIRF images with dual-view system

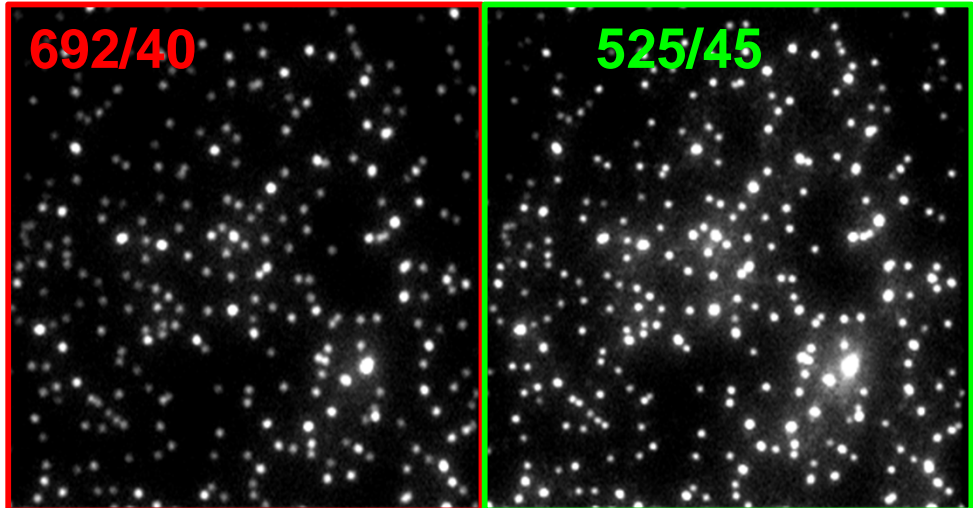
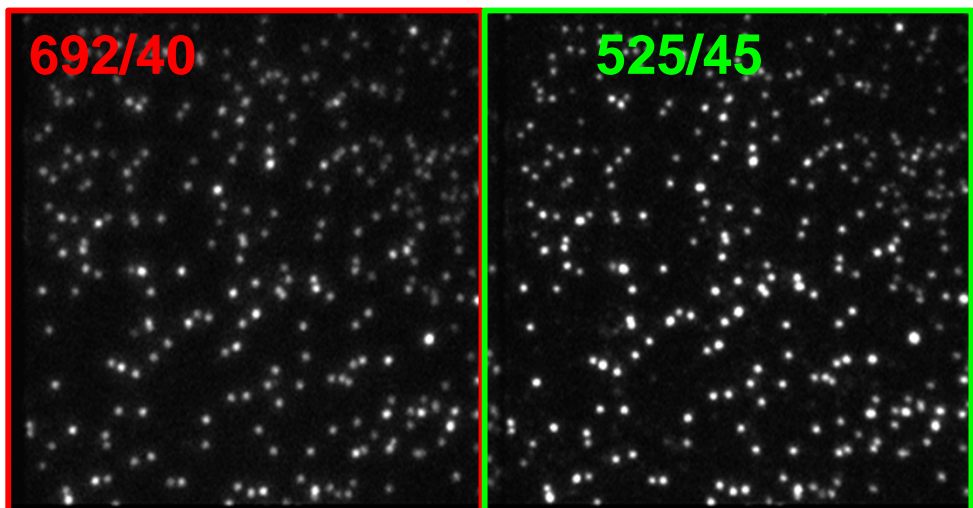


Image 2

$$T_2 = \begin{bmatrix} \tilde{t}_{11} & \tilde{t}_{12} & \tilde{t}_{13} \\ \tilde{t}_{21} & \tilde{t}_{22} & \tilde{t}_{23} \\ \tilde{t}_{31} & \tilde{t}_{32} & \tilde{t}_{33} \end{bmatrix}$$



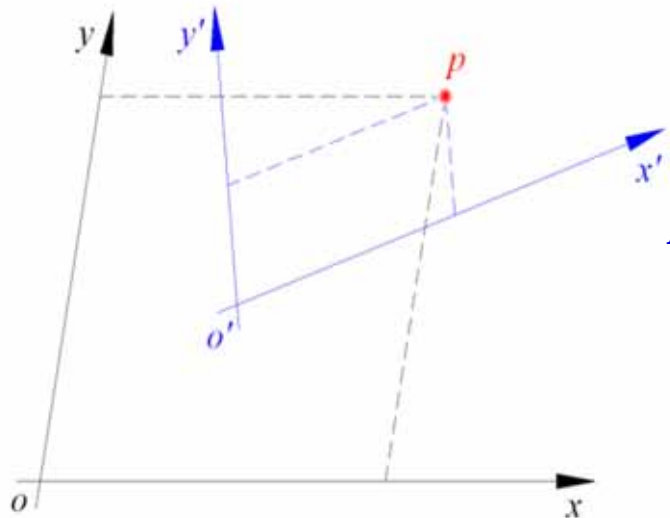
# Coordinates alignment of dual color imaging

$$U = TV = \begin{bmatrix} x \\ y \\ 1 \end{bmatrix} = T \begin{bmatrix} x' \\ y' \\ 1 \end{bmatrix} = \begin{bmatrix} r_1 & r_2 & t_1 \\ r_3 & r_4 & t_2 \\ p_1 & p_2 & 1 \end{bmatrix} \begin{bmatrix} x' \\ y' \\ 1 \end{bmatrix}$$

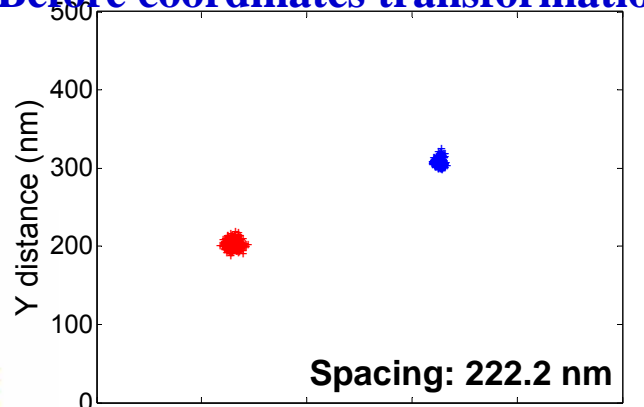
*T: the coordinates transformation matrix  
x,y: the coordinates of control points  
x',y': the coordinates of transformed points*

## Alignment concept

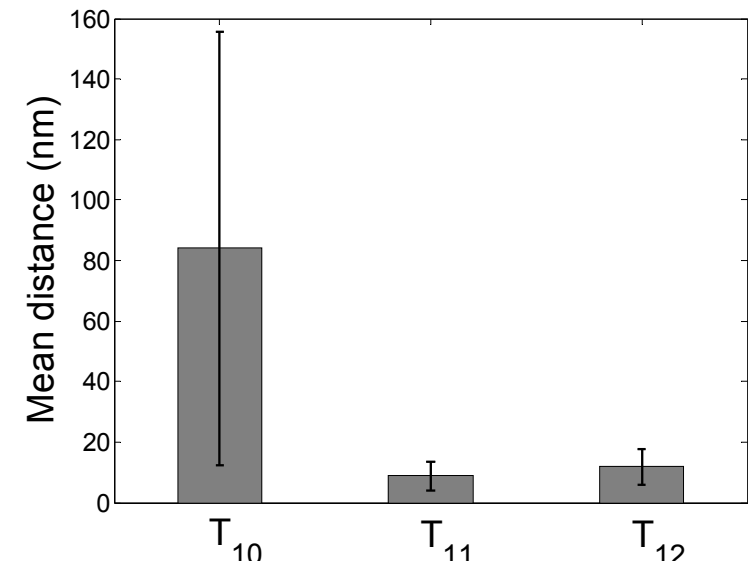
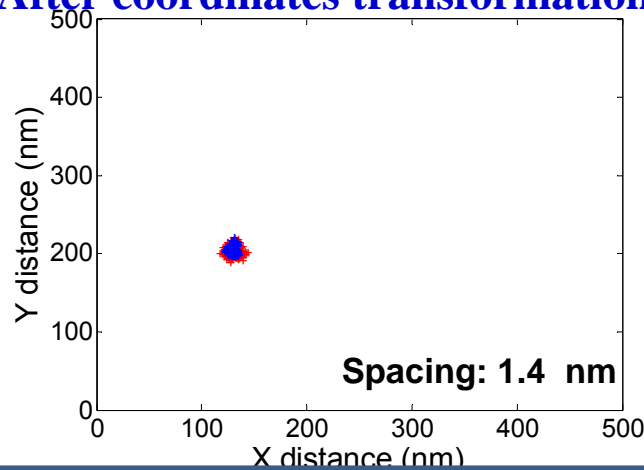
*Corrected with 25 reference markers  
in the image*



Before coordinates transformation



After coordinates transformation



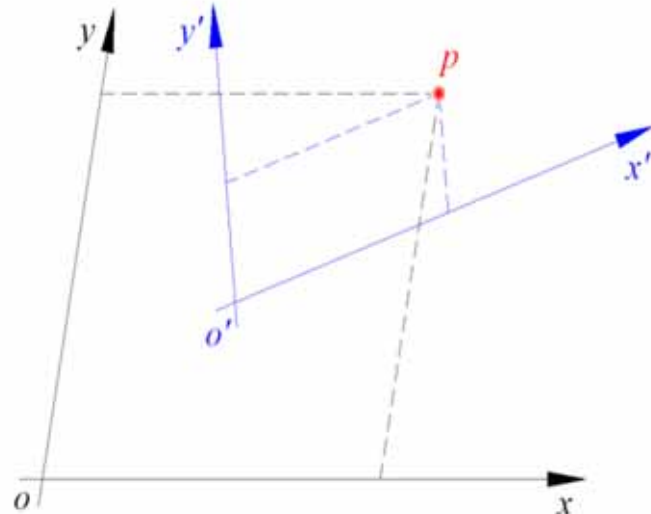
# Coordinates alignment of dual color imaging

$$U = TV = \begin{bmatrix} x \\ y \\ 1 \end{bmatrix} = T \begin{bmatrix} x' \\ y' \\ 1 \end{bmatrix} = \begin{bmatrix} r_1 & r_2 & t_1 \\ r_3 & r_4 & t_2 \\ p_1 & p_2 & 1 \end{bmatrix} \begin{bmatrix} x' \\ y' \\ 1 \end{bmatrix}$$

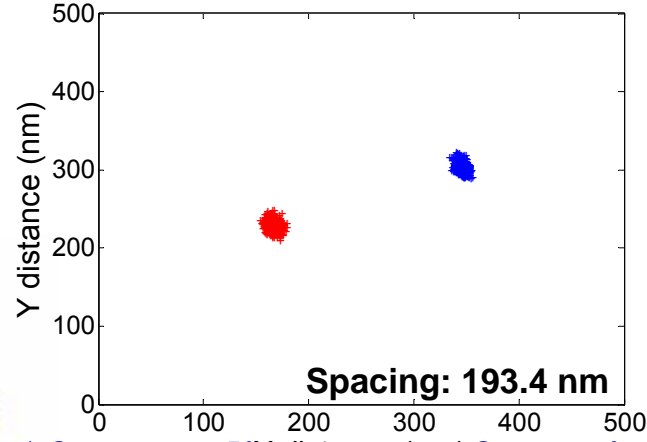
*T: the coordinates transformation matrix  
x,y: the coordinates of control points  
x',y': the coordinates of transformed points*

## Alignment concept

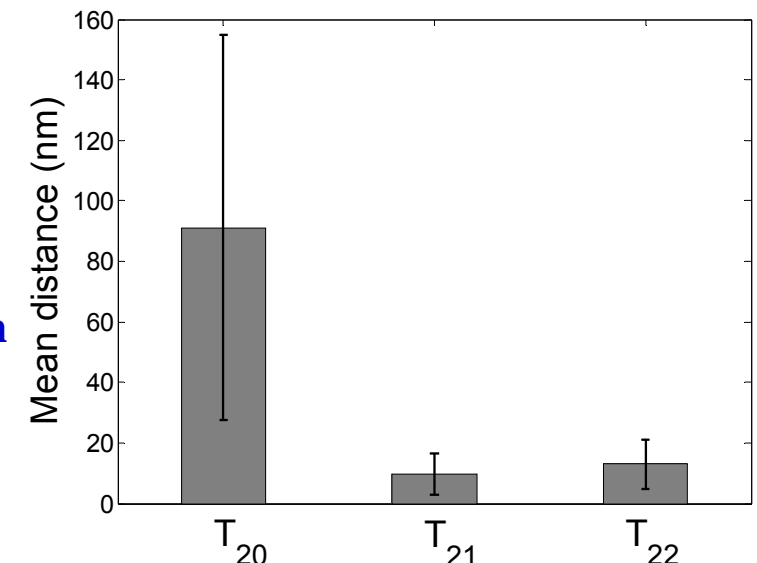
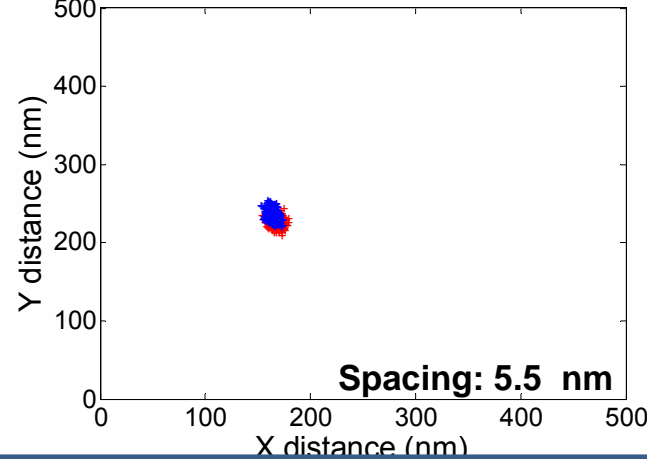
*Corrected with 25 reference markers in the image*



Before coordinates transformation

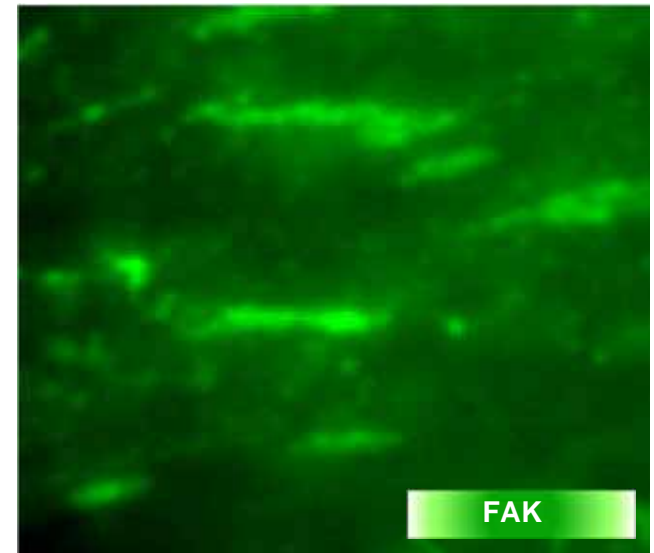
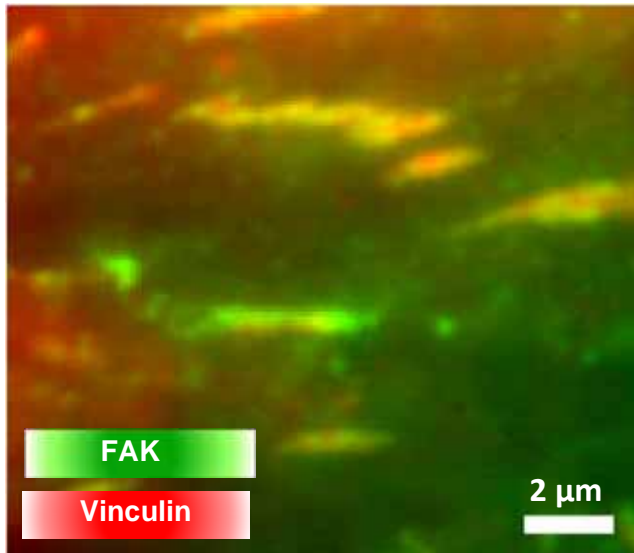


After coordinates transformation

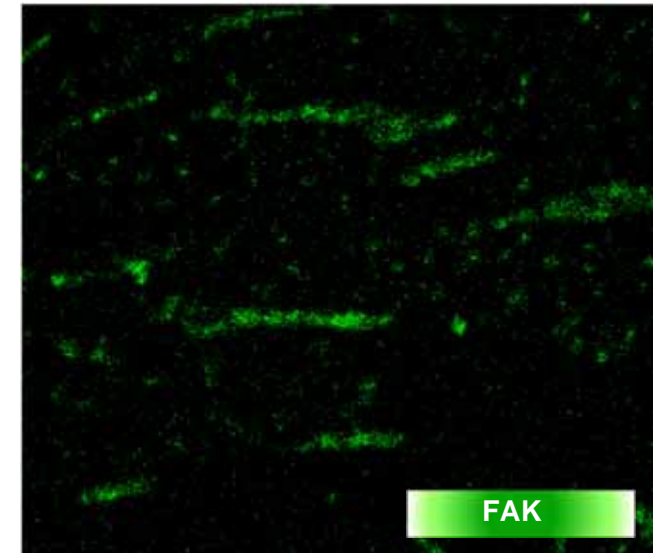
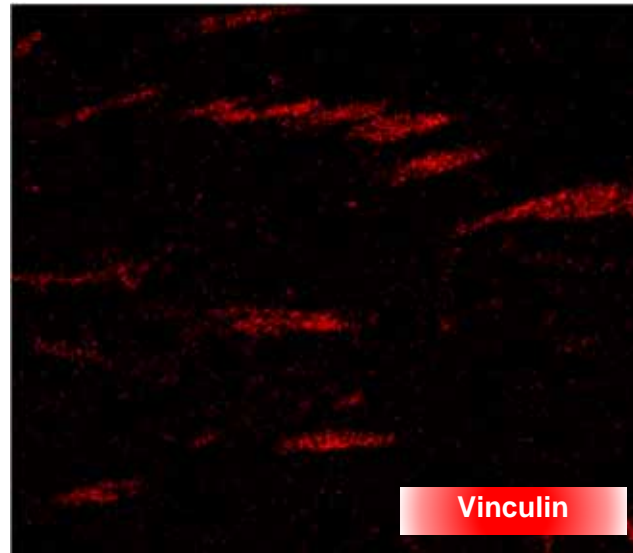
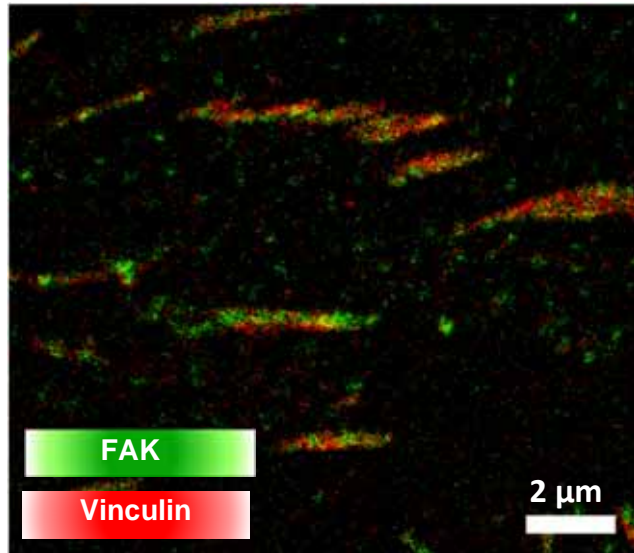


# Super-resolution localization imaging of focal adhesion complexes

TIRF images

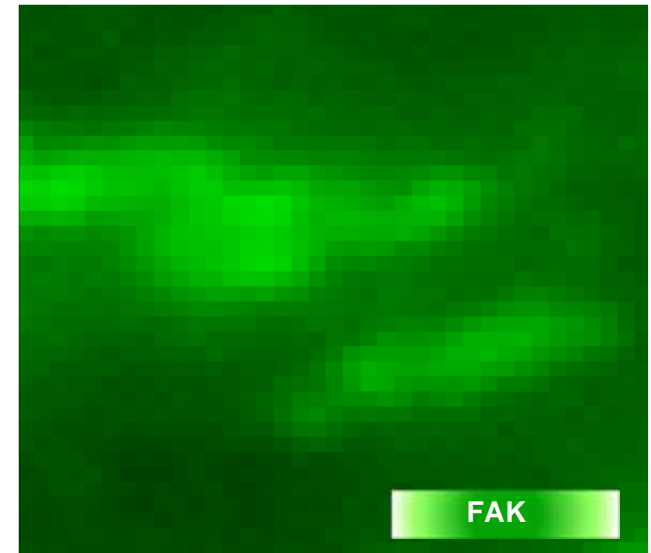
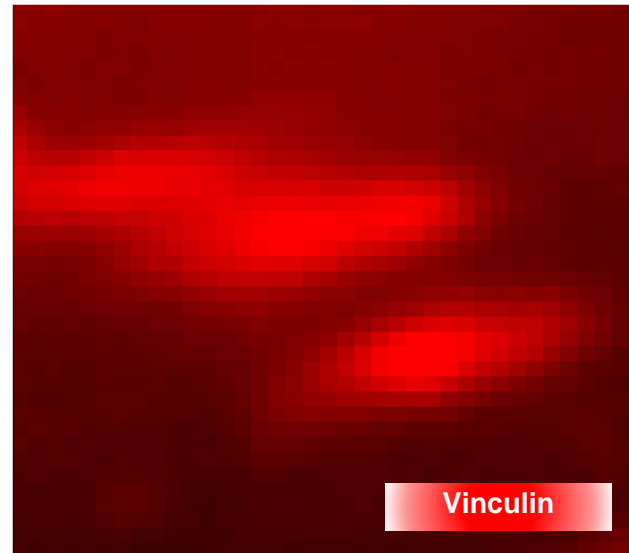
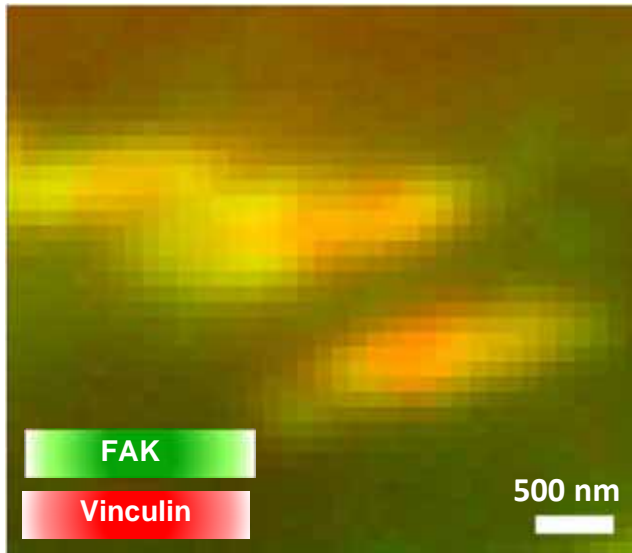


Super-resolution images

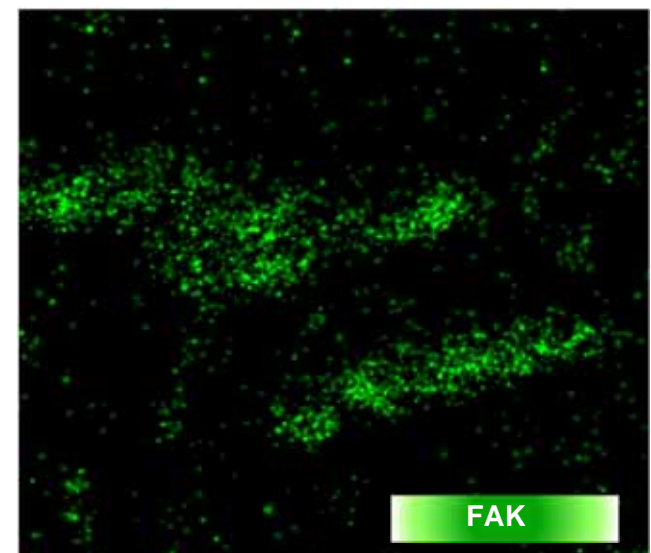
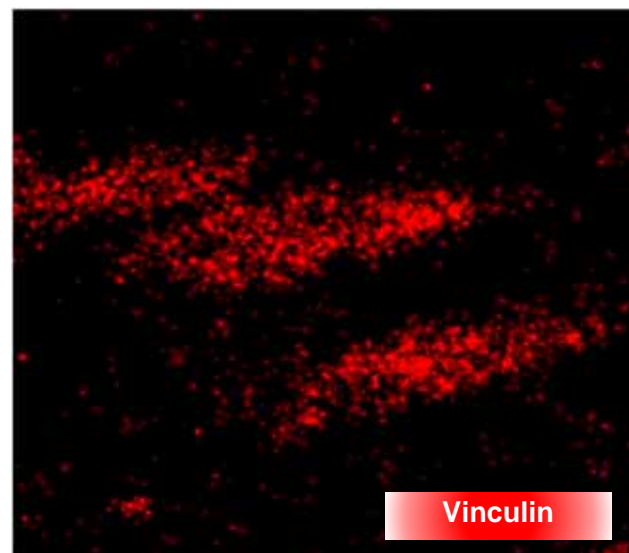
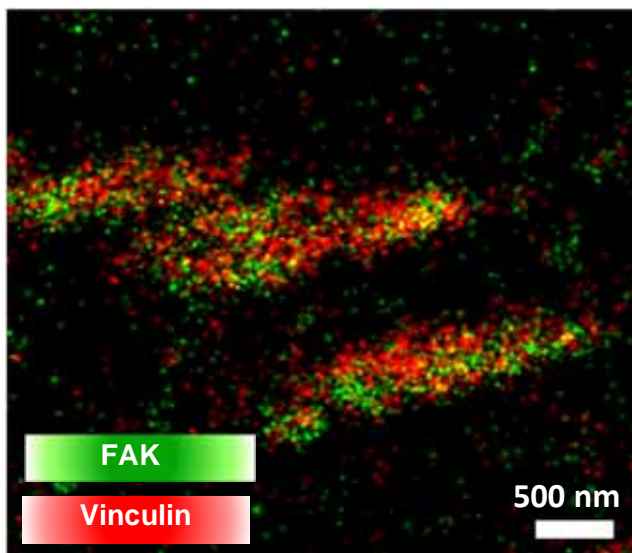


# Super-resolution localization imaging of focal adhesion complexes

TIRF images

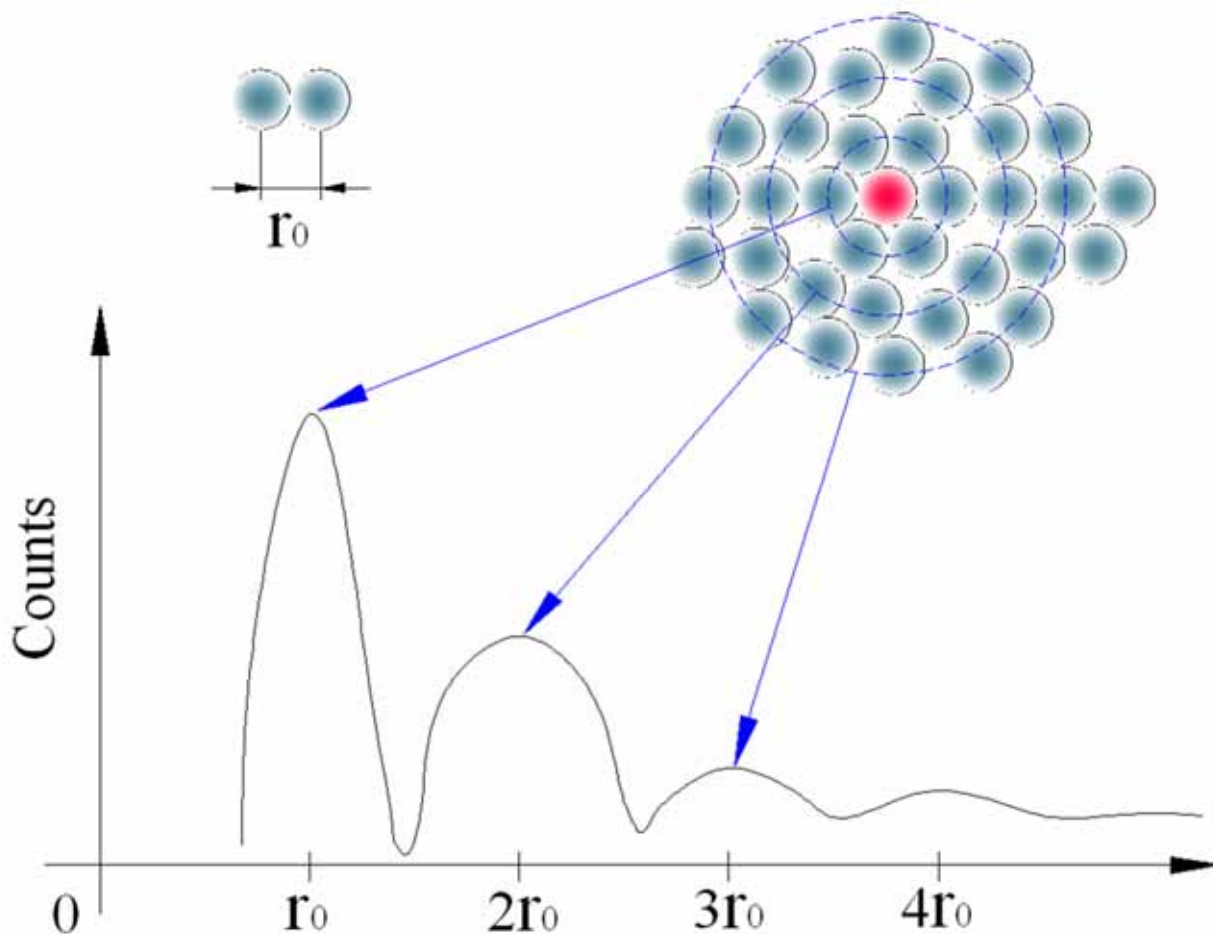


Super-resolution images



# Pair distance analysis

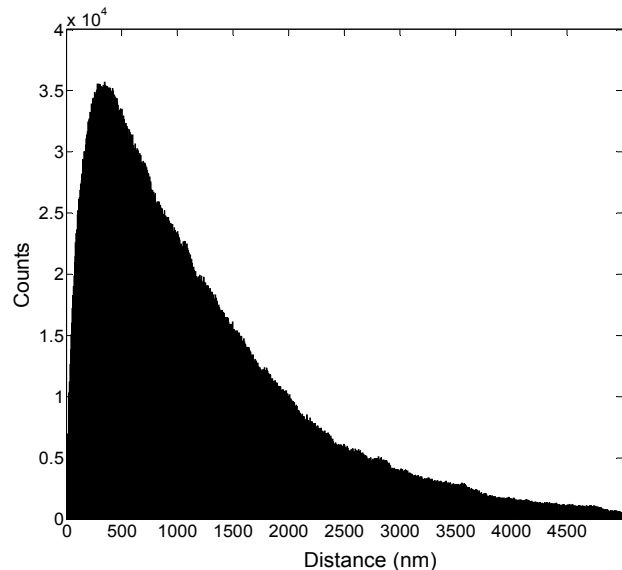
## Concept



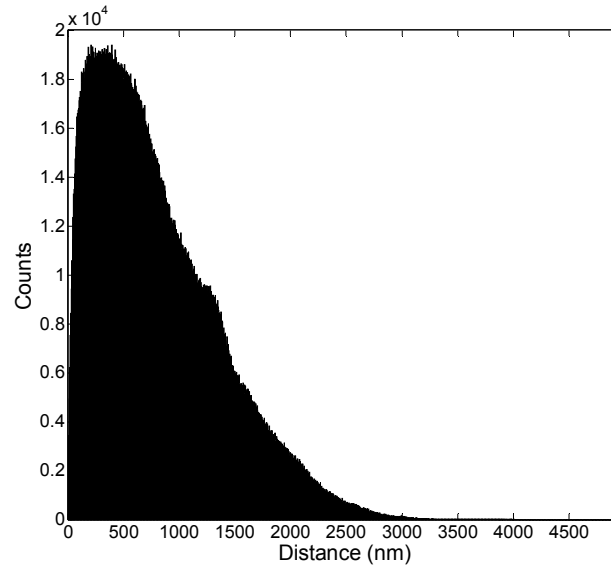
# Pair distance analysis

## Autocorrelation and Cross-correlation

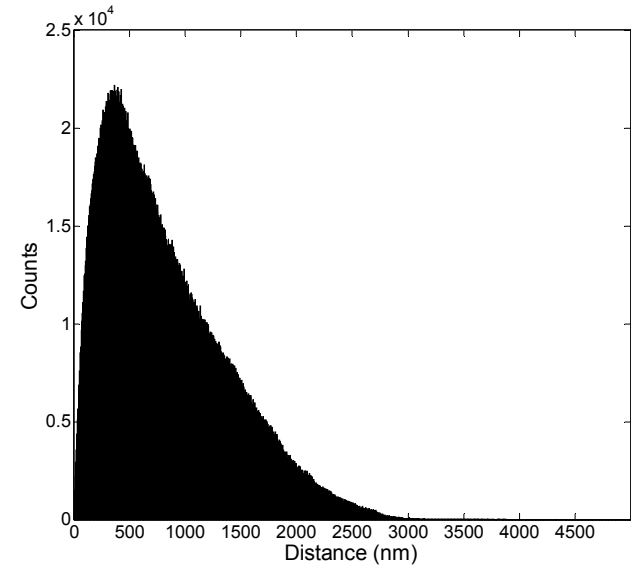
Vinculin-Vinculin



FAK-FAK



Vinculin-FAK

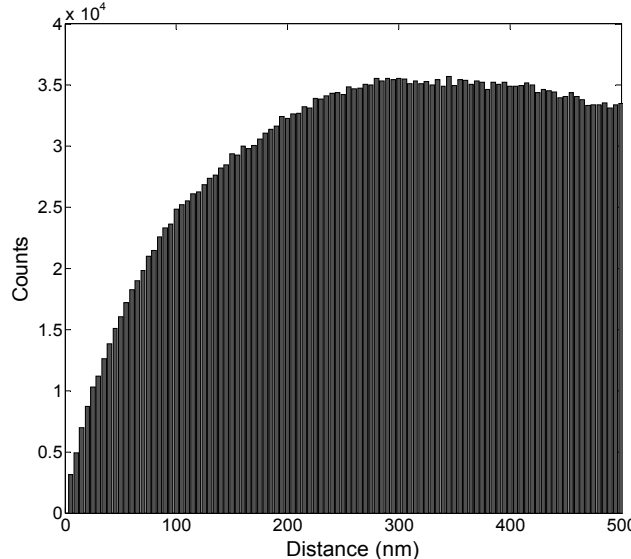


	Vin-Vin	FAK-FAK
Total molecular number	<b>16469</b>	<b>9484</b>
Molecular number of per adhesion	<b><math>1029.3 \pm 561.2</math></b>	<b><math>862.2 \pm 356.3</math></b>

# Pair distance analysis

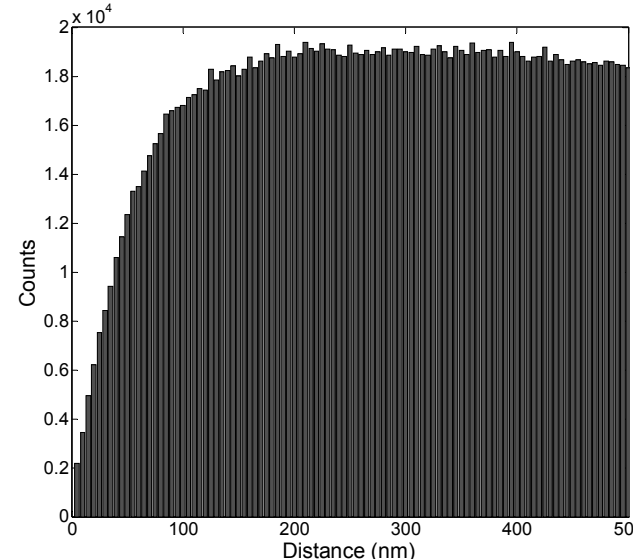
## Autocorrelation and Cross-correlation

Vinculin-Vinculin



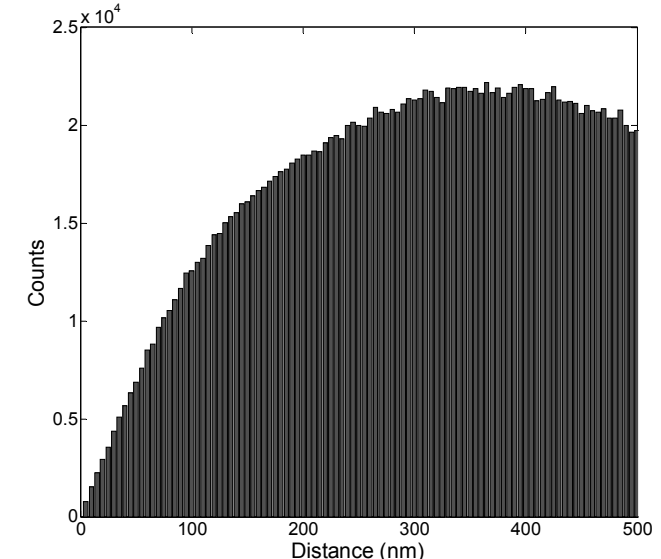
Pair distance 100 nm  
 $D_{avg}: 62.6 \pm 25.0$  nm

FAK-FAK



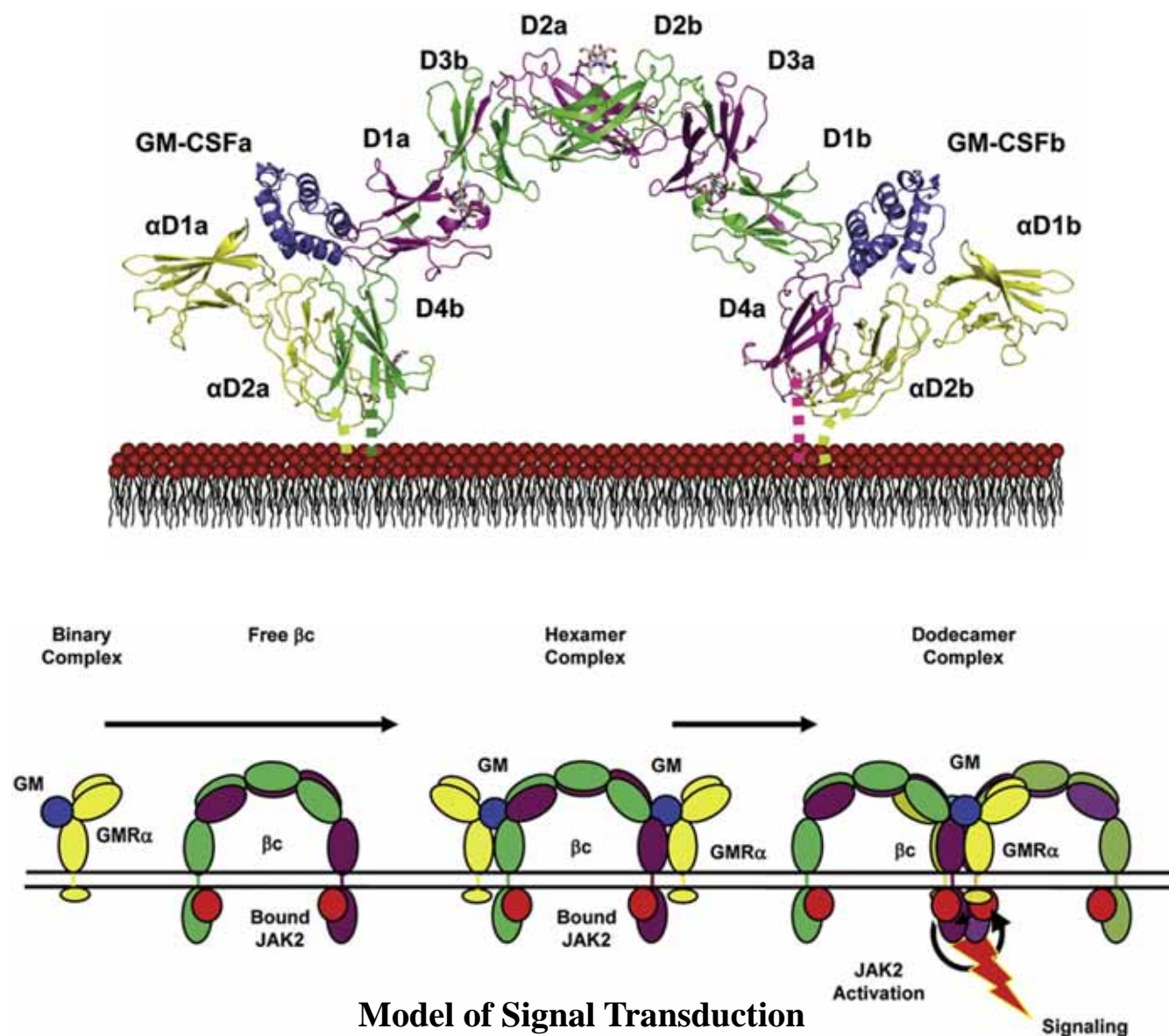
Pair distance 100 nm  
 $D_{avg}: 62.3 \pm 24.7$  nm

Vinculin-FAK



Pair distance 100 nm  
 $D_{avg}: 65.7 \pm 23.8$  nm

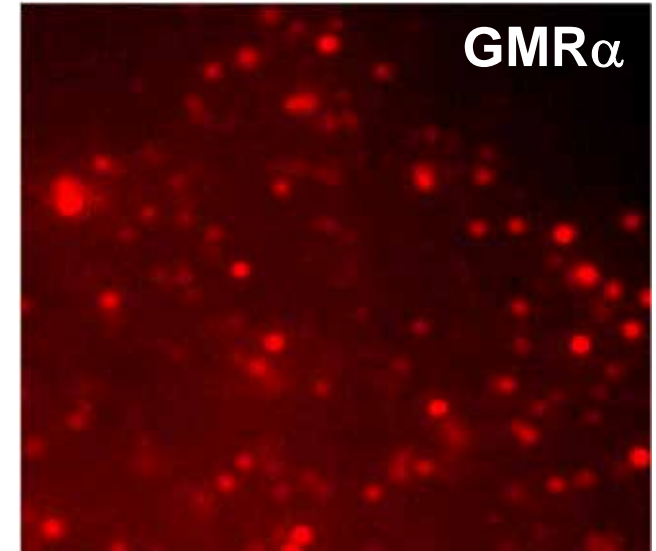
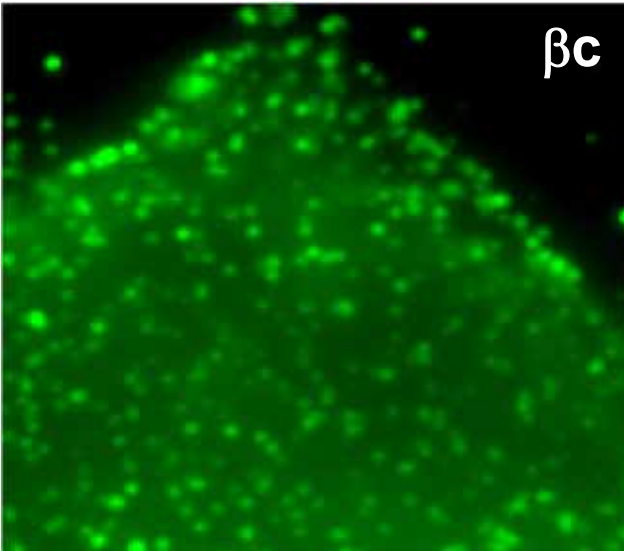
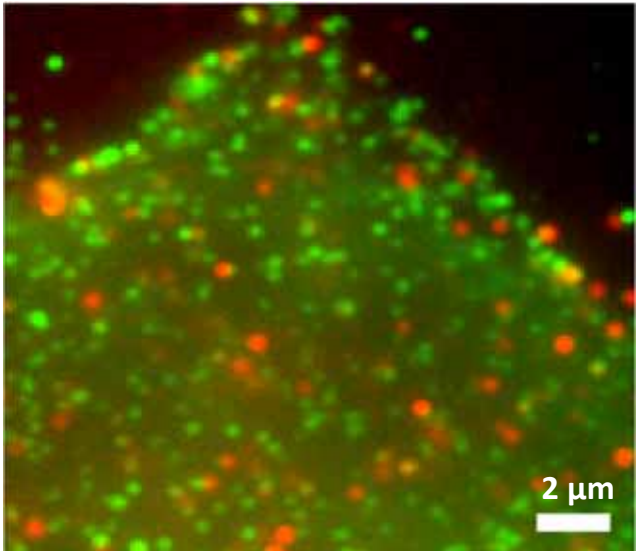
# Granulocyte-macrophage colony-stimulating factor (GM-CSF)



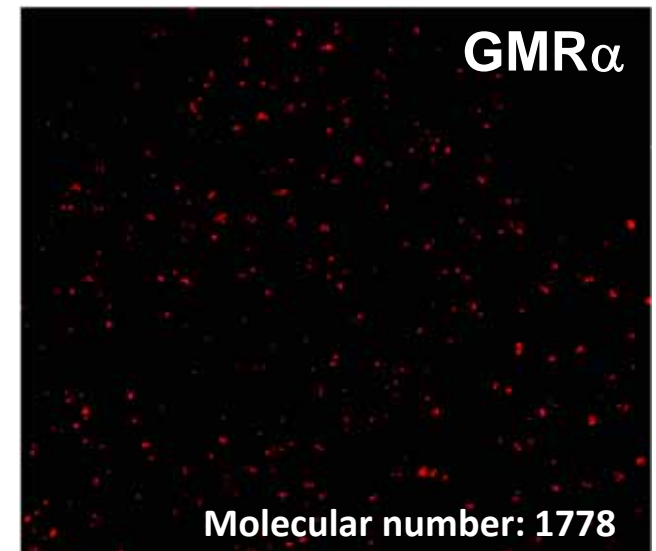
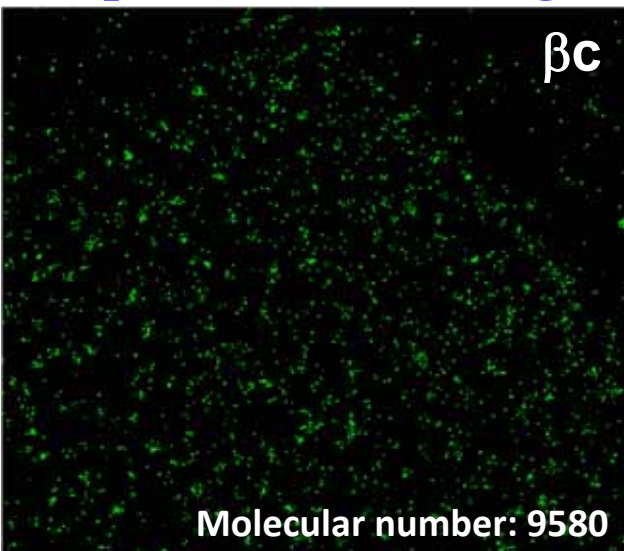
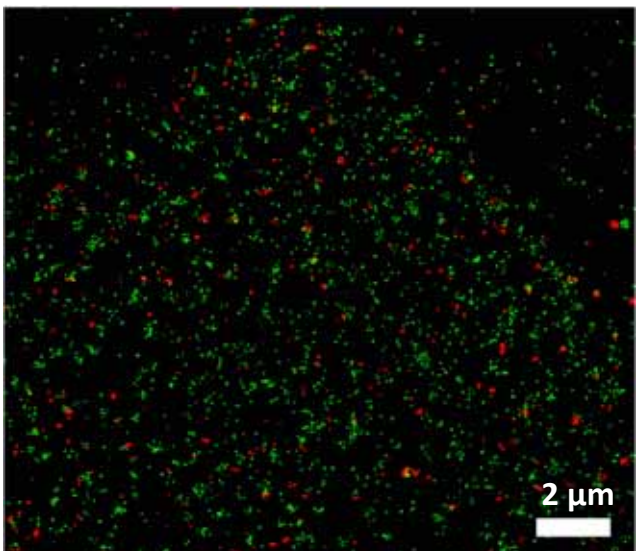
# Super-resolution localization imaging

Sample: AB+

TIRF images

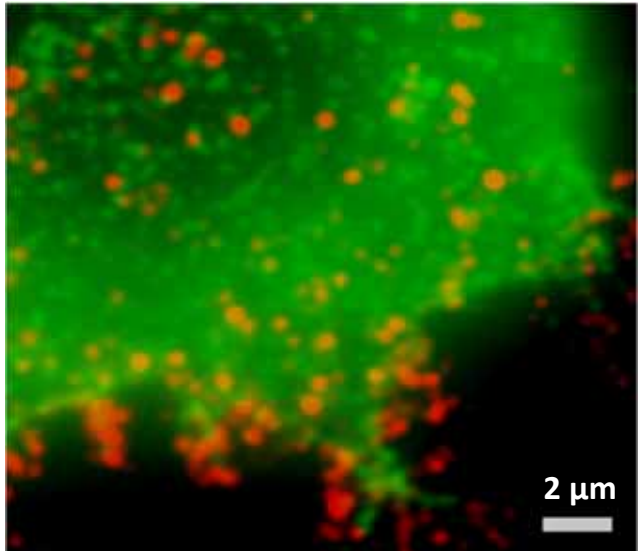


Super-resolution images

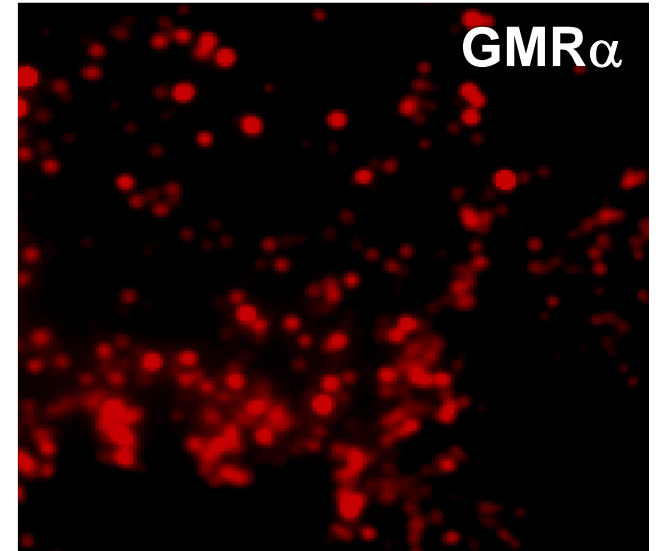
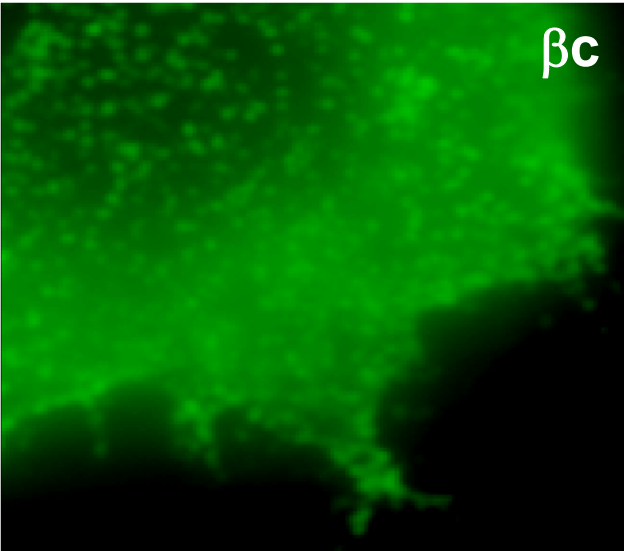


# Super-resolution localization imaging

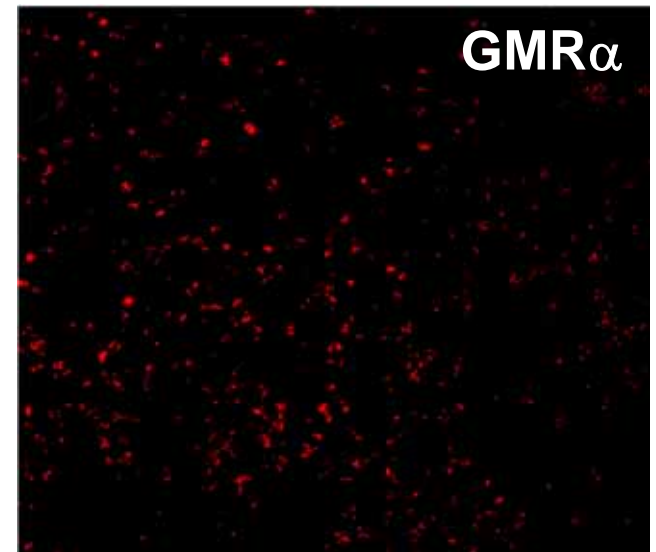
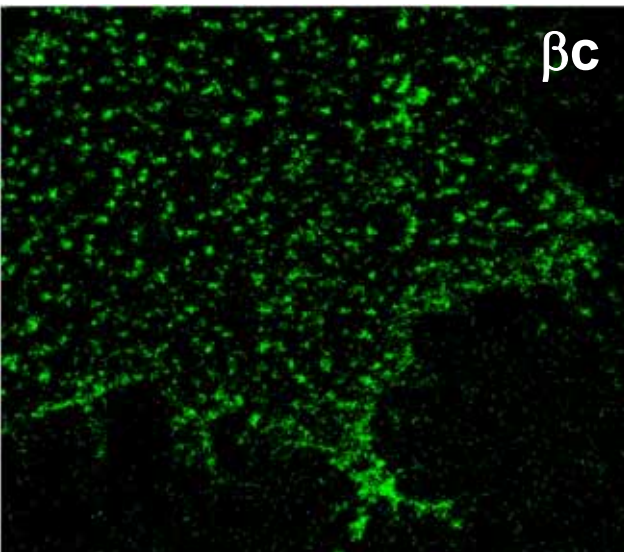
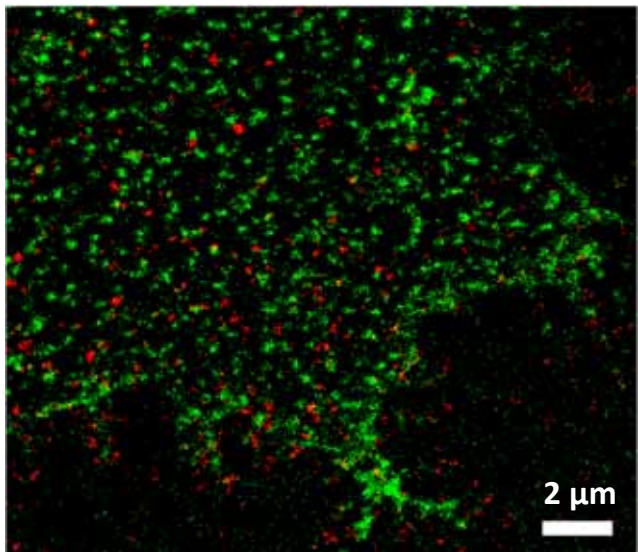
Sample: W+



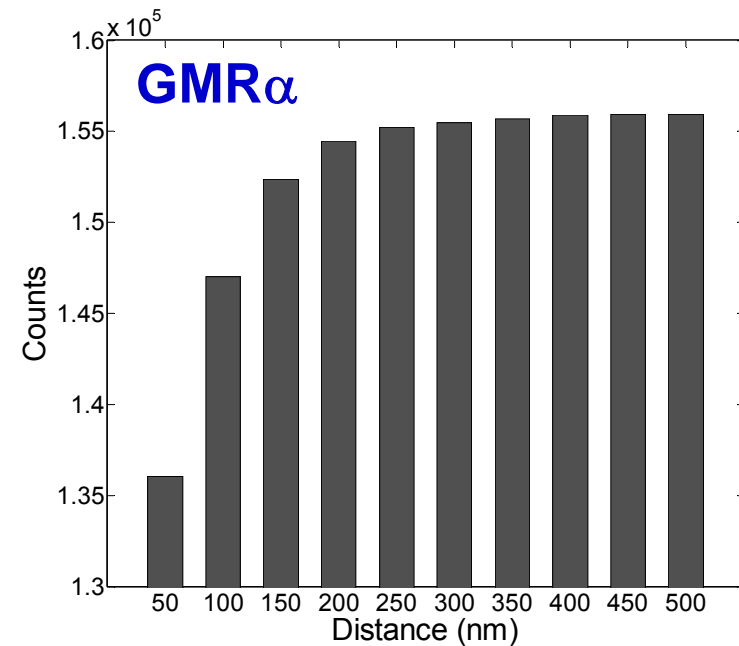
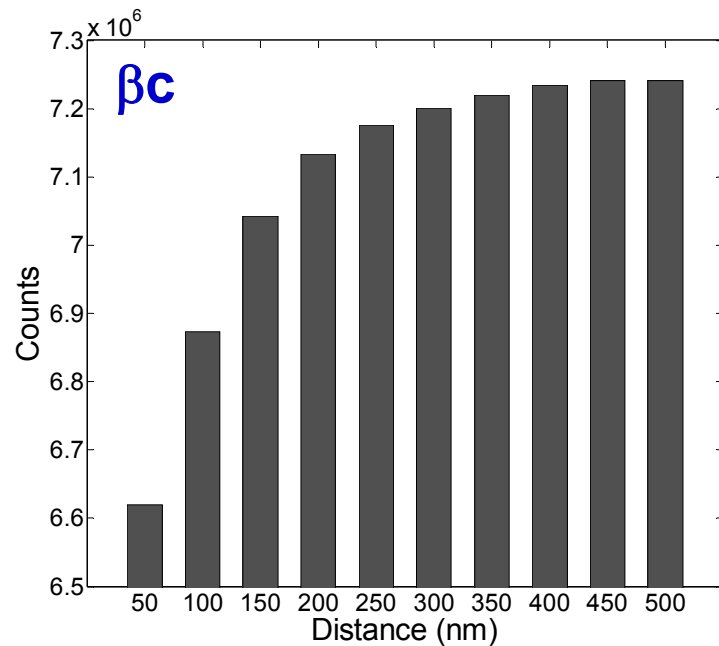
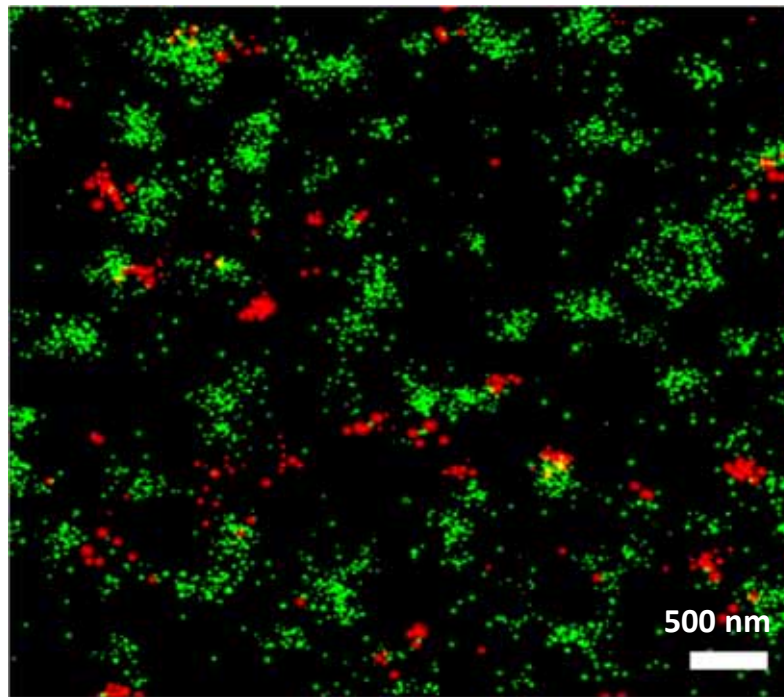
TIRF images



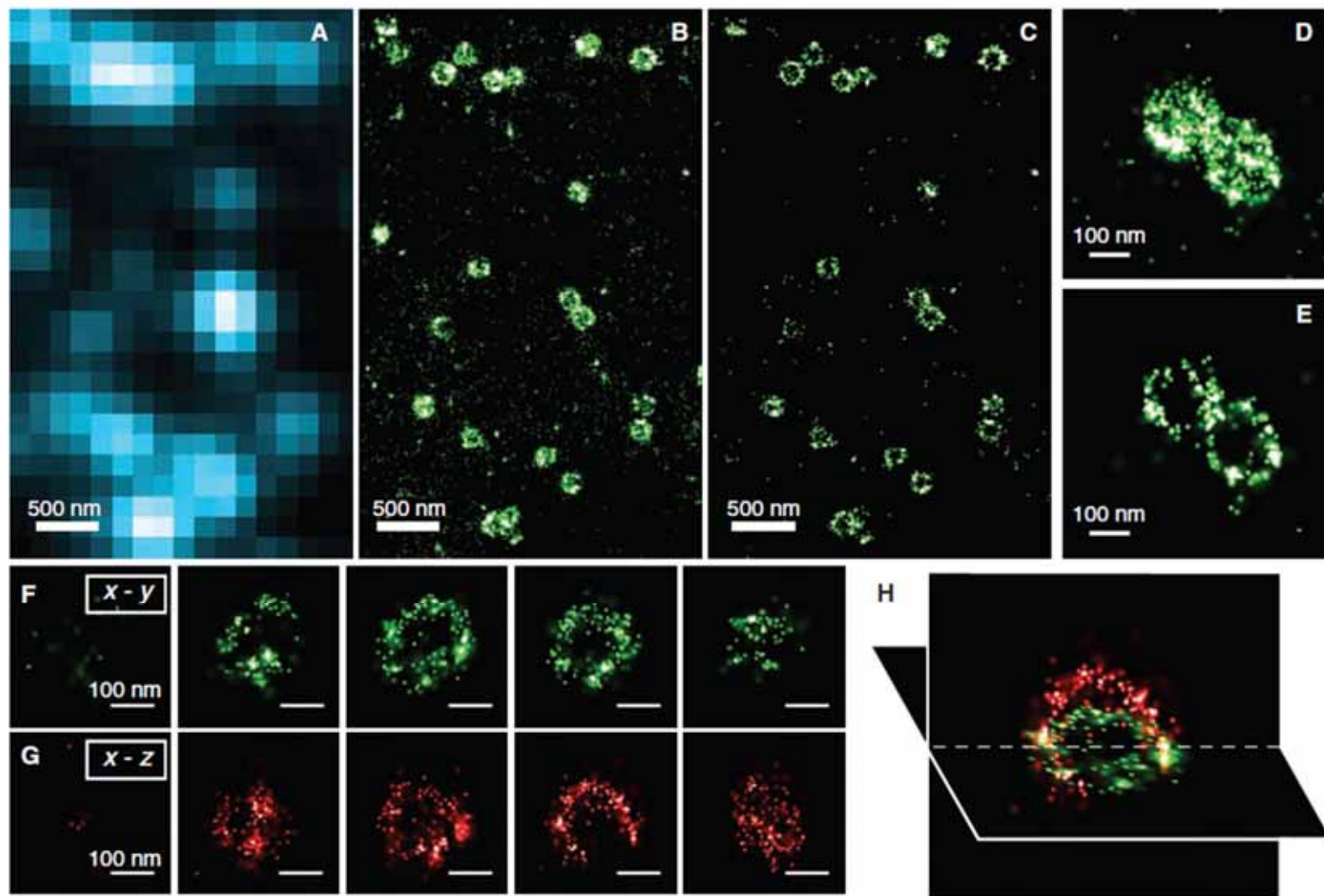
Super-resolution images



# Clustering analysis



# Clathrin-coated pits (CCPs) in BS-C-1 cells



## Pair correlation analysis

$$g(r) = \left\langle \frac{\rho(r)}{\bar{\rho}} \right\rangle$$

$\rho(r)$  is the density of molecules at distance.

$r$  from a given molecule.

$\bar{\rho}$  is the average density of molecules, with this ratio averaged over the entire ensemble of molecules.

